NASA/TP—1998–206864

Technique for Predicting the RF Field Strength Inside an Enclosure

M. Hallett, J. Reddell

National Aeronautics and
Space Administration

Goddard Space Flight Center
Greenbelt, Maryland 20771

August 1998

The NASA STI Program Office ... in Profile

Since its founding, NASA has been dedicated to the advancement of aeronautics and space science. The NASA Scientific and Technical Information (STI) Program Office plays a key part in helping NASA maintain this important role.

The NASA STI Program Office is operated by Langley Research Center, the lead center for NASA's scientific and technical information. The NASA STI Program Office provides access to the NASA STI Database, the largest collection of aeronautical and space science STI in the world. The Program Office is also NASA's institutional mechanism for disseminating the results of its research and development activities. These results are published by NASA in the NASA STI Report Series, which includes the following report types:

- TECHNICAL PUBLICATION. Reports of completed research or a major significant phase of research that present the results of NASA programs and include extensive data or theoretical analysis. Includes compilations of significant scientific and technical data and information deemed to be of continuing reference value. NASA's counterpart of peer-reviewed formal professional papers but has less stringent limitations on manuscript length and extent of graphic presentations.
- TECHNICAL MEMORANDUM. Scientific and technical findings that are preliminary or of specialized interest, e.g., quick release reports, working papers, and bibliographies that contain minimal annotation. Does not contain extensive analysis.
- CONTRACTOR REPORT. Scientific and technical findings by NASA-sponsored contractors and grantees.
- CONFERENCE PUBLICATION. Collected papers from scientific and technical conferences, symposia, seminars, or other meetings sponsored or cosponsored by NASA.
- SPECIAL PUBLICATION. Scientific, technical, or historical information from NASA programs, projects, and mission, often concerned with subjects having substantial public interest.
- TECHNICAL TRANSLATION. English-language translations of foreign scientific and technical material pertinent to NASA's mission.

Specialized services that complement the STI Program Office's diverse offerings include creating custom thesauri, building customized databases, organizing and publishing research results . . . even providing videos.

For more information about the NASA STI Program Office, see the following:

- Access the NASA STI Program Home Page at http://www.sti.nasa.gov/STI-homepage.html
- E-mail your question via the Internet to help@sti.nasa.gov
- Fax your question to the NASA Access Help Desk at (301) 621-0134
- Telephone the NASA Access Help Desk at (301) 621-0390
- Write to:
  NASA Access Help Desk
  NASA Center for AeroSpace Information
  Parkway Center/7121 Standard Drive
  Hanover, MD 21076-1320

NASA/TP—98–206864

Technique for Predicting the RF Field Strength Inside an Enclosure

M. Hallett, Goddard Space Flight Center, Greenbelt, Maryland
J. Reddell, Boeing Corp., Seabrook, Maryland

National Aeronautics and
Space Administration

Goddard Space Flight Center
Greenbelt, Maryland 20771

August 1998

Available from:

NASA Center for AeroSpace Information
Parkway Center/7121 Standard Drive
Hanover, MD 21076-1320
Price Code: A17

National Technical Information Service
5285 Port Royal Road
Springfield, VA 22161
Price Code: A10

Abstract

This Memorandum presents a simple analytical technique for predicting the RF electric field strength inside an enclosed volume in which radio frequency radiation occurs. The technique was developed to predict the radio frequency (RF) field strength within a launch vehicle's fairing from payloads launched with their telemetry transmitters radiating and to the impact of the radiation on the vehicle and payload. The RF field strength is shown to be a function of the surface materials and surface areas. The method accounts for RF energy losses within exposed surfaces, through RF windows, and within multiple layers of dielectric materials which may cover the surfaces. This Memorandum includes the rigorous derivation of all equations and presents examples and data to support the validity of the technique.

Table of Contents

List of Figures

Figure Title — Page Number

List of Tables

Title Page Number

1.0 INTRODUCTION

An analysis technique has been developed to predict the RF field strength, within the Delta fairing, arising from radio frequency transmission inside the fairing. This analysis is required to evaluate the impact of the radiation that could be caused by payloads launching with their telemetry transmitters radiating. This memorandum discusses the development of the analytical technique (mathematically derived in Appendix B) for predicting the RF electric field strength inside an enclosed volume in which radio frequency radiation occurs. The basic analytical approach is presented in Appendix A and Reference (2).

The analysis provides the ability to account for losses associated with the acoustic blankets which line the fairing wall. A method for evaluating the RF losses within the acoustic blankets is also provided and presented in Appendix D. This memorandum provides experimental data which validates the method. The technique is then used to estimate the RF fields inside the Delta fairing developed by the transmitters on the KoreaSat and XTE satellites. The computations were performed using the mathmatical functions of the Microsoft Excel spreadsheets.

The attached appendices provide rigorous derivations of all equations used in the analysis and provide insight into the technique for acoustic blanket modeling. Thorough study of these appendices can provide insight into the factors involved. This memorandum addresses the analytical concept, analytical steps, summary of background and efforts, validation of the analytical model, recommendation for composite fairing, and conclusions.

2.0 ANALYTICAL CONCEPT

The analysis is based on the technique and hypothesis presented by M. P. Hallett in Appendix A. This concept (derived from the conservation of energy) is that the field inside the fairing will increase, due to reflections, until all the energy being supplied by the transmitter is absorbed by the surface areas exposed to the RF field. Due to the combined reflected and scattered waves, the magnitude of the RF field is hypothesized to be equivalent to the magnitude of a single incident wave which would dissipate the total transmitter RF energy in the surface areas. The approach is an application of "*Poynting's theorem*" which states: **The power delivered by internal sources (the payload transmitter) to a volume is accounted for by the power dissipated in the resistance of the media (air) plus the time rate of increase in power stored in the electric and magnetic fields in the volume plus the power leaving through the closed surface(s).**

In our problem the power dissipated in the resistance of the media (air) inside the volume is extremely small and can be considered to be zero. Also, since the concern is for a stabilized system, the time rate of increase of the power stored in the electric and magnetic fields in the volume has become zero. Thus the theorem is reduced to the following: the power supplied by the transmitter is equal to the power leaving through the closed surface(s).

Mathematically the concept is implemented in Appendix B, equation (B55).

$$\left|\overset{V}{E_o^i}\right| = \sqrt{\frac{\langle P \rangle}{\sum_{k=1}^{k=m} 2A_{k-surf}\, real\left\{\frac{\eta_k}{|\eta_o + \eta_k|^2}\right\}}}$$

Where: P is the radiated power,

E_0^i is the absolute value of the surface incident wave,
$A_{k\text{-}surf}$ is the area in square meters of the surface k,
η is the complex impedance of the surface k material, and
η_0^k is the complex impedance of the media (air) inside the enclosure.

This equation shows the field is dependent on the area and impedance of each surface. The impedances of the surface areas are, in general, a function of frequency for homogeneous materials. The acoustic blanket covered surface area impedance is very complex being a composite function of the properties and thickness of each material, the order of layers of material, and the impedance of the wall material.

3.0 ANALYTICAL STEPS

The analytical steps which are performed during an analysis are briefly outlined here:

a) Compute the surface area in square meters of each of the different types of materials exposed to the RF field.
b) Compute the intrinsic RF characteristics of each material exposed to RF field. These characteristics are usually described as complex numbers. The equations for computing the characteristics of most materials, including air and aluminum, are provided in Appendix C.
c) Determine the effective RF impedance of the blanket covered fairing walls. The necessary mathematical equation derivation and the methodology used is described in Appendix D.
d) Compute the incident wave's RF electric field strength using equation (B55) of Appendix B and the results of the three previous steps.

Appendix A and Reference (1) provide initial explanations of the method and its application to early models of the fairing. These original explanations and computations did not include, or consider, the affects of the acoustic blankets.

4.0 SUMMARY OF BACKGROUND AND EFFORTS

Early in the development of the Small Expendable Launch Vehicle (SELVs) service, a need arose to estimate the fields created by RF radiation within the launch vehicle's fairing. At that time, no analytical tools were readily available. Therefore, a simple test was performed using a 1-watt S-band source radiating inside the fairing, and measuring the resulting field strength at several points inside the fairing. The results were alarming; with measured field strengths approaching 100 v/m. Consequently, the SELVs program does not allow RF radiation within their fairing.

During the launch processing of an Atlas-E mission, a NOAA spacecraft reported experiencing unexpected noise and interference of instrumentation data during ground testing. The test included RF transmitter radiation while encapsulated in the fairing. The noise and interference vanished when the transmitter was powered off, indicating that the spacecraft was operating at the edge of its limit. The RF field levels were not known.

Because of the SELVs data and anecdotal information from the Atlas-E program, we began to question the validity of past decisions allowing RF radiation within the Medium Expendable Launch Vehicle (MELVs)

sevice (Delta) fairing. It appeared that these decisions had been based on either free space calculations of the field strength, or similarity to an earlier (successful) mission. Neither approach could be supported on a rigorous engineering basis.

We then started development of a method which could be justified by sound engineering principles to estimate the field strength inside a fairing. Considerable effort was expended examining computationally intensive approaches using resonant cavity theory, ray tracing theory, etc. The mathematics involved were extensive and the results questionable, although indicating that fields were high, as expected. Theoretically, a finite difference program (such as GEMACS) is capable of solving this class of problem. However, the physical dimensions of the problem resulted in huge matrices that demanded the capabilities of large, fast computers. An additional shortcoming was that these programs offered little visibility into the factors involved, such as program implementation limits, or the ability to vary parameters within the model.

The basic technique is outlined in sections 2.0 and 3.0. This technique involves computations that can be performed within a spreadsheet, yielding results that are reasonably accurate and tend to bound the upper limit of the field. **The reader is cautioned that this technique yields an assumed uniform field strength, not an exact solution of the field distribution.**

The first attempts to model the Delta vehicle, spacecraft, and fairing resulted in prediction of very high field strengths. Incident RF fields of about 115 volts per meter and a standing wave of about 230 volts per meter were computed for 1 watt transmitted. Further investigation indicated that the RF window established a limiting factor on the buildup of the internal fields. Given the typical size of the current window (approximately 0.5 m^2), our model shows that the field developed by a 1 watt source would be an incident wave in the order of 30 volts per meter with a possible standing wave to 60 v/m. This is still high, and one can reasonably question the validity of the result in light of many successful launches without indications of EMI.

A review of the various items contained within the fairing was then initiated, searching for materials that might further reduce the fields. We concluded (and later proved by testing) that the acoustic attenuation blankets which line the fairing are also quite effective absorbers of RF energy. This conclusion then demanded development of a model for the acoustic blankets, thus completing our model of vehicle, spacecraft, and fairing. This blanket model and vehicle model were subsequently validated by experimental data, as described in section 5.0 of this memorandum.

5.0 VALIDATION OF THE ANALYTICAL MODEL

The validation of the analytical technique and equations is addressed in four parts. The four parts are presented in the chronological order that the test data and analysis model developed. The first (section 5.1) addresses the equations and modeling of the acoustic blankets. The second (section 5.2) addresses the application of our technique to an aluminum room. The third (section 5.3) deals with analysis and measurements made within actual vehicle fairing enclosures. The fourth part (section 5.4) provides a correlation of measured RF field data with the results of the analytical technique and equations as applied to a six foot diameter composite fairing test article.

It should be noted that three different types of acoustic blankets are discussed in this memorandum. The first is the blanket that has flown in the metal fairing for many years. It is built somewhat like a large pillow

with fiberglass batting covered all around by a thin cover. This first blanket is discussed in sections 5.1, 5.2, 5.3.1, and 5.3.2. The second acoustic blanket is the original design for the composite fairing. It is a foam in contact with the fairing wall and having the surface facing the center of the fairing covered by a sheet of highly reflective aluminized kapton. This second blanket is discussed in section 5.3.3. The third acoustic blanket, discussed in section 5.4, is a foam in contact with the fairing wall with it's inner surface (facing the center of the fairing) covered with a sheet of carbon loaded kapton.

5.1 Acoustic blanket modeling

The computations required by our model were initially frustrated by the presence of dielectric materials in the blankets. The blankets' unknown electrical properties and the inability to accurately evaluate their affect on the fields presented serious problems. The need for an accurate method of evaluating the acoustic blanket's affects became the major goal in arriving at a good analytical model.

Initial evaluation of the RF losses in the acoustic blanket began as a series expansion of the reflected and transmitted waves between the boundaries of the many layers of materials in the blanket and the fairing wall. This initial method convinced us the blankets were a dominant factor in reducing the field strength inside the fairing. The series expansion technique presented several difficulties which caused an increase in efforts to define another method. A method to accurately determine the effective impedance of the area covered by the blankets was sought. Reference (4), Section 7-08, provided the insight to allow the derivation of the Appendix D equations.

The Appendix D equation (D17) eventually proved to accurately provide the complex impedance for the blanket covered wall area. The validity of the blanket model is confirmed by classical theory and experimental testing, which demonstrates that the results are reasonably accurate.

5.1.1 Classical Theory

The RF characteristic of homogeneous materials can be computed using the known conductivity, permeability and permitivity of the materials. Many texts provide simplified equations for their computation and testify to their validity. Appendix C provides a thorough development of the generic equations, which can be simplified, using appropriate assumptions, to the equations presented in most texts. This testifies to their theoretical validity.

While the impedance of many materials can be easily computed, the equivalent impedance of several layers of material is not easily computed nor is it a subject treated thoroughly or effectively in text books. The text typically make a brief reference to transmission line corollaries, present highly simplified equations (with no explanation of the simplifying assumptions which were used), and then launch into activities with Smith charts etc. In contrast to this, the rigorous mathematical derivation of equation (D17) in Appendix D indicates it is theoretically sound. This derivation makes no confusing references to transmission line theory or Smith charts. This equation defines the complex impedance at the surface of a single layer of material (media 1) of thickness, $T = \ell$, which covers a plate (media 2). The subscript 1, designates the single layer material and subscript 2 is the plate. Alpha and beta are for the single layer of material (media 1). Successive application of the equation is required to determine the impedance of several layers of materials.

$$\eta_L(l) = \eta_1 \left\{ \frac{\left[(\eta_2+\eta_1)e^{\alpha_1 l} + (\eta_2-\eta_1)e^{-\alpha_1 l}\right]\cos\beta_1 l + j\left[(\eta_2+\eta_1)e^{\alpha_1 l} - (\eta_2-\eta_1)e^{-\alpha_1 l}\right]\sin\beta_1 l}{\left[(\eta_2+\eta_1)e^{\alpha_1 l} - (\eta_2-\eta_1)e^{-\alpha_1 l}\right]\cos\beta_1 l + j\left[(\eta_2+\eta_1)e^{\alpha_1 l} + (\eta_2-\eta_1)e^{-\alpha_1 l}\right]\sin\beta_1 l} \right\}$$

The equation matches the simplified equation (with the appropriate simplifying assumption, $\alpha_1 = 0$) which is normally presented in text books. This correlation with the texts supports its validity. Other evidence is also available. Since most texts use transmission line theory as a corollary for analyzing RF transmission through media, the characteristics from transmission line theory will be used here to demonstrate the validity of the equation application. The optics world also has corollaries to these characteristics which will not be discussed here.

5.1.1.1 Half Wavelength Characteristics

One well known impedance characteristic of a transmission line is that a transmission line of length equal to a multiple half wavelength behaves as if the transmission line is not present. In other words, the load at the source is the same as the impedance terminating the line. Equation (D17) of Appendix D was used to calculate the equivalent impedance of fiberglass batting on air and batting on aluminum. Figures 1 and 2 show the results as a function of the batting thickness in wavelengths. At multiples of the half wavelength, Figure 1 shows the effective impedance to be that of air. Figure 2 shows the effective impedance to be that of aluminum at the half wavelength points. Both examples demonstrate the effective half wavelength characteristic expected from its corollary transmission line theory and confirm its validity.

Classical transmission line theory shows that the impedance repeats at half wavelength increments. This repeating characteristic is demonstrated in the examples shown in Figures 1, 2, 3, 5, and 7.

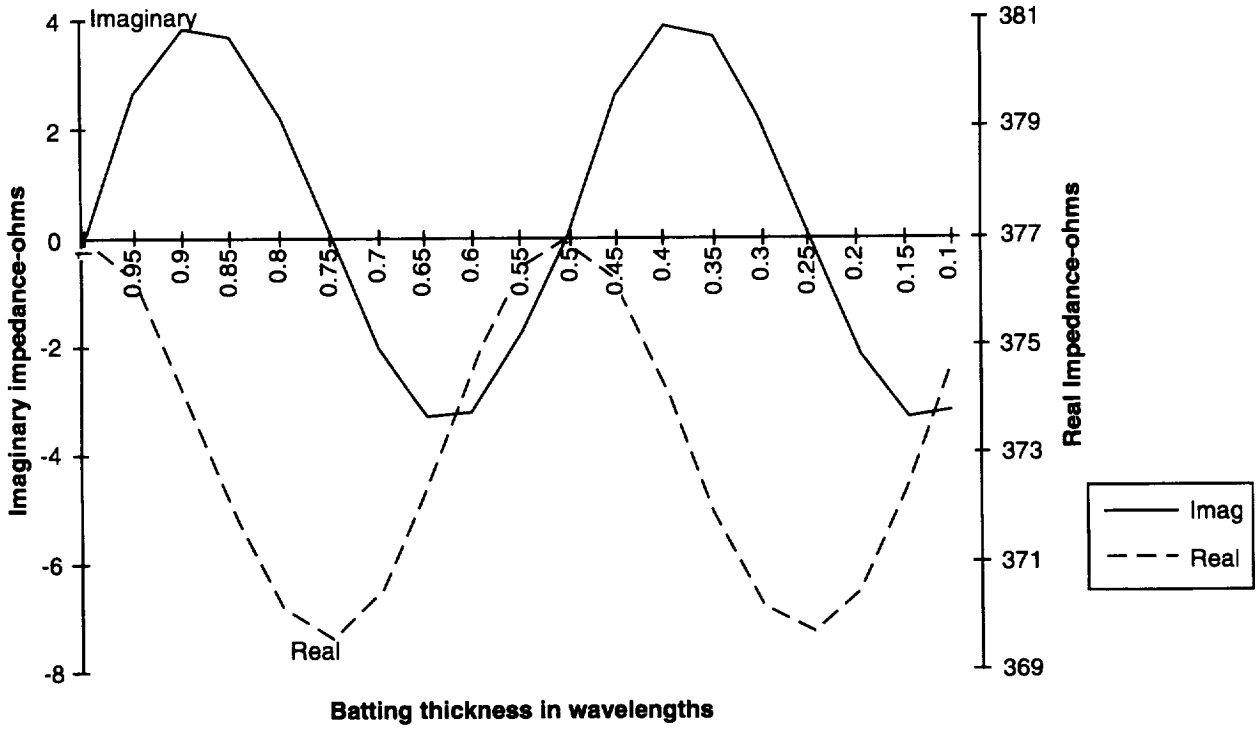

Figure 1. Effective impedance of batting on air.

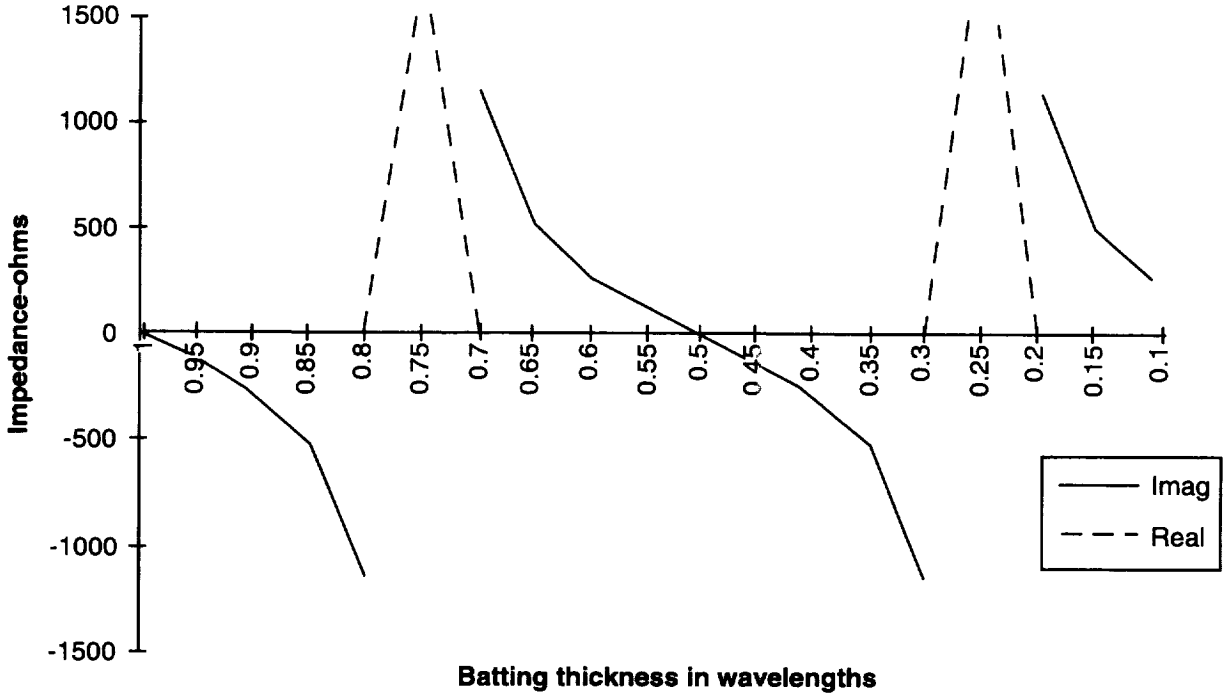

Figure 2. Batting on aluminum.

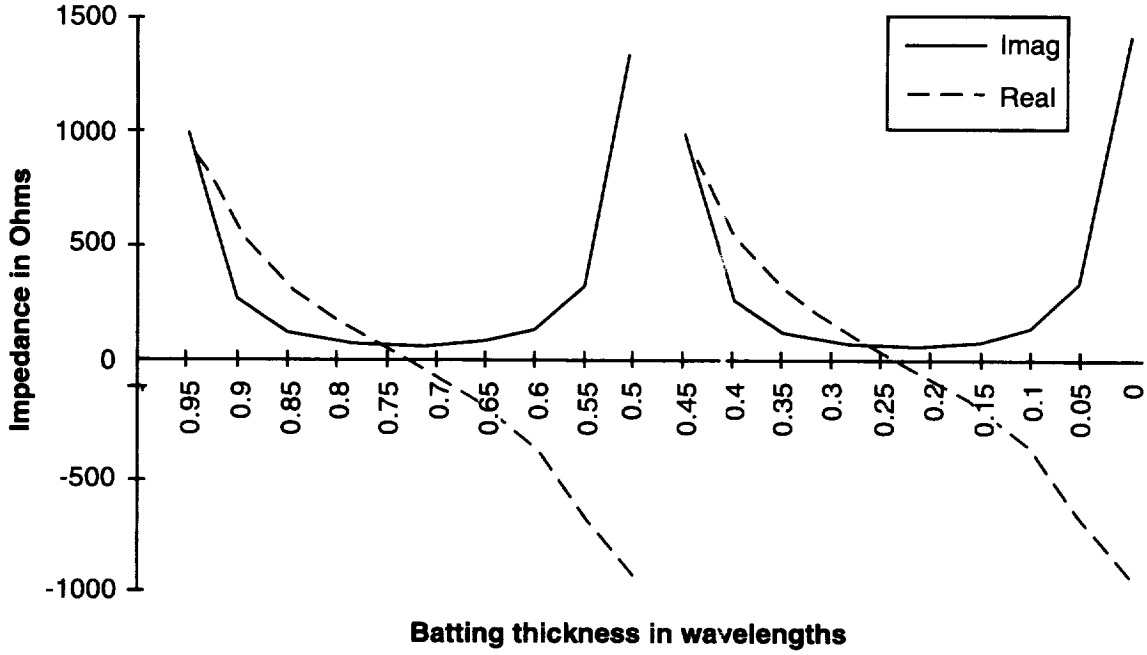

Figure 3. Impedance of batting on high impedance plate.

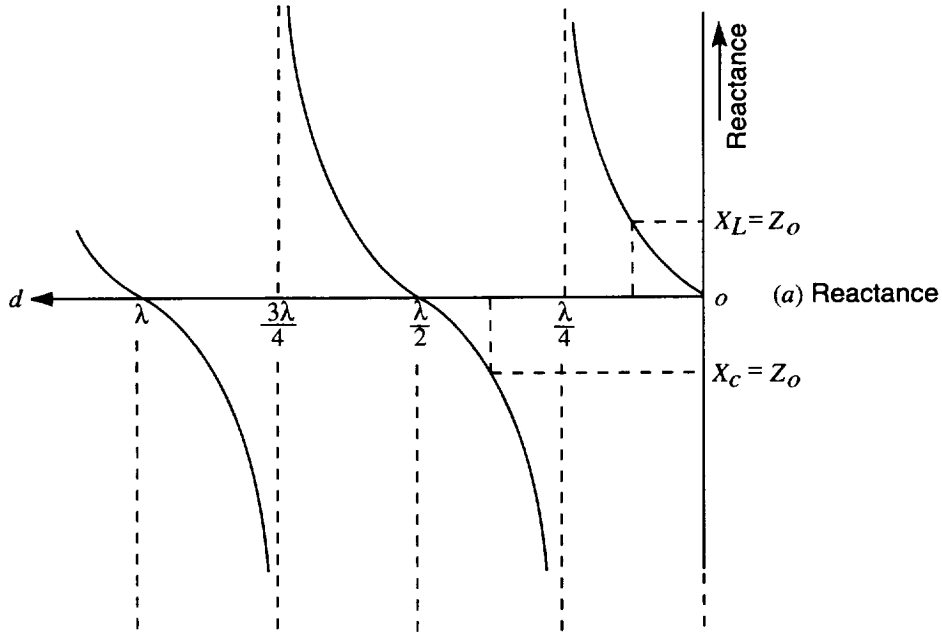

Figure 4. The variation of reactance along a lossless short-circuited transmission line.

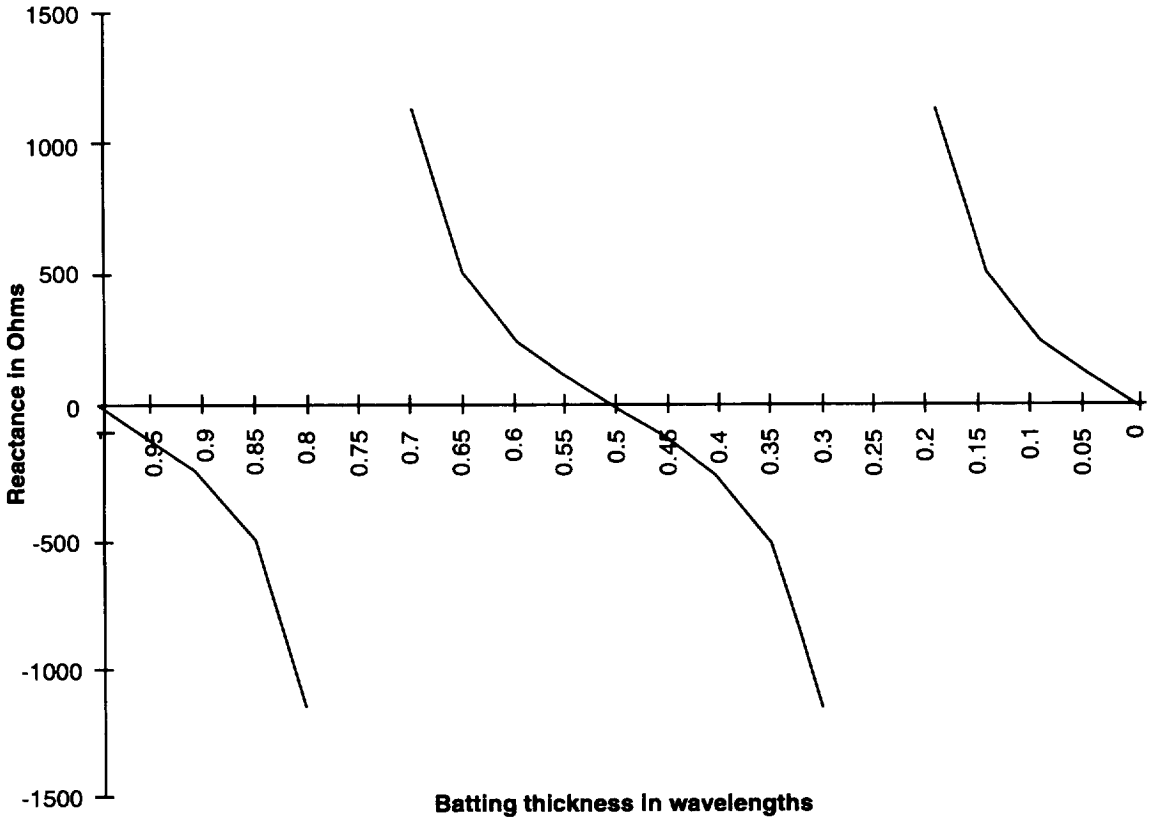

Figure 5. Reactance of batting on aluminum.

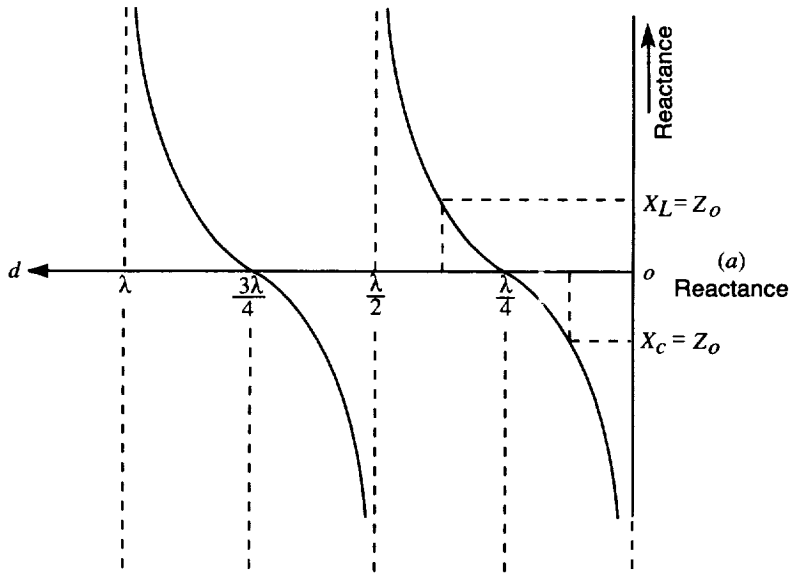

Figure 6. The variation of reactance along a lossless open-circuited transmission line.

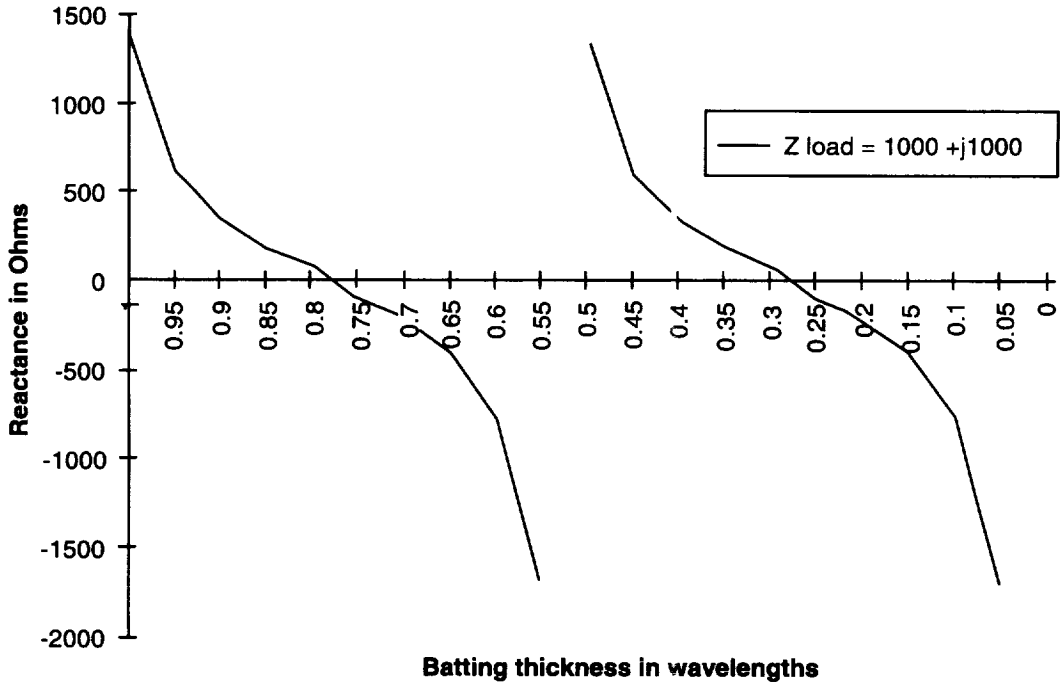

Figure. 7 Reactance of batting on high impedance.

5.1.1.2 Quarter WaveLength Characteristics

Another characteristic suggested by the transmission line corollary is the impedance characteristics for odd multiples of lossless quarter wavelength line which is terminated by the characteristic impedance of the source. That is, if the line length (batting thickness) is an odd multiple of a quarter wavelength then the equivalent impedance at the source has an imaginary part which is zero and the real part has a minimum magnitude. Figure 1 demonstrates this low value for the real part and a zero value for the imaginary part

at the quarter wavelength intervals.

The quarter wavelength transmission line is also an impedance inverter. This characteristic says that for a "shorted" load (a perfect conductor), at odd multiplies of quarter wavelength line, the effective impedance is infinite . Figure 2 is for batting on aluminum and shows that the real and imaginary parts are off scale at the odd multiple quarter wavelengths. (Actual computations were on the order of millions of ohms for both the real and imaginary parts). Similarly, the theory says an open circuit would be inverted to an effective impedance of zero at the quarter wavelength distances. Figure 3 shows the computation for the batting on an high impedance circuit and shows the expected low (zero) impedance at the quarter wavelength.

5.1.1.3 Shorted and Opened Transmission Line

The computed impedance terms also follow the classical shapes for the shorted transmission line of varying length. Figure 4 is a typical figure given in textbooks showing the reactance for a transmission line terminated in a short circuit as a function of transmission line length. Figure 5 shows the computed reactance for the batting on aluminum which matches the Figure 4 form. Figure 6 (typically in textbooks) shows the reactance for a transmission line with an open circuit load. Figure 7 shows the computed reactance for the batting on a plate with a relatively high impedance, which matches the Figure 6 characteristics.

5.1.1.4 Classical Theory Conclusions on Equation

Each of these computations show that the Appendix D equation (D17) agrees with the corollaries to transmission line classical theory. The equation demonstrates the expected quarter wave inverting characteristic, the expected half wave transparency, repeating impedance for each half wavelength, and provides the expected capacitive and inductive nature of the impedance with length (thickness). This correlation indicates the mathematical model (equation (D17) of Appendix D) is valid for the application to the acoustic blanket installation in the fairing.

A significant point of this discussion is that for any given frequency, one may expect the RF impedance of the acoustic blanket to vary as a function of the batting thickness. In fact, it will vary between a rather high loss level (medium impedance, low reflection) defined by the cover sheet material and a rather low loss level (small impedance or highly reflective) defined by the wall behind the blanket. This leads us to still another observation. At S-band frequencies, it is theoretically possible for the blankets to become "transparent" due to compression and billowing, leaving the RF window the dominant factor in establishing the upper boundary of the RF field. This will be discussed in greater detail in sections 5.3.1 and 5.3.2.

5.1.2 Cover Sheet Model Validation

Determination of the characteristics of the blanket's cover sheets is difficult because it is not a homogeneous material. It is made of several layers of different material. Fortunately the composite properties can be determined experimentally by insertion loss measurements. The measurements provide the complex dielectric constant and loss tangent at various frequencies. Test data on the carbon loaded cover sheets of the acoustic blankets was provided by McDonnell Douglas Aerospace (MDA). This data defined the sheet's thickness, dielectric constant, loss tangent, insertion loss, phase angle, and conductivity. Appendix E provides the equations for computing the resistance, impedance, attenuation, and phase shift constants

for the sheet using the complex dielectric constant and the loss tangent. The Appendix E equations computed comparable results to the test data. These cover sheet computations results were used with equations (D17) and (D21) of Appendix D to compute the insertion loss of the single cover sheet at frequencies from 2 to 13 GHz. Table 1 provides the computed and the measured values. Reasonable agreement is apparent at all frequencies. This data indicates the mathematical model for the cover sheet is valid.

Table 1.
Carbon Loaded cover sheet, insertion loss

Frequency- GHz	Measured* Insertion Loss	Calculated Insertion Loss
2	2.86	2.862
3	2.91	2.908
4	2.95	2.955
5	3.00	3.000
6	3.05	3.047
7	3.09	3.093
8	3.14	3.140
9	3.18	3.187
10	3.23	3.232
11	3.28	3.277
12	3.32	3.324
13	3.37	3.371

*Test data provided by DuPont, Circleville, OH to MDA; FAX dated 8/24/95.

5.1.3 Blanket on RF Window Model Validation

The sheet model developed in the previous step was then combined (using Appendix D technique) with the characteristics for a 1.5 inch fiberglass batting, thus providing a model for the 1.5 inch blanket on the RF window. The model provided insertion loss calculations of about 5.2 dB. Measured data for the insertion loss of the blanket varied from 3.4 to 4.4 dB. Reasonable comparison with the test data exists. This correlation provides further confidence that the mathematical model and technique are valid and that a valid model for the blanket's performance has been accomplished.

5.1.4 Conclusions on Acoustic Blanket Modeling

Classical theory supports the use of the equation. Its applications to blanket components show agreement with experimental test data confirming its validity.

5.2 VALIDATION OF THE BASIC TECHNIQUE

The next step in the validation of the technique is to demonstrate the model in an enclosed volume. To accomplish this an aluminum room was constructed measuring 8 feet by 8 feet by 8 feet. Measurements of RF field strength inside the room were made while transmitting 1 watt at S-band frequencies. Reference (2) describes the test and results. These measurements were compared to the model predictions for three cases:

1. The room with bare aluminum surface.
2. The room with a small area covered with acoustic blankets.
3. The room with a larger area covered with acoustic blankets.

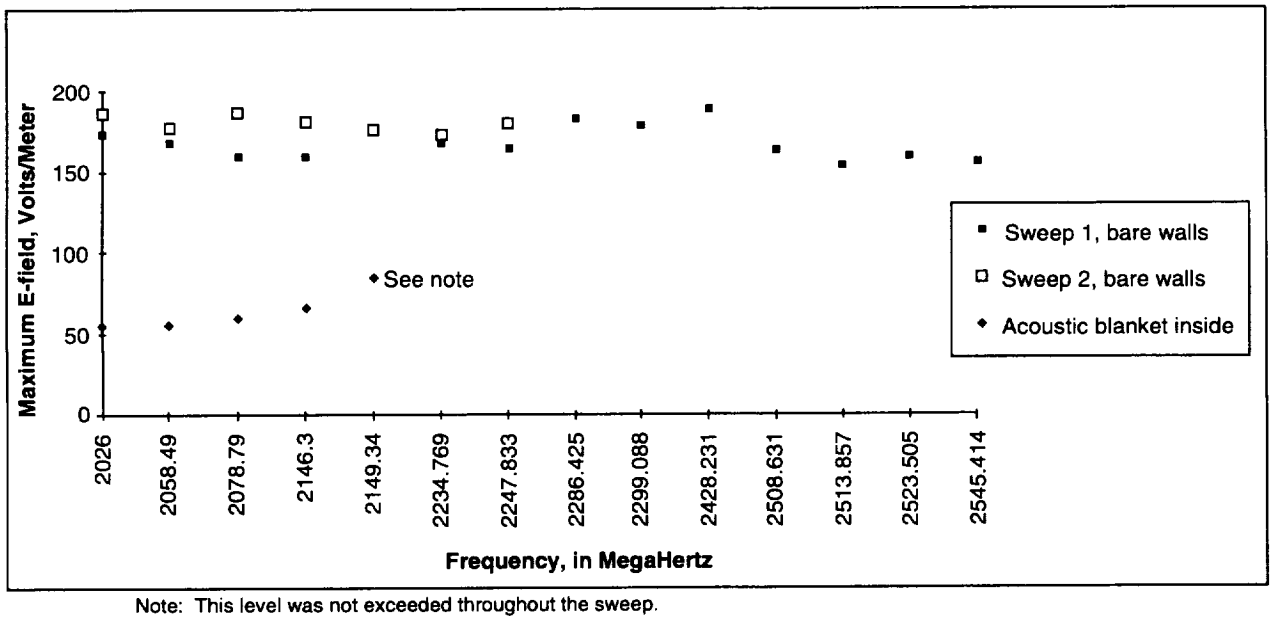

Note: This level was not exceeded throughout the sweep.

Figure 8. Effect of acoustic blanket on maximum fields.

5.2.1 Bare Aluminum Walls

Predictions for the bare aluminum surfaces of the cube room were 254 volts per meter for the incident wave giving rise to a possible 508 volts per meter for the standing wave. The 254 volts per meter is the RMS value of the wave incident on the wall to give the power loss. The 508 volts per meter corresponds to the RMS value of the standing wave inside the enclosure. Figure 8 shows the fields measured at one point in the room as the frequency of the signal was varied. The hypothesis is that the peak standing wave for a fixed frequency is very close to the receiving probe and is comparable to the peak field measured with the frequency varying. Measurements showed levels averaging 85 volts per meter and a maximum standing wave measurement of 197 volts per meter. The concern is for the maximum field. A very large standing wave is present with peaks located very close to one another. The average distribution of the measurements is what one would expect with the large standing wave. Subsequent assessments of the antenna loading characteristics indicated the actual power being radiated could have been reduced to about 0.7 watt. Making the corrections indicated the maximum measured fields could have been as high as 236 volts per meter. This 236 V/m (or the uncorrected 197 V/m) compare favorably with the predicted incident wave level of 254 V/m. Another loss factor not accounted for was the dielectric material used for the antenna stand and the probe stand. The presence of the very high field strength would likely cause appreciable losses in these stands. The model bounded the measured levels providing an upper limit and demonstrating a reasonable close agreement with the test data.

5.2.2 Small Area of Blanket-Covered Wall

The batting data and sheet model discussed is section 5.1 were used to define the model for the blanket on aluminum. This model was then used to predict the RF fields which would result in the 8 foot aluminum cube room. Slight variations in the thickness of the batting material in the blanket cause significant effects

on the predicted RF fields inside the room. Figure 9 shows the predicted effect of batting thickness on the field strength inside the room. Figure 10 shows the effect on the impedance of the covered area and Figure 11 shows the effect on the reflectance of the covered area.

Initial testing with an acoustic blanket used one blanket segment approximately 15 inches wide by 14 feet long and 3 inches thick. The model predictions for this blanketed area were an incident field of 14 volts per meter for the most lossy batting thickness and 250 volts per meter for the least lossy batting thickness. The least loss condition allows the covered wall area to behave as bare aluminum. The predictions indicate incident fields could be between 14 and 250 volts per meter depending on the installation and manufacturing tolerances of the blanket . This means the standing wave field value could be as high as 500 volts per meter. The most likely values would be the average of the predicted incident fields as thickness varies (reference Figure 9) which gives an incident value of 54 and a standing wave of 110 volts per meter. Figure 8 shows the measured values. Test measurements showed average fields of 55 volts per meter with the maximum of 85 volts per meter. Using the possible correction for antenna loading, the measured fields could have been at higher values (an average of 66 and maximum of 102 volts per meter). Our model predicted the possibility of high fields and bounded the upper limit of the problem. The model suggests that the blankets could have provided a much lower field value if the installed thickness was made smaller.

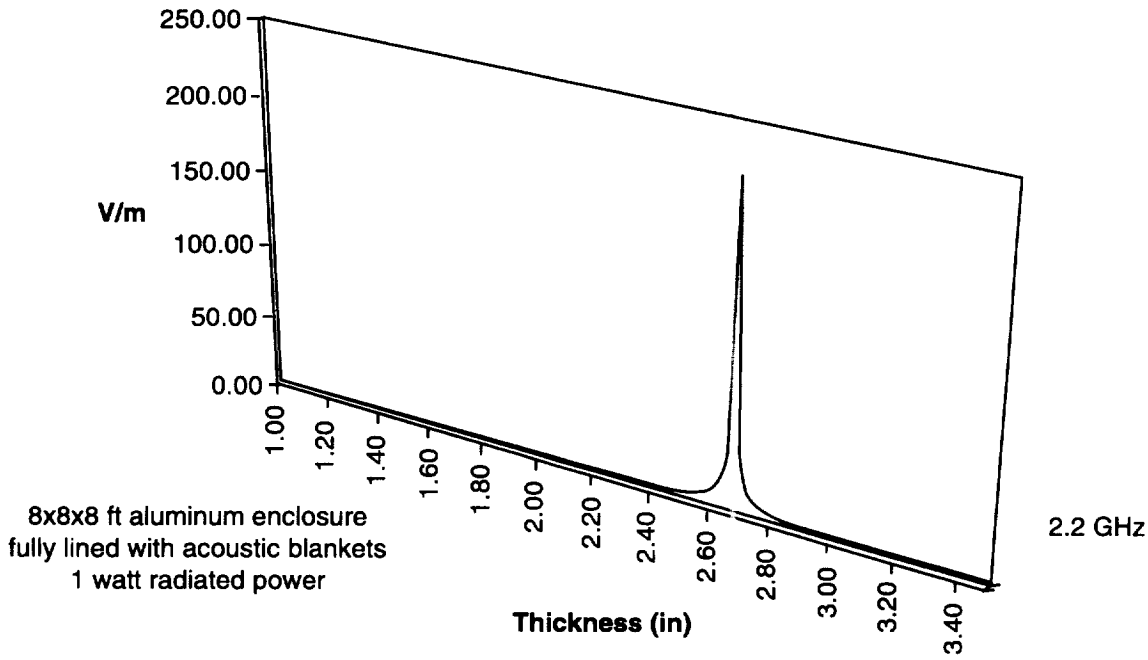

Figure 9. Effect of blanket thickness on field strength inside enclosure.

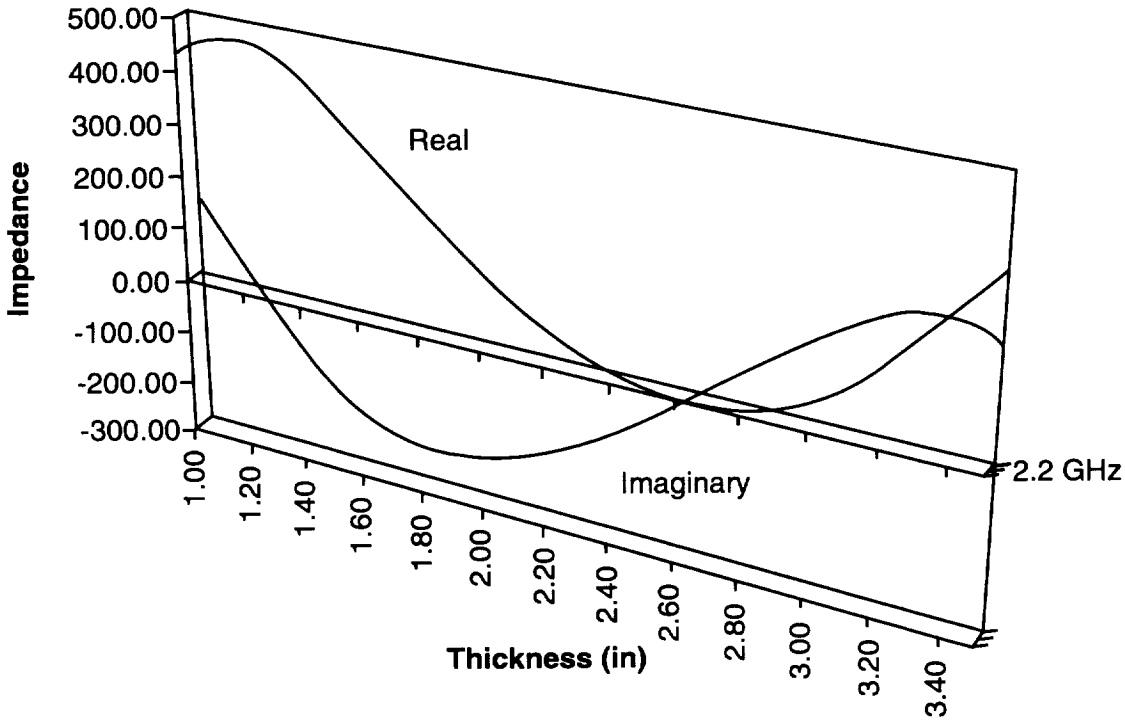

Figure 10. Effect of blanket thickness on equivalent impedance.

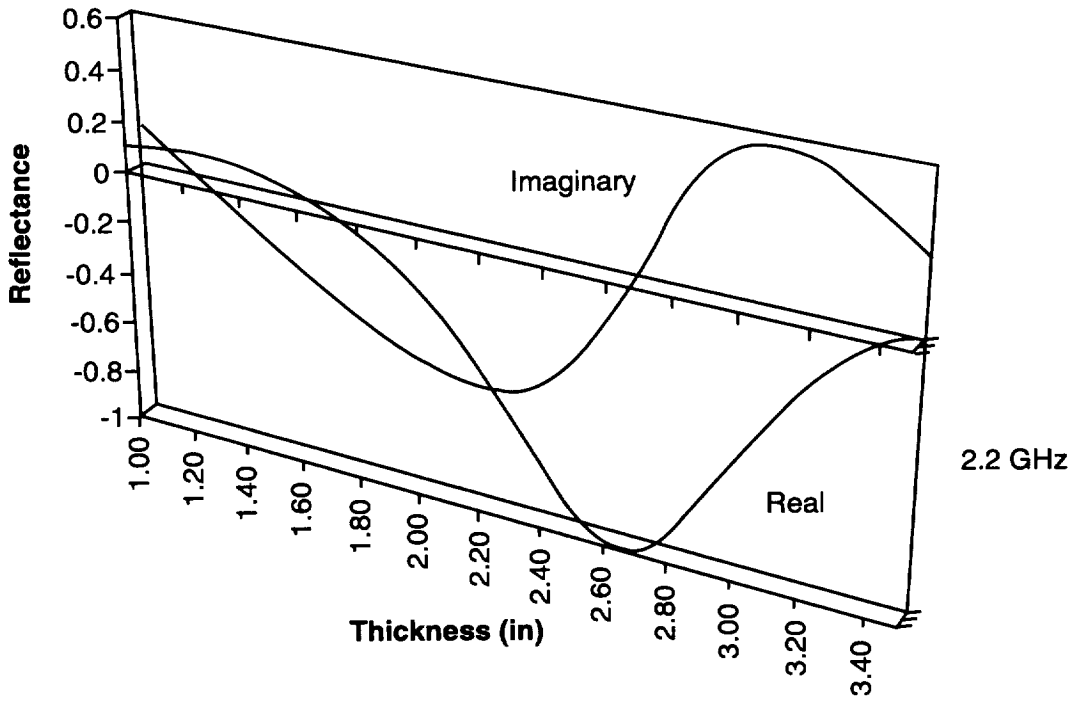

Figure 11. Effect of blanket thickness on reflectance.

5.2.3 Large Area of Blanket-Covered Walls

Subsequent testing with blankets covering 42% of the wall surface, measured average field strength of 17 volts per meter, and a maximum level of 33 volts per meter. Antenna loading could indicate the fields could be as high as 40 volts per meter. This reduction, caused by added blanket area, supports the model's use of surface area as a prime factor. The model predicts the incident RF field could be as low as 6 volts per meter for blanket thickness in the most lossy condition. The model predicts incident fields could still be as high as 250 volts per meter for the least lossy thickness. The standing wave could be as high as 500 volts per meter. It is believed that the conditions are such that the most likely value of incident RF field would be an averaging of the effects giving the most likely calculated incident value of 26 volts per meter and a standing wave of 52 volts per meter. The 33 to 40 volts per meter measured compares very well with the 26 to 52 volts per meter predicted, further demonstrating the validity of our method.

5.2.4 Aluminum Room Model Conclusions

The model definitely predicts the blankets can be extremely lossy. It also warns that the loss could be dramatically affected by construction tolerances, installation, and billowing during launch. The variations of loss suggest the possibility of very high fields developing. The model also provides some valuable insight into the nature and characteristics of the losses. The model established an upper limit which encompassed the test results.

5.3 VEHICLE VALIDATION

5.3.1 KoreaSat RF Measurements

The RF fields inside the 9.5 foot aluminum fairing were measured during ground testing of the KoreaSat mission. The model predictions were compared to the fields measured.

The model for the KoreaSat vehicle included:

- Frequency of 12.5 GHz
- Transmitter power of 1.3 watts
- Bare aluminum area of 137.5 square meters
- 3 inch acoustic blanket covered area of 18.5 square meters
- 1.5 inch acoustic blanket covered area of 15.5 square meters
- 1.5 inch blanket covered RF window of 0.5 square meter

Models for the 3 inch and 1.5 inch blankets were developed. The acoustic blankets included the validated batting data and sheet characteristics. The model predicted incident field value of 3.5 to 6 volts per meter with blankets installed. The standing wave was expected to be less than 12 volts per meter. The unpredictability of the blankets' losses cause the RF window losses to establish an incident wave of 30 volts per meter and a corresponding standing wave of 60 volts per meter. Consequently we expected to see fields as low as 3.5 to 12 volts per meter with a possible high of 60 volts per meter. Testing indicated values of 3 to 8 volts per meter at various locations within the fairing. The maximum test data was bounded by the model predictions showing that the data measured on KoreaSat agrees well with the model. The test data supports the validation of the technique.

5.3.2 XTE Mission RF Levels

Measurements were made for the XTE mission during ground testing. The model for the XTE vehicle included:

- Frequency of 2.2875 GHz
- Transmitter power of 1.0 watt
- Bare aluminum area of 128.5 square meters
- 3 inch acoustic blanket covered area of 35 square meters
- 1.5 inch acoustic blanket covered area of 18 square meters
- 1.5 inch blanket covered RF window of 0.5 square meter

The model for the XTE 10 foot fairing and vehicle (including 3 inch acoustic blankets, and 1.5 inch acoustic blankets) was developed. The acoustic blankets included the validated batting data and sheet characteristics. The model predicted an incident field value ranging from 2.2 to 5 volts per meter for the blanket installation. The standing wave was expected to be less than 10 volts per meter but the unpredictability of the blankets defaults to the RF window established upper boundary of 30 volts per meter. The bulk of the measurements on XTE were below 5 volts per meter, and a few measurements were about 9 volts per meter. One point measured 20.4 volts per meter. This high point was at some distance from the antenna and demonstrates the magnitude of the standing wave and the unpredictability of the blanket losses.

5.3.3 Composite Fairing Testing

Two configurations for the composite fairing were tested. One configuration was a fairing with no acoustic blankets installed which was also used as the structural test article. This configuration is referred to here as the "bare" composite fairing test. The second configuration had 3-inch acoustic blankets installed and was used for the acoustic testing. The second configuration is referred to in this memorandum as the composite fairing with acoustic blankets test. The acoustic blankets were a different design from those discussed in the previous section and were not expected to be lossy.

5.3.3.1 Bare Composite Fairing Test

A one watt source was radiated (using a horn directional antenna) at 2 to 13 GHz and RF field measurements made. The tests were performed with the radiating antenna located in the center of the fairing at approximately 2/3 the fairing height. The radiating antenna was pointed up toward the nose of the fairing. The test probe was at three locations. During test 1, it's location was about 30 inches from the side wall, at 1/2 the fairing height. During test 2, the test probe was located about 3 feet from the side wall at about 2/3 the fairing height. For tests 3, the test probe was located approximately 2 feet from the side wall at about 2/3 the height of the fairing. Table 2 presents a summary of the RF field strengths measured.

Table 2.
RF Fields Measured in the Bare Composite Fairing.

Position	Test 1 volt/meter	Test 2 volts/meter	Test 3 volts/meter
Maximum	39.0	39.0	63
Minimum	6.6	2.2	7.9
Average	20.0	14.0	25.0

The analytical model for the bare composite fairing configuration, predicted an incident wave of 39 volts per meter and a corresponding standing wave of 78 volts per meter. This test provides reasonable correlation with the analytical model predictions.

5.3.3.2 Composite Fairing with Acoustic Blankets Test

A one watt source was radiated (using a horn directional antenna) at 2 to 13 Ghz and RF field measurements made. Tests were performed with the radiating antenna at three orientation positions and the test probe at two locations. During test 1 and 2, the transmit antenna was pointed toward the top of the fairing and was located at about 40 inches from the side wall at approximatel mid-height of the fairing. For test 3 the radiating antenna was also pointed up, but was located at about 1/4th the fairing height. The test 3 location for the radiating antenna was about 40 inches from the side wall, at 1/4 the fairing height , but pointed toward the closest fairing wall. During test 1, the test probe was located about 1 foot from the side wall at about 1/3 the fairing height. For tests 2,3, and 4, the test probe was located approximately three feet from the side wall at about 2/3 the height of the fairing. Table 3 presents a summary of the RF field strengths measured.

Table 3.
RF fields Measured in the Composite Fairing With 62.4% Blanket Coverage.

Position	Test 1 volts/meter	Test 2 volts/meter	Test 3 volts/meter	Test 4 volts/meter
Maximum	43.8	52.8	53.2	53.6
Minimum	7.8	13.4	7.8	12.4
Average	22.8	28.8	25.3	29.8

These measurements confirmed predictions that the blankets were not lossy and would probably result in an increase of field over the bare fairing. The data indicates an increase in field strength when compared to the data in Table 2. The analytical model for this configuration, predicted an incident wave of 29 volts per meter and a corresponding standing wave of 58 volts per meter. This test provides reasonable correlation with the analytical model predictions.

5.3.4 Vehicle Validation Conclusions

The analytical model provides reasonable agreement with the tests performed and consistently predicts a conservative upper bound of the field.

5.4 VALIDATION USING A 6-FOOT DIAMETER COMPOSITE FAIRING TEST ARTICLE.

The previously discussed testing tended to support the use of our technique. Each of these previous tests, however, had factors which introduced some level of uncertainty in the results. The sources of uncertainties included unstable walls (aluminum room), actual installed blanket thickness, surfaces areas of unknown materials and RF properties (spacecraft surfaces), limited access limited radiation frequency, and the radiated RF power. A development six foot diameter composite fairing was selected as a test article to allow more exacting and thorough testing with no interference with vehicle development, production, or processing schedule.

We performed the calculations to estimate the field strength that a 1 watt transmitter would create by radiating within the envelope of the six foot diameter fairing. These calculations were carried out for two different boundary conditions. First, for a fairing with bare walls. Second, for a fairing with blanketed walls. We then performed a series of tests to compare our calculated estimates with actual measured values for the two boundary conditions. The results of these tests showed that our technique can provide useful estimates of the resulting fields within the fairing volume. **The reader is once again cautioned that our technique yields an assumed uniform field strength, not an exact solution of the field distribution.**

We intend to use our technique to estimate the field strength created when operating a transmitter within a fairing envelope. This information will then be used to evaluate the electromagnetic interference margins for equipment located within the volume.

5.4.1 The Analysis

We begin the analysis by determining the interior surface area of the test fairing. The surface area of the interior wall was determined to be approximately 27 m^2, with an approximate 3 m^2 aluminum aft closure. Figure 12 illustrates the fairing configuration and the construction of the blanket.

Figure 12. Test Fairing and Blanket Configuration.

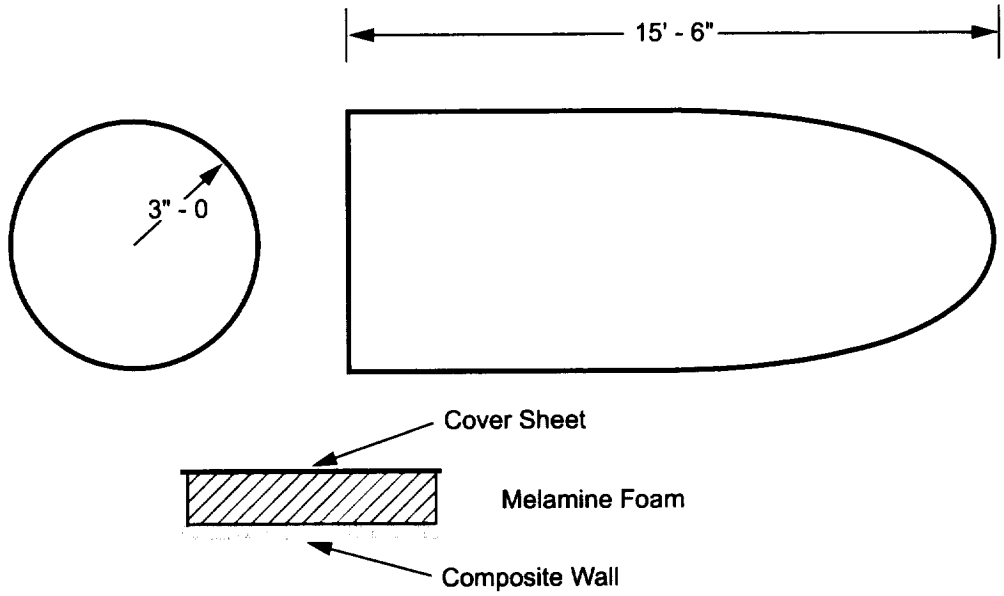

Next, we determined the electrical properties of the materials. The properties of some of these materials were readily available in handbooks, other materials required laboratory measurement.

We employed a computer spreadsheet to organize our data and to perform the many calculations required to complete the analysis. We found the spreadsheet's "built in" capability to perform mathematical operations using complex numbers to be quite helpful. However this capability is not mandatory; the spreadsheet can be set up in a classical manner to perform the required operations. We strongly recommend that the user spend some time reviewing the mathematics of complex numbers before attempting to set up an analysis such as this. A Pascal program to perform the problem setup and analysis is being developed.

The various material properties and required physical constants are summarized in Table 4. It should be noted that the e' and e" (the real and imaginary components of permittivity) have a strong frequency dependence in some materials. The cover sheet is an example of this, as it is designed to be a lossy dielectric. Therefore, the data in the Table 4 is valid only at the noted frequency of 2.2 GHz. For our analysis, the cover sheet permitivity was measured over a wide frequency range. We then developed a curve fit function within the spreadsheet to evaluate e' and e" as a function of frequency. In the case of foam, the permittivity was measured and found to be essentially constant across a wide frequency band. For the Composite and Aluminum materials, the e" was computed using Appendix E equation E6, based on conductivity values. The conductivity value used for aluminum is a handbook value, while that of the composite material is a value estimated by the authors.

Table 4.
RF Properties of Materials in Construction of the Fairing and Blankets (Valid at 2.2 Ghz)

Material	Air	Cover Sheet	Melamine	Composite	Aluminum
Mu (permeability)	1.26E-06	1.26E-06	1.26E-06	1.26E-06	1.26E-06
epsilon zero	8.85E-12	8.85E-12	8.85E-12	8.85E-12	8.85E-12
conductivity (mho/m)	0.00E+00	6.68E+01	1.22E-04	3.00E+05	3.72E+07
e'	1.00E+00	7.33E+01	1.02E+00	1.00E+00	1.00E+00
e"	0.00E+00	5.46E+02	1.00E-03	2.45E+06	3.04E+08
0.5 arc tan(e"/e')=	0.00E+00	7.19E-01	4.92E-04	7.85E-01	7.85E-01

The next step in the analysis is to compute the propagation constant, attenuation constant and phase constant using Appendix E equations E13, E14, E17 & E18. The intrinsic impedance of each of the materials is also computed using Appendix E equations E9, E10 & E11. As discussed earlier, these computations were set up and performed in a spreadsheet. The results are summarized in Table 5.

Table 5.
RF Characteristics of Materials Used in Fairing and Blanket. (Valid at 2.2 GHz)

Material	Air	Cover Sheet	Melamine	Composite	Aluminum
gamma	4.62E+01	1.08E+03	4.65E+01	7.23E+04	8.05E+05
alpha	0.00E+00	7.13E+02	2.29E-02	5.11E+04	5.69E+05
beta	4.62E+01	8.15E+02	4.65E+01	5.11E+04	5.69E+05
|n|	3.77E+02	1.61E+01	3.74E+02	2.41E-01	2.16E-02
n_real	3.77E+02	1.21E+01	3.74E+02	1.70E-01	1.53E-02
n_imag	0.00E+00	1.06E+01	1.84E-01	1.70E-01	1.53E-02

The next step was to determine the RF fields that would be developed in the fairing if a 1 watt transmitter was to radiate within the fairing envelope. Our first set of boundary conditions assumed an unblanketed fairing (bare composite walls). We can directly apply Appendix B equation B55 (using the impedance of the composite walls) to determine the anticipated field. The results are shown in Figure 13 below.

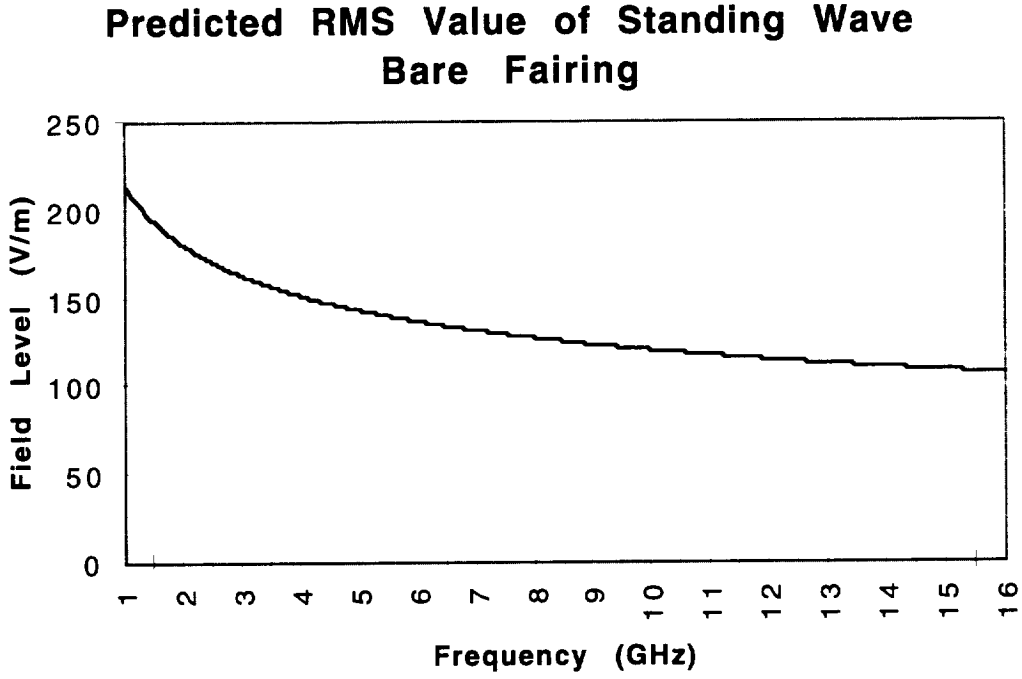

Figure 13. Predicted RMS Value of Standing Wave in Bare Fairing.

Two intermediate steps in the analysis were performed to enhance understanding the effects of the blanket materials on the RF fields and the performance of the blanket as a system. It will be shown that the system performance is much more than the sum of their parts. Neither the foam alone or the coversheet alone is adequate to reduce the field.

One intermediate step evaluated the RF fields with the cover sheet material lining the fairing wall. In other words, no foam was present and the cover sheet (0.0015 inches thick) was in contact with the wall. The equivalent load impedance of the sheet covered wall was computed (using the cover sheet and composite material RF properties in Appendix D equation D17) before proceeding to Appendix B equation B55. This configuration resulted in RF fields essentially the same as the bare fairing. Figure 13 also represents the fields that result from the fairing with only the cover sheet installed.

The second intermediate step in our analysis, was to determine the RF field that would result inside the test fairing when lined with only the 3 inch thick Melamine foam (no cover sheet installed). The foam is installed against the composite walls of the fairing. The equivalent load impedance of the foam covered wall must be computed before proceeding to Appendix B equation B55. The equivalent load impedance of the blanketed wall was computed using the foam and composite material RF properties in Appendix D equation D17. The resulting fields are shown in Figure 14.

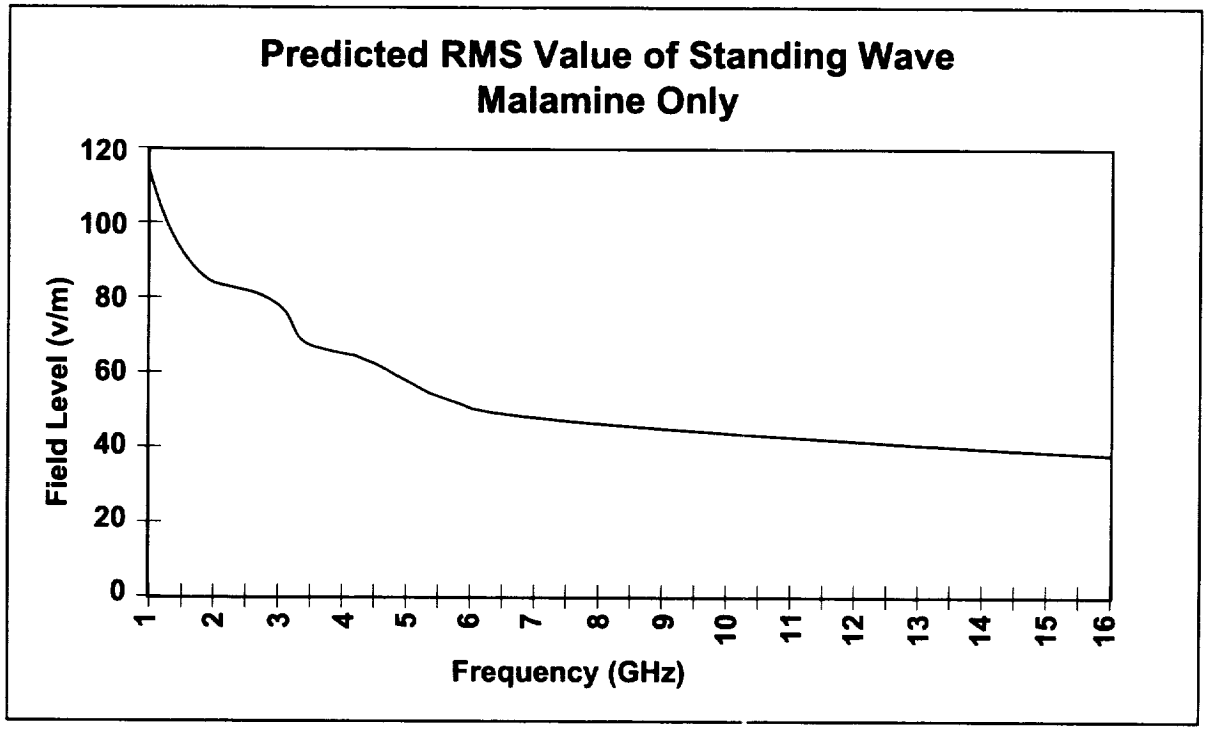

Figure 14. Predicted RMS Value of the Standing Wave, Fairing with Foam Only.

It is observed by comparing Figures 13 and 14, that the shape and trend of the foam only curve is much the same as the bare fairing. However, the RF fields are reduced by about 6 dB from the bare fairing. This reduction of the RF fields is not readily expected since the properties of the foam are very close to those of air. This is one example of how a relatively small loss factor can have a large effect on overall system performance. It is also apparent, however, that the fields are still unacceptably high. Additional reduction of the field is needed.

The final step in our analysis, was to determine the field that would be created by a 1 watt transmitter radiating inside a blanketed (foam and coversheet) fairing. The results for the coversheet only and the foam only analyses seems to imply that the total blanket will not be effective. We will see that this impression is incorrect. In this blanketed fairing case, the equivalent load impedance of the blanketed wall must be computed before proceeding to Appendix B equation B55. The equivalent load impedance of the blanketed wall was computed by successive applications of Appendix D equation D17, working from the wall toward the fairing center line through the layer of Melamine, then through the cover sheet. The blanket consisted of a 3" layer of Melamine foam with a .0015" thick cover sheet. The blanket is installed with the Melamine against the composite walls of the fairing and the cover sheet facing the interior volume of the fairing. The results of the field strength calculations are shown in Figure 15.

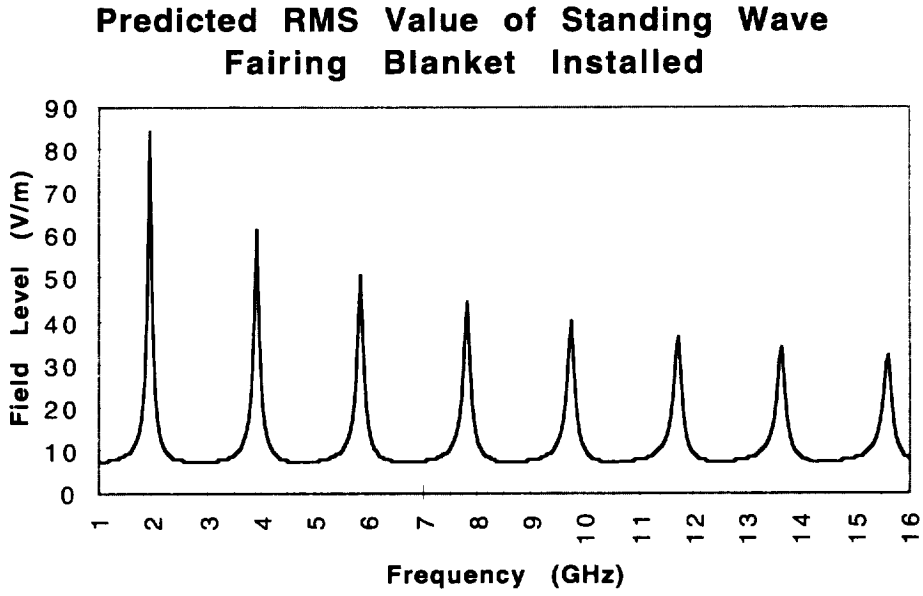

Figure 15. Predicted RMS Value of Standing Wave with the Fairing Blanket Installed.

The results show uniformly separated RF field peaks with values corresponding to the "foam only" installation of Figure 14. The RF field at frequencies between the peaks are drastically reduced to relatively low levels. This dramatic reduction is used to provide equipment protection for relatively wide frequency bands centered about the expected radiating frequency.

Further examination of the field strength behavior in a blanketed fairing reveals that the frequencies at which the high level "spikes" occur are a function the spacing between the cover sheet and the wall (in other words, a function of the foam thickness). Such behavior is implicit in Appendix D equation D17, but it is not obvious until the data is plotted with respect to frequency. In simplistic terms; at certain frequencies (determined primarily by the foam thickness), the cover sheet becomes "transparent". The RF energy must then be absorbed by the Melamine/wall system instead of the more lossy cover sheet thus higher RF fields are necessary to dissipate the RF power. One can examine this "spiking" behavior in more detail (using Appendix D equations D21 and D22) to further evaluate the field levels and power dissipated within the blanket/wall system.

At this point, one could reasonably ask where the energy is being dissipated. The energy loss distribution for the blanketed fairing configuration is shown in Figure 16 for frequencies about the "spike" at about 2 GHz.

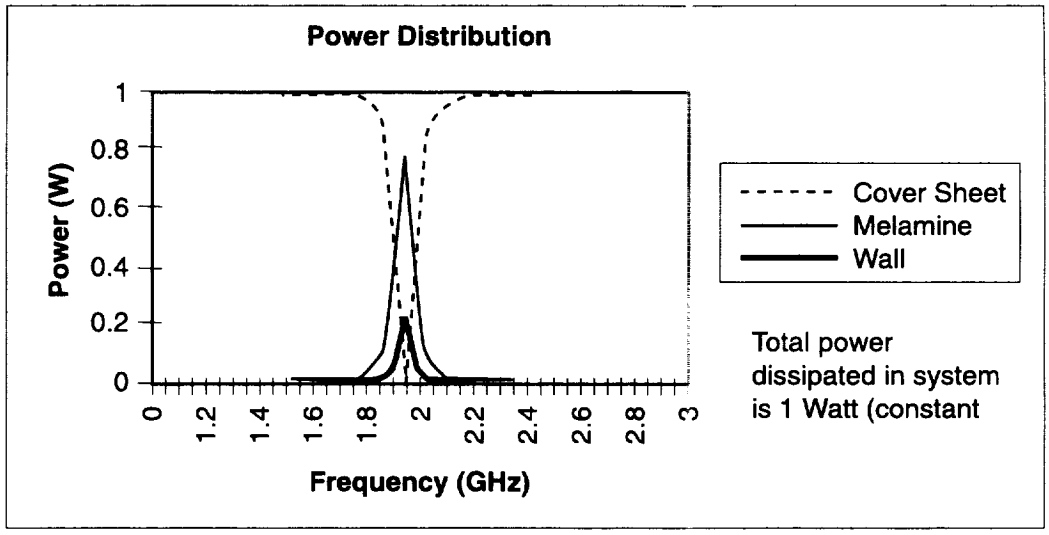

Figure 16. Distribution of Power within the Blanket-wall System.

The Figure 16 shows that the energy at the low RF field frequencies is primarily dissipated within the coversheet of the blanket with very little being absorbed by the foam or the Fairing wall. The opposite is true for the frequencies corresponding to the peak field values. Essentially no energy is lost in the coversheet while the bulk is going to the foam with a significant dissipation within the fairing wall.

There are some additional interesting facts to be observed when we review the results of the analyses we have just completed. First, our analysis predicts that a 1 watt transmitter is capable of developing quite high RF fields within a bare fairing envelope. Second, it is possible to design a blanket system that can provide significant field strength reductions over specific frequency bands.

As one further examines the theoretical behavior of the system, it is possible to postulate several approaches that might improve the RF absorption capabilities of the blanket system. Some of these will be discussed later.

5.4.2 Test Results and Comparison to Analytical Predictions.

Once our analysis was complete, we were ready to attempt to validate our technique by measuring the actual fields created by a 1 watt RF source installed within our test fairing. We hoped that our analytical results would "envelope" the actual test data, thereby validating a tool that could then be used to estimate field levels in an enclosed environment.

Our first tests were conducted inside a bare composite fairing. Typical results are shown in Figure 17.

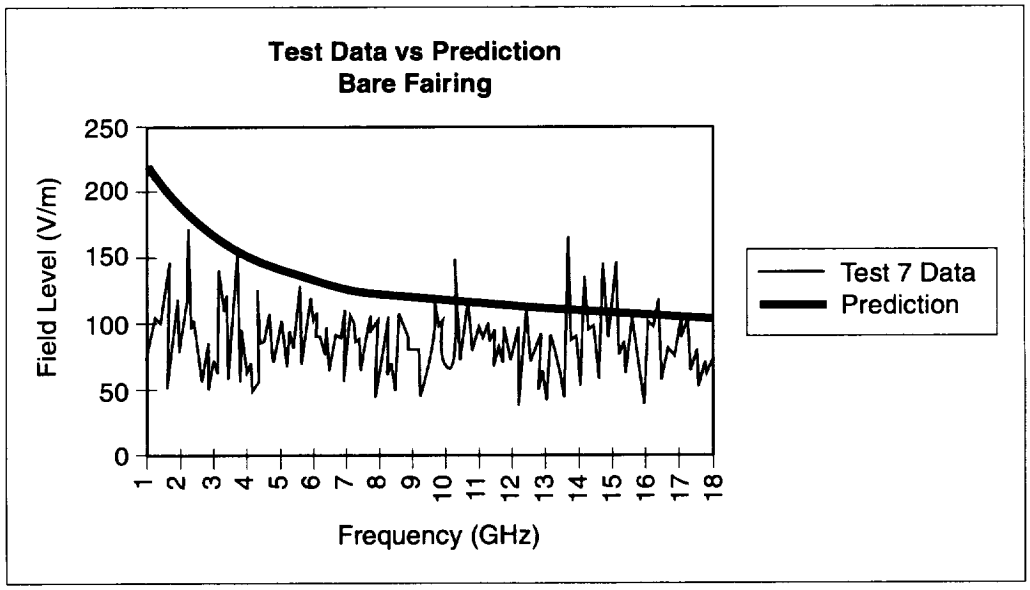

Figure 17. Test Data Versus Analytical Prediction for the Bare Fairing.

Similarly, a second series of tests were performed in a blanketed fairing. Representative results are shown in Figure 18.

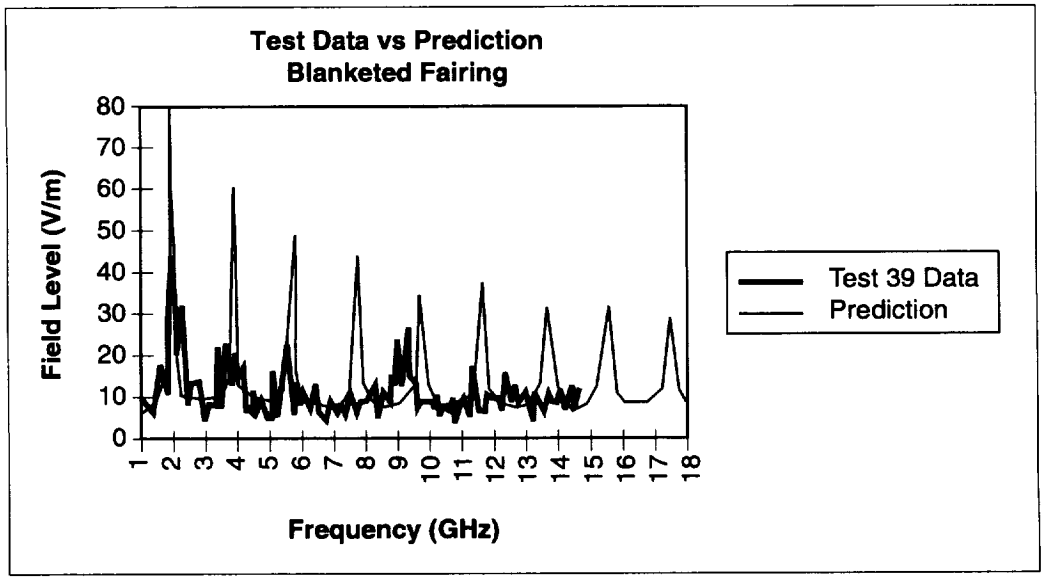

Figure 18. Test Data Versus Analytical Prediction for Blanketed Fairing.

5.4.3 Composite Fairing Test Article Conclusions.

As stated previously, the data is representative of a large number of tests performed with varying antenna locations (both transmit and field level sensor). While the data sets were expectedly "noisy", the test results confirmed the general characteristics predicted by our analytical approach. That is, the fields developed inside a bare fairing were quite high (peaks approaching 200 V/m from a 1 watt source). In addition, we confirmed the general behavior of the blanket system and its ability to provide significant reduction to the RF fields in specific frequency bands. The test data also showed the expected field "peaking" resulting from the spacing between the cover sheet and the wall. It was also shown that (as predicted) the field levels developed inside a bare composite fairing were quite similar to those developed inside a metallic fairing. Essentially the composite fairing exhibits RF behavior much the same as a metallic fairing. It is highly reflective to RF energy and provides significant attenuation from one side of its skin to the other.

Our analytic approach assumes an isotropic source and good scattering, thus assuring the development of a uniform field within the enclosed volume. This is seldom the case in the real world, especially when the volume begins to be filled with a payload. A few exploratory tests were performed with a simulated payload in the fairing volume, and as might be expected, some portions of the volume were "shadowed" or "choked off." But in general, the overall field levels remained enveloped by our predictions. It is obvious that significant shadowing and blockage would require re-assessment of the absorbing area. It is probable that an engineering judgment would be required, to arrive at a reduced effective area of the absorbing blanket.

Mil-Std-1541A requires an inter system EMI safety margin of at least 6 dB for tested systems (12 dB for systems qualified solely by analysis). The authors certainly concur that the inter system safety margin for tested systems should be at least 6 dB if our technique is used to estimate the field level. We have observed test to test variation in measured field levels approaching 3 dB, and recommend caution in approaching demonstrated safety margins. Although our analysis provides a conservative envelope for the predicted field levels, approaching a 6 dB safety margin should be done with great care.

As was mentioned earlier, our analysis indicated several approaches that might improve the effectiveness of the blanket system. One obvious approach is to adjust the blanket thickness such that the maximum loss is coincident with the frequency of operation.

A second approach would be to use blankets of two or more thickness. Here the objective is to have one blanket provide at least some loss when the other is at its minimum. We tested a configuration that employed two different thickness blankets in the hope of creating a more uniform field level, with lower "spikes". While the results from this test showed a general tendency to behave as predicted, the overall improvement was less than expected. We believe the poor performance was due to less than optimum scattering of the incident field. The transmitting antenna used for this test was highly directive. Hence the bulk of the incident power was directed at one blanket or the other causing that blanket to dominate the system response. These results point out that if a highly directive antenna is used to radiate within the fairing, care must be taken to evaluate the effective surface area of the absorbing material.

A third approach towards improving the blanket effectiveness is suggested when the power absorption behavior of the blanket is examined. If we were to replace the Melamine with a different (more lossy)

dielectric material, the blanket system would exhibit higher losses in the frequency range where the cover sheet becomes "transparent." We do not know if such a material exists, or if one could be found that is compatible with its intended use (weight, cleanliness, etc.). This approach is simply suggested by the mathematics of the problem.

6.0 RECOMMENDATION FOR COMPOSITE FAIRING

The technique described in Appendix D provides insight into the acoustic blankets' RF performance. This leads to some recommendations to ensure the composite fairing and acoustic blanket designs provide an RF environment no worse than the Delta vehicle aluminum fairing and blankets.

6.1 REPLACE ALUMINIZED KAPTON

The layer of aluminum deposited on the kapton cover sheet is too thick, dramatically increasing the reflection and decreasing the loss. The aluminized kapton sheet should be replaced with a carbon loaded kapton (or equivalent) which has a reduced conductivity and reflection. This change alone can substantially reduce the RF fields.

6.2 STABILIZE THE THICKNESS OF THE BLANKET

The thickness of the blanket should not change easily since the changes perturbate the losses within the blanket. The metal fairing blankets are subject to easy changes in thickness due to installation method, venting, vibration, air flow, etc. The thickness changes cause the losses in the blanket to fluctuate greatly and to be unpredictable. The melamine foam is flexible but it is also much more stable than the batting material so its loss should be more predictable.

6.3 SELECT PROPER COMBINATION OF BLANKET THICKNESS

One of the most obvious recommendations is to provide some blankets of thickness less than a half wavelength. Three-inch blankets in the cylindrical section combined with 3.25 or 3.5-inch blankets in the nose section can reduce the RF field 'peaking' effects at certain frequencies. Blanket thickness should avoid even number multiples or divisions of the RF wavelength. This will ensure a lossy blanket area that will limit the RF field to a relatively low value at a wide band of frequencies.

6.4 MAKE THE MELAMINE FOAM CONDUCTIVE

Implementation of the proper conductivity for the foam will dramatically reduce the RF fields at virtually all frequencies. The conductivity can be increased by mixing graphite, carbon, or other conductive powder with the melamine.

The design of a blanket that would give large loss when installed on aluminum should also provide large loss for the composite fairing since the composite is more lossy than aluminum. The analysis technique described in Appendix D can be used to perform trade studies to ensure a good blanket design. The following activities will ensure that design:

1. Determine the thickness, dielectric constant and loss tangent for the candidate cover sheets for the acoustic blankets. Application of Appendices D and E equations should allow for the design and selection of an appropriately lossy cover material.

2. Determine the dielectric constant and loss tangent for the proposed foam material for the blankets. Use the Appendices D and E technique to establish the proper material and thickness.

3. Use the technique of Appendices B and D to compare the fairing RF fields for each candidate blanket design.

The technique of Appendix E can be used to determine the RF characteristics of the composite fairing wall. Use the equipment which measured the blanket cover sheet properties to determine the complex dielectric constant and loss tangent for the various layers of the composite fairing wall, then use Appendix E to compute the effective RF impedance for bare composite wall surface.

7.0 CONCLUSIONS

The analytical technique presented in Appendix B is shown to be relatively simple. The greatest effort is in determining the surface areas and type of materials involved. The equations presented for the complex values of media characteristic wave impedance and the magnitude of the incident wave are exact and simple. The model can account for the presence of items comparable to the acoustic blankets by using the technique of Appendix D to define the effective surface impedance. The simplicity of the concept and its computation suggests it is a viable technique for first order quantification of the RF fields inside any enclosure. The value is an equivalent wave which would dissipate the transmitted power into the surface areas. In the real world, large standing waves exist which are approximately twice the magnitude of the equivalent incident wave.

The technique can provide a methodology for evaluating various blanket designs for the composite fairing and could be used to establish the RF characteristics of the fairing composite surface.

References

1) Computation of RF fields in Delta Fairing; by J. P. Reddell, 21 September 1994.

2) Shielded Enclosure and Aluminum Enclosure RF Strength Test Report; J. P. Huynh, McDonnell Douglas Aerospace, Huntington Beach, 9 June 1995.

3) Transmission Lines and Networks; Walter C. Johnson, McGraw-Hill Book Company, 1950.

4) Fields and Waves in Modern Radio; Simon Ramo and John R. Whinnery, John Wiley & Sons, Inc., July, 1962.

List of Acronyms

GEMACS	General Electromagnetic Model for the Analysis of Complex Systems
MDA	McDonnell Douglas Aerospace
MELV	Medium Expendable Launch Vehicle
NOAA	National Oceanic and Atmospheric Administration
RF	Radio Frequency
RMS	Root Mean Square
SELV	Small Expendable Launch Vehicle
XTE	X-Ray Timing Explorer

APPENDIX A

A Method for the Estimation of the Field Strength of Electromagnetic Waves Inside a Volume Bounded by a Conductive Surface

by
M.P. Hallett

Recent requests from a number of spacecraft projects to operate their transmitters during launch processing and throughout the launch itself, has led us to investigate the nature of the RF field created within the fairing envelope under such situations. This analysis was further prompted by data obtained from another OLS project, indicating that significant amplification of the electromagnetic fields occur when a transmitter radiates inside a conductive enclosure such as a payload fairing.

In an attempt to establish some limits on the field strengths experienced, first consider the case of no fairing at all. For equipment in view of an isotropic transmitting antenna, a reasonable estimate of the field strength will be given by the free space radiation formula:

$$\phi = P_t / 4\pi r^2 \qquad \text{(A1)}$$

Where: ϕ = Power density (watts / m^2),
P_t = Transmitter power (watts), and
r = Distance to the source (m).

and

$$E = \sqrt{377\phi} \qquad \text{(A2)}$$

Where: E = Electric field strength (volts/m), and
377 = impedance of free space.

If necessary, these equations can be modified to account for antenna gain and directivity, transmission losses, etc. See any good text on antenna theory, such as "Antennas" by John Kraus (McGraw-Hill, 1950) for a complete treatment of this subject. These equations provide a reasonable estimate of the lower bound on the field strength at any given point. To get some idea of the magnitudes involved, a quick computation for a point 1 meter away from a 1 watt isotropic source (in free space) gives us a power density of .079 watts / m^2 and an electric field strength of 5.5 volts/m.

If the entire system is enclosed within a conductive surface (payload fairing), one intuitively expects the field strengths to increase. Instead of radiating out into free space the transmitter power is trapped within the enclosed volume. The power is reflected back and forth from the conductive surfaces enclosing the volume, with higher conductivity equating to greater reflection. The energy contained within the fields will continue to build up until the power lost into the enclosing surface comes into balance with the power supplied by the source. This is a rather simplistic restatement of the Poynting Theorem. In this model, the only mechanism for energy loss is through ohmic heating in the enclosing walls or other objects contained within the enclosing surface. In Ramo and Whinnery's "Fields and Waves in Modern Radio" (Wiley, 1959) 241, it is shown that the average power loss in a plane conductor can be directly computed, knowing the strength of the incident field and the surface resistance of the conductor using the following equation:

$$W_L = (1/2)R_s|J|^2 = (1/2)R_s|H_{inc}|^2 \qquad \text{(A3)}$$

Where: W_L = Average power lost in conductor per unit area,
J = Surface current (amps / meter),
R_s = Surface resistance (ohms), and
H_{inc} = Incident magnetic field intensity (amps / meter).

The surface resistance is frequency dependent (skin effect) and may be computed given the frequency of interest and the conductivity of the material. For aluminum, R_S = 3.26E-7 $\sqrt{f}$.

It should also be noted that for a perfect conductor, the conductivity becomes infinite and the surface resistance goes to zero. For aluminum at S band, frequency f = 2.2E9, we compute R_S = .015 ohms. To be precise, this is just the real part of the surface resistance. There is an imaginary component that can be computed as well. A full treatment of skin effect and surface resistance can be found in Ramo and Whinnery (Op. cit.) or Magnusson's "Transmission Lines and Wave Propagation" (Allyn and Bacon, 1965).

Inspecting the power loss equation, we see that to sustain a given power loss, the incident field must increase as the surface resistance gets smaller. In the case of our fairing, as the walls become more perfect conductors, increasingly large fields will be required to dissipate the power being supplied by the transmitter. In the case of perfect conductors, the fields grow infinitely large. This confirms our intuitive feel for the problem. Enclosing the system with a conductive surface causes the fields to increase. In a way, this is somewhat analogous to the interior of a microwave oven. However, an upper bound of infinity for the field in our enclosed volume is not very helpful. A model that establishes a more reasonable upper bound needs to be developed. To do this, we shall account for the fact that the enclosing surface is a non-ideal conductor and ohmic losses will occur. We then strike a balance where the field strength rises to the value required to dissipate the power being supplied. Power out equals power in.

Returning to the equation for the power loss per unit area in a conductive surface, rearrange the terms to solve for H_{inc}

$$|H_{inc}|^2 = 2W_L/R_s \text{ and}$$

$$|H_{inc}| = \sqrt{2W_L/R_s}. \tag{A4}$$

For a plane wave normally incident on a perfect conductor, boundary condition analysis shows that the E field is zero and all the energy is contained in the magnetic field. To meet this condition, the value for H_{inc} must be twice the peak value of the H field in free space. See Ramo and Whinnery (Op. cit.) 285, for discussion of this topic.

What follows is based on the assumption that the energy in the enclosed volume will be made up of randomly directed plane waves, uniformly distributed within the volume. In essence, a uniform energy density impinges on the walls. An equivalent wave can then be computed that will produce the same energy loss in the surface. This new wave can be viewed as the sum of the normal incident components of all the random waves.

Recalling that:

$$|H_{inc}| = 2H_0 \text{ and}$$

$$|H_0| = \sqrt{W_L/2R_s}. \tag{A5}$$

For plane waves in a perfect dielectric, it has been shown that E and H are related by Z_0:

$$H = E/Z_0 ;$$

where

$$Z_0 = \sqrt{\mu/\varepsilon}, \tag{A6}$$

which is 377 ohms for free space. Substituting (A6) into (A5) results in:

$$|E_0| = Z_0\sqrt{W_L/2R_s} . \tag{A7}$$

For plane waves, the energy stored per unit volume is the sum of the energy in the magnetic field and the energy in the electric field. This has been shown to be:

$$U_t = U_m + U_e . \tag{A8}$$

In free space:

$$U_m = U_e . \tag{A9}$$

Where

$$U_e = \varepsilon E^2/2 \quad \text{(Electric Field) and} \tag{A10}$$

$$U_m = \mu H^2/2 \quad \text{(Magnetic Field).} \tag{A11}$$

In other words, the uniform energy density within the volume contains the same electric field energy density as a wave of magnitude E_0 everywhere within the volume. This concept has been used in the analysis of RF test chambers. The object of these chambers is to create a space containing large, uniform electromagnetic fields. For further discussion, see IEEE Transactions on Electromagnetic Compatibility, February 1990.

Now examine a numerical example for a simple case of a 1 watt isotropic source enclosed by a cylindrical surface 3 meters in diameter and 13 meters high. This is a crude representation of the volume between the top of the fuel tank and the top of the fairing. The enclosing surface area (A) can be found to be 136.66 m^2. The power delivered by the 1 watt source must be absorbed by the enclosing surface. Assuming a uniform power distribution, the average power density at the surface must be:

$$W_L = < P_t >/A = 1 / 136.66 = 0.00732 \text{ watts / } m^2. \tag{A12}$$

Computing the equivalent wave that will produce this power loss at the surface:

Where $Z_0 = 377$ ohms, $R_S = 0.015$ ohms, and $W_L = 0.00732$ w/m^2 with

$$|E_0| = Z_0\sqrt{W_L/2R_s} ; \tag{A13}$$

gives

$$E_0 = 377\sqrt{0.00732/((2)(0.015))} = 377\ (.494) = 186.2 \text{ v/m}. \tag{A14}$$

This result shows us that even moderate sources will create large fields when fully enclosed by a conductive surface. It also shows that the model needs to be refined a bit more.

Insert a solid cylinder 2 meters in diameter and 10 meters high within the previously defined volume. This becomes a crude representation of second stage/spacecraft stack. This solid is defined as being electrically connected to the original enclosing surface. This added solid provides additional surface area (for the power to be dissipated into). A quick calculation reveals that the added solid has a surface area of 69.11 m^2 associated with it. Thus the total surface area into which the power is being dissipated becomes 205.77 m^2 and $W_L = 1 / 205.77 = 0.00486$ w/m^2.

Thus for: $Z_0 = 377$ ohms, $R_S = 0.015$ ohms, and $W_L = 0.00486$ w/m^2 with

$$|E_0| = Z_0\sqrt{W_L/2R_s};$$

gives

$$E_0 = 377\sqrt{.00486/((2)(.015))} = 377\ (0.402) = 151.7\ \text{v/m}. \tag{A15}$$

This result certainly warns us against radiating inside a fully sealed conductive fairing. It also gives us some indication of the dominant factors in this process which are: the total surface area absorbing the incident power; the surface resistance of that area; and the magnitude of the source.

There is one final refinement that we can add to this model. It is a RF window, or aperture, in the enclosing surface. Here, the power supplied by the source is equal to the sum of the power lost out the aperture, and the power absorbed by the walls.

$$< P_t >= \left(A_{surf}\right)\left(W_{surf}\right) + \left(A_{aper}\right)\left(W_{aper}\right) \tag{A16}$$

It has been shown that the surface energy density for a plane wave in free space is given by the Poynting vector S = E x H, and that the average value of the Poynting vector is:

$$< S >= (1/2)\left(E^2/Z\right) \tag{A17}$$

Thus <S> describes the energy density of the waves leaving the enclosure via the aperture.

$$W_{aper} =< S >= (1/2)\left(E^2/Z\right). \tag{A18}$$

Recalling from earlier, the surface loss is given by

$$W_{surf} = (1/2)(R_s)|2H_0|^2 = (2)(R_s)\left(|E_0|^2/Z^2\right). \tag{A19}$$

Thus:

$$< P_t >= \left(A_{surf}\right)(2)(R_s)\left(|E_0|^2/Z^2\right) + \left(A_{aper}\right)(1/2)\left(E_0^2/Z\right). \tag{A20}$$

Rearranging:

$$|E_0|^2 = < P_t > \Big/ \Big(\big(2A_{surf}(R_s)/Z^2\big) + \big((1/2)\big(A_{aper}\big)/Z\big) \Big). \tag{A21}$$

Thus:

$$|E_0| = \sqrt{< P_t > \Big/ \Big(\big(2A_{surf}(R_s)/Z^2\big) + \big((1/2)\big(A_{aper}\big)/Z\big) \Big)}. \tag{A22}$$

Returning to our crude model, we insert a 0.5 m^2 aperture in the enclosing surface which is an approximate value for a typical RF window area.

Thus: $A_{aper} = 0.5\ m^2$, $A_{surf} = 205.27\ m^2$,

$Z = 377$ ohms, $R_S = .015$ ohms, and $P_t = 1$ w.

Solving:

$$E_0 = \sqrt{1/\Big(\big(2(205.27(.015))/377^2\big) + (.5/(2)(377)) \Big)},$$

$$E_0 = \sqrt{1/(4.33E-5+6.63E-4)} = \sqrt{1/7.06E-4}, \text{ and}$$

$$E_0 = 37.6v/m. \tag{A23}$$

This result reveals the significant effect of an aperture in the enclosing surface. It also provides a clue for the absence of reports of effects from RF radiation in the fairing in the past. It would seem that the field strength under such conditions is probably greater than the qualification limits to which the equipment has been tested. However, they are probably not sufficiently large to overcome simple shielding techniques, shadowing, and inefficient coupling mechanisms.

Recalling that this analysis began with the purpose of establishing a bound for the field strength within the fairing, we have determined the following:

- The field strength at any given point within the fairing envelope is greater than the value determined by the free space radiation formula.
- The field strength is less than the value determined by a balance between the power supplied by the source, and the power lost in the walls and apertures.

It is our judgment that the energy balance approach provides a reasonable estimate of the field strength while also yielding a conservative upper bound.

APPENDIX B

Derivation of Equation for Electric Field Inside an Enclosure

by
Jerry Reddell

B.1 INTRODUCTION

This Appendix defines the equations used to calculate the RF field strength resulting from RF transmission within an enclosure. The surface of the enclosure (fairing) is, in general, an area of several materials. Developing the equation for the RF field inside the enclosure, requires an understanding of the boundary of two media. One media represents the air (media of the enclosed volume). The other media correlates to the surface of the enclosure. Once an understanding of the RF wave relationships for the boundary is reached, the solutions for the field inside the enclosure can be defined for the more general situation where several different materials make up the surface of the enclosure. Equations for the electric field intensity, the magnetic field intensity, and the power are derived. The equations are in terms of the incident wave's electric field intensity and the characteristic impedances of the surface media. The approach is:

a) develop the boundary equations for two media,
b) define the equations for the RF waves in each media,
c) define the equations for RF power in multiple materials, and
d) define the equations for RF field in an enclosed volume.

The equations for a media's intrinsic wave impedance and characteristics are developed in Appendix D. It is important to remember the goal is to determine the relationship between the RF power absorbed by the enclosure surface area and the incident RF field within the enclosed volume.

B.2 EQUATIONS FOR THE BOUNDARY OF TWO MEDIA

The equations defining the RF waves in two media are needed. Media 1 represents the enclosure surface material. Media 0 represents the internal volume material. Figure B-1 illustrates the boundary of the two media at z=0 which is normal to the z-axis. An RF wave traveling along the z-axis in media 0 is incident upon media 1 (which acts as a plate) at z = 0. Z is negative in media 0. Three waves are of concern: the incident wave in media 0, the reflected wave in media 0, and the transmitted wave in media 1. This section develops the equations for the electric field (E field) intensity and the magnetic field (H field) intensity at the boundary of the two media. These fields can be written in terms of the incident wave electric field intensity and the wave impedance of the media.

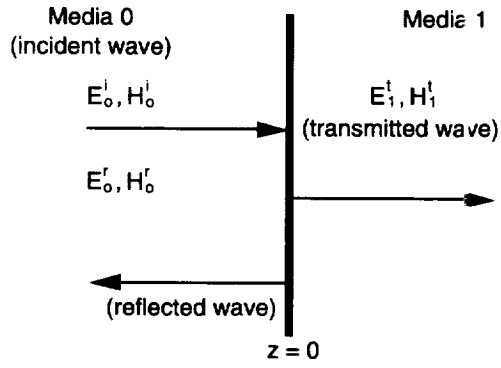

Figure B-1. RF waves at the boundary of two media.

B.2.1 BOUNDARY CONDITIONS OF MEDIA 0 AND MEDIA 1

This section derives the coefficients which relate the reflected and transmitted waves to the incident wave fields. The boundary conditions require that the following relationships exist at the boundary:

a) The tangential component of the electric field intensity is continuous across the boundary. This means:

$$\vec{n}x\left(\vec{E}_1^t - \vec{E}_0\right) = 0,$$
$$\vec{n}x\left(\vec{E}_1^t - \vec{E}_0^i - \vec{E}_0^R\right) = 0, \text{ and}$$
$$\vec{E}_o^i + \vec{E}_o^r = \vec{E}_1^t; \tag{B1}$$

b) The tangential component of the magnetic field intensity is continuous across the boundary. This means:

$$\vec{n}x\left(\vec{H}_1^t - \vec{H}_0\right) = 0,$$
$$\vec{n}x\left(\vec{H}_1^t - \vec{H}_0^i - \vec{H}_0^R\right) = 0, \text{ and}$$
$$\vec{H}_o^i + \vec{H}_o^r = \vec{H}_1^t. \tag{B2}$$

The relationship between the electric field intensity and magnetic field intensity within a media is:

$$\frac{|E|}{|H|} = \eta = \text{intrinsic or wave impedance of the media.} \tag{B3}$$

Using equation (B3) and the boundary conditions the following relationships are determined:

$$\frac{E_o^i}{H_o^i} = \eta_o, \quad \text{Incident wave fields in media 0;} \tag{B4}$$

$$\frac{E_o^r}{H_o^r} = -\eta_o, \text{ Reflected wave fields in media 0; and} \tag{B5}$$

$$\frac{E_1^t}{H_1^t} = \eta_1, \quad \text{Transmitted wave fields in media 1.} \tag{B6}$$

B.2.1.1 Determine the Reflected E Field

Solve equations (B4), (B5), and (B6) for the H fields and substitute into equation (B2) to get:

$$\frac{E_o^i}{\eta_o} - \frac{E_o^r}{\eta_o} = \frac{E_1^t}{\eta_1} = \frac{1}{\eta_o}\left(E_o^i - E_o^r\right). \tag{B7}$$

Solving for the transmitted E field gives:

$$E_1^t = \frac{\eta_1}{\eta_o}\left(E_o^i - E_o^r\right). \tag{B8}$$

Substituting (B8) into equation (B1) gives:

$$\bar{E}_1^t = \bar{E}_o^i + \bar{E}_o^r = \frac{\eta_1}{\eta_o}\left(E_o^i - E_o^r\right) = \frac{\eta_1}{\eta_o}E_o^i - \frac{\eta_1}{\eta_o}E_o^r . \tag{B9}$$

Collecting terms:

$$\begin{aligned} &\bar{E}_o^i - \frac{\eta_1}{\eta_o}E_o^i = -\bar{E}_o^r - \frac{\eta_1}{\eta_o}E_o^r \text{ and} \\ &\bar{E}_o^i\left(\frac{\eta_o - \eta_1}{\eta_o}\right) = -\bar{E}_o^r\left(\frac{\eta_o + \eta_1}{\eta_o}\right) \end{aligned} \tag{B10}$$

Therefore, the reflected E field is related to the incident E field by

$$\frac{\bar{E}_o^r}{\bar{E}_o^i} = \frac{\eta_1 - \eta_o}{\eta_o + \eta_1}. \tag{B11}$$

This is the familiar reflection coefficient term presented in the text books. This defines the relationship of the incident and reflected waves within the media "0," at the boundary; the traveling wave within the media is discussed in section B.3.2.1.

B.2.1.2 Determine the Transmitted E Field

Solve equation (B11) for the reflected electric intensity:

$$\bar{E}_o^r = \left(\frac{\eta_1 - \eta_o}{\eta_o + \eta_1}\right)\bar{E}_o^i. \tag{B12}$$

Substitute into equation (B1):

$$\bar{E}_o^i + \left(\frac{\eta_1 - \eta_o}{\eta_o + \eta_1}\right)\bar{E}_o^i = \bar{E}_1^t \text{ and}$$

$$\bar{E}_1^t = \bar{E}_o^i\left(1 + \frac{\eta_1 - \eta_o}{\eta_o + \eta_1}\right) = \bar{E}_o^i\left(\frac{\eta_o + \eta_1 + \eta_1 - \eta_o}{\eta_o + \eta_1}\right) = \bar{E}_o^i\left(\frac{2\eta_1}{\eta_o + \eta_1}\right) \tag{B13}$$

So that the transmitted coefficient for the electric field intensities is:

$$\frac{\bar{E}_1^t}{\bar{E}_o^i} = \frac{2\eta_1}{\eta_o + \eta_1}. \tag{B14}$$

This is the term normally presented in texts. Remember, this coefficient only defines the relationship at the boundary. For the more general case of a traveling wave within the media see section B.3.3.1.

B.2.1.3 Determine the Reflected H Field

Solving equations (B4), (B5), and (B6) for the E fields and substituting into equation (B1) gives:

$$\eta_o\bar{H}_o^i - \eta_o\bar{H}_o^r = \eta_1\bar{H}_1^t = \eta_o\left(\bar{H}_o^i - \bar{H}_o^r\right). \tag{B15}$$

Solving for the transmitted H field:

$$\bar{H}_1^t = \frac{\eta_o}{\eta_1}\left(\bar{H}_o^i - \bar{H}_o^r\right). \tag{B16}$$

Substituting into equation (B2):

$$\bar{H}_o^i + \bar{H}_o^r = \bar{H}_1^t = \frac{\eta_o}{\eta_1}\left(\bar{H}_o^i - \bar{H}_o^r\right) \text{ and}$$

$$\bar{H}_o^i\left(1 - \frac{\eta_o}{\eta_1}\right) = -\bar{H}_o^r\left(1 + \frac{\eta_o}{\eta_1}\right). \tag{B17}$$

Therefore the reflected H field is related to the incident H field by:

$$\frac{\bar{H}_o^r}{\bar{H}_o^i} = \frac{\eta_o - \eta_1}{\eta_o + \eta_1}. \tag{B18}$$

This is the reflection coefficient normally presented in texts. Remember, this coefficient only defines the relationship at the boundary. For the more general case of a traveling wave within the media see section B.3.2.1.

B.2.1.4 Determine the Transmitted H Field

Solving equation (B18) for the reflected magnetic field intensity and substituting into equation (B2) gives:

$$\begin{aligned} &\bar{H}_o^i + \bar{H}_o^i\left(\frac{\eta_o - \eta_1}{\eta_o + \eta_1}\right) = \bar{H}_1^t \text{ and} \\ &\bar{H}_o^i\left(\frac{\eta_o + \eta_1 + \eta_o - \eta_1}{\eta_o + \eta_1}\right) = \bar{H}_1^t. \end{aligned} \tag{B19}$$

Solving for the transmission coefficient for the magnetic field intensity:

$$\frac{\bar{H}_1^t}{\bar{H}_o^i} = \frac{2\eta_o}{\eta_o + \eta_1}. \tag{B20}$$

This term is the form presented in text books. Remember, this coefficient only defines the relationship at the boundary. For the more general case of a traveling wave within the media see section B.3.3.1.

B.3 DETERMINE THE EQUATIONS FOR THE WAVES IN EACH MEDIA

Derive the equations defining the wave propagation and boundary conditions. Assuming a RF wave is traveling in (media 0) and incident upon a plate (media 1), the conditions and relationships for the incident, reflected, and transmitted waves at the boundary between the media 0 (air) and plate will be developed. The wave is traveling along the z-axis.

B.3.1 DERIVE THE EQUATIONS FOR THE INCIDENT WAVE

B.3.1.1 Components of the Incident Wave

The components of a wave are the electric field intensity and the magnetic field intensity. The incident wave, which is traveling in media 0, is defined by:

$$\begin{aligned} &\bar{E}^i(z,t) = E_o^i e^{-\gamma_{01} z} e^{j\omega t}\bar{a}_x; \\ &\bar{H}^i(z,t) = H_o^i e^{-\gamma_{01} z} e^{j\omega t}\bar{a}_y. \end{aligned} \tag{B21}$$

The wave components can be related using the relationship between the electric and magnetic fields within a media. For the wave in media 0:

$$\left|\bar{H}_o^i\right| = \frac{\left|\bar{E}_o^i\right|}{\eta_0}. \tag{B22}$$

The incident wave is therefore defined by substituting equation (B22) into equations (B21) giving:

$$\bar{E}_o^i(z,t) = \bar{E}_o^i e^{-\gamma_0 z} e^{j\omega t}\bar{a}_x \text{ and} \tag{B23}$$

$$\overset{V}{H}_o^i(z,t) = \left(\frac{\overset{V}{E}_o^i}{\eta_0}\right)e^{-\gamma_0 z}e^{j\omega t}\overset{V}{a}_y = \left(\frac{\overset{V}{E}_o^i}{\eta_0}\right)\left(\frac{\eta_0^*}{\eta_0^*}\right)e^{-\gamma_0 z}e^{j\omega t}\overset{V}{a}_y = \left(\frac{\overset{V}{E}_o^i}{|\eta_0|^2}\right)(\eta_0^*)e^{-\gamma_0 z}e^{j\omega t}\overset{V}{a}_y. \quad \text{(B24)}$$

Where the term (η_0^*) is the conjugate of the media's complex impedance. Since the conjugate of the product of two complex numbers is equal to the product of the conjugates of each of the complex numbers, the conjugate of the magnetic field is determined directly from equation (B24) as:

$$\overset{V}{H}_o^i(z,t)^* = \left(\frac{\overset{V}{E}_o^{i*}}{|\eta_0|^2}\right)(\eta_0)e^{-\gamma_0 z}e^{j\omega t}\overset{V}{a}_y. \quad \text{(B24a)}$$

B.3.1.2 Incident Power

A wave, composed of complex phasors, has its instantaneous power per unit area defined by the cross product of the electric field and the conjugate of the magnetic field. Therefore the instantaneous power per unit area traveling in media 0 is the product of equation (B23) and (B24a):

$$\overset{V}{S}_o^i = \overset{V}{E}_o^i(z,t)x\overset{V}{H}_o^i(z,t)^* = \overset{V}{E}_o^i\left(\frac{\overset{V}{E}_o^{i*}}{|\eta_0|^2}\right)(\eta_0)e^{-2\gamma_0 z}e^{j2\omega t}\overset{V}{a}_z = \left(\frac{|\overset{V}{E}_o^i|^2}{|\eta_0|^2}\right)(\eta_0)e^{-2\gamma_0 z}e^{j2\omega t}\overset{V}{a}_z. \quad \text{(B25)}$$

For sine waves, the average power per unit area is defined as one half the real part of the instantaneous power, which gives from equation (B25):

$$\langle\overset{V}{S}_o^i\rangle = \frac{1}{2}real\left\{\left(\frac{|\overset{V}{E}_o^i|^2}{|\eta_0|^2}\right)(\eta_0)e^{-2\gamma_0 z}e^{j2\omega t}\overset{V}{a}_{zz}\right\}. \quad \text{(B26)}$$

The average power per unit area incident on the plate is therefore the average power traveling in media 0 at the boundary. It is calculated using equation (B26) with z = -0:

$$\langle\overset{V}{S}_o^i\rangle = \frac{1}{2}real\left\{\left(\frac{|\overset{V}{E}_o^i|^2}{|\eta_0|^2}\right)(\eta_0)e^{-2\gamma_0 z}\overset{V}{a}_z\right\} = \frac{1}{2}\left(\frac{|\overset{V}{E}_o^i|^2}{|\eta_0|^2}\right)real(\eta_0). \quad \text{(B27)}$$

The average power incident on the plate at the boundary is given by the product of equation (B27) and the surface area of the plate (media 1):

$$P^i = \langle\overset{V}{S}\rangle A_{surf} = \frac{|\overset{V}{E}_o^i|^2}{|\eta_0|^2}A_{surf}real(\eta_0). \quad \text{(B27a)}$$

B.3.2 REFLECTED WAVE EQUATIONS

B.3.2.1 Components of the Reflected Wave

The reflected wave (also traveling in media 0) is defined by:

$$\begin{aligned}\overset{\vee}{E}^r(z,t) &= E_o^r e^{\gamma_0 z} e^{j\omega t} \overset{\vee}{a}_x \text{ and} \\ \overset{\vee}{H}^r(z,t) &= H_o^r e^{\gamma_0 z} e^{j\omega t} \overset{\vee}{a}_y .\end{aligned} \tag{B28}$$

The reflected wave components traveling in media 0 can be determined using the relationship between the electric and magnetic fields within a media. For the wave in media 0:

$$\left|\overset{\vee}{H}_o^r\right| = \frac{\left|\overset{\vee}{E}_o^r\right|}{\eta_0}. \tag{B29}$$

The components of the reflected wave at the boundary are related to the incident wave components by using equation (B29) in equation (B18) giving:

$$\overset{\vee}{H}_o^r = \left(\frac{\eta_0 - \eta_1}{\eta_0 + \eta_1}\right)\overset{\vee}{H}_o^i = \left(\frac{\eta_0 - \eta_1}{\eta_0 + \eta_1}\right)\frac{\overset{\vee}{E}_o^i}{\eta_0}. \tag{B30}$$

Equation (B4) states:

$$\overset{\vee}{E}_0^r = \left(\frac{\eta_1 - \eta_0}{\eta_0 + \eta_1}\right)\overset{\vee}{E}_o^i. \tag{B31}$$

The reflected wave is therefore defined by substituting equation (B30) and (B31) into equations (B28) giving:

$$\overset{\vee}{H}_o^r(z,t) = \left(\frac{\eta_0 - \eta_1}{\eta_0(\eta_0 + \eta_1)}\right)\overset{\vee}{E}_o^i e^{\gamma_0 z} e^{j\omega t}\overset{\vee}{a}_y. \tag{B32}$$

The conjugate of the magnetic field is:

$$\overset{\vee}{H}_o^i(z,t)^* = \left(\frac{(\eta_0 - \eta_1)^* \eta_0(\eta_0 + \eta_1)}{|\eta_0|^2 |\eta_0 + \eta|^2}\right)\overset{\vee}{E}_o^{i*} e^{\gamma_0 z} e^{j\omega t}\overset{\vee}{a}_y \text{ and} \tag{B32a}$$

$$\overset{\vee}{E}_o^r(z,t) = \left(\frac{\eta_1 - \eta_0}{\eta_0 + \eta_1}\right)\overset{\vee}{E}_o^i e^{\gamma_0 z} e^{j\omega t}\overset{\vee}{a}_x. \tag{B33}$$

B.3.2.2 Reflected Power

A wave, composed of complex phasors, has its instantaneous power per unit area defined as the cross product of the electric field and the conjugate of the magnetic field. Therefore the instantaneous power per unit area reflected is the cross product of equation (B33) and (B32a) giving:

$$\overset{\vee}{S}_o^r = \overset{\vee}{E}_o^i(z,t) x \overset{\vee}{H}_o^i(z,t)^* = -\left|\overset{\vee}{E}_o^i\right|^2 \left(\frac{|\eta_0 - \eta_1|}{|\eta_0 + \eta_1|}\right)^2 \frac{\eta_0}{|\eta_0|^2} e^{2\gamma_0 z} e^{j2\omega t} \overset{\vee}{a}_z. \tag{B34}$$

For sine waves, the average power per unit area traveling in the plate is defined as one half the real part of the instantaneous power, which gives from equation (B34):

$$\left\langle \overset{\vee}{S}_o^r \right\rangle = \frac{1}{2}\left(\frac{|\eta_0 - \eta_1|}{|\eta_0 + \eta_1|}\right)^2 \frac{\left|\overset{\vee}{E}_o^i\right|^2}{|\eta_0|^2} \left\{e^{2\gamma_0 z} \overset{\vee}{a}_z\right\} real\{\eta_0\}. \tag{B35}$$

The average power per unit area reflected from the plate is therefore the average power at the boundary of media 0 and media 1. It is calculated using equation (B35) with z=0:

$$\left\langle \overset{\vee}{S}_o^r \right\rangle = \frac{1}{2}\left(\frac{|\eta_0 - \eta_1|}{|\eta_0 + \eta_1|}\right)^2 \frac{\left|\overset{\vee}{E}_o^i\right|^2}{|\eta_0|^2} real\{\eta_0\}. \tag{B36}$$

The average power reflected from a plate at the boundary is given by the product of equation (B36) and the surface area of the plate:

$$P^r = \left\langle \overset{\vee}{S}_o^r \right\rangle A_{surf} = \frac{1}{2}\left(\frac{|\eta_0 - \eta_1|}{|\eta_0 + \eta_1|}\right)^2 \frac{\left|\overset{\vee}{E}_o^i\right|^2}{|\eta_0|^2} A_{surf}\, real\{\eta_0\}. \tag{B37}$$

B.3.3 DETERMINE THE EQUATIONS FOR THE TRANSMITTED WAVE

B.3.3.1 Components of the Transmitted Wave

The transmitted wave, traveling in the plate (media 1), is defined by:

$$\begin{aligned} \overset{\vee}{E}^t(z,t) &= E_1^t e^{-\gamma_1 z} e^{j\omega t} \overset{\vee}{a}_x \text{ and} \\ \overset{\vee}{H}^t(z,t) &= H_1^t e^{-\gamma_1 z} e^{j\omega t} \overset{\vee}{a}_y . \end{aligned} \tag{B38}$$

The wave components entering the plate can be determined using the relationship between the electric and magnetic fields within a media. For the wave in media 1:

$$\left|\overset{\vee}{H}_1^i\right| = \frac{\left|\overset{\vee}{E}_1^i\right|}{\eta_1}. \tag{B39}$$

The components of the wave entering the plate at the boundary are related to the incident wave components by using equation (B39) in equations (B20) giving:

$$\overset{v}{H}_1^t = \left(\frac{2\eta_0}{\eta_0+\eta_1}\right)\overset{v}{H}_o^i = \left(\frac{2\eta_0}{\eta_0+\eta_1}\right)\frac{\left|\overset{v}{E}_o^i\right|}{\eta_o} = \frac{2\overset{v}{E}_o^i}{\eta_0+\eta_1}. \tag{B40}$$

Equation (B14) states:

$$\overset{v}{E}_1^t = \left(\frac{2\eta_1}{\eta_0+\eta_1}\right)\overset{v}{E}_o^i. \tag{B41}$$

The wave within the plate is therefore defined by substituting equation (B40) and (B41) into equations (B38) giving:

$$\overset{v}{H}^t(z,t) = \left(\frac{2\overset{v}{E}_o^i}{\eta_0+\eta_1}\right)e^{-\gamma_1 z}e^{j\omega t}\overset{v}{a}_y. \tag{B42}$$

The conjugate of the magnetic field is:

$$\overset{v}{H}^t(z,t)^* = \left(\frac{2\overset{v}{E}_o^{i*}(\eta_0+\eta_1)}{|\eta_0+\eta_1|^2}\right)e^{-\gamma_1 z}e^{j\omega t}\overset{v}{a}_y \text{ and} \tag{B42a}$$

$$\overset{v}{E}^t(z,t) = \left(\frac{2\eta_1\overset{v}{E}_o^i}{\eta_0+\eta_1}\right)e^{-\gamma_1 z}e^{j\omega t}\overset{v}{a}_x. \tag{B43}$$

B.3.3.2 Transmitted Power

Figure B-2 illustrates the incident, reflected, and transmitted power per unit area at the boundary of media 0 and the media 1 plate made of one material.

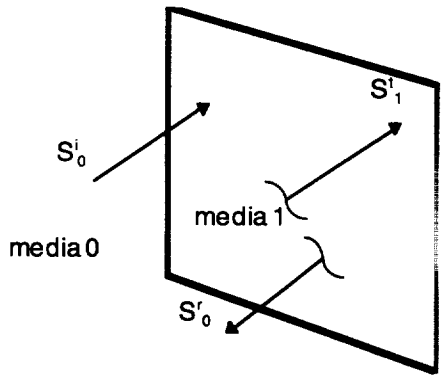

Figure B-2. RF power at boundary with a single material.

A wave, composed of complex phasors, has instantaneous power per unit area defined as the cross product of the electric field and the conjugate of the magnetic field. Therefore, the instantaneous power per unit area traveling in the plate is the cross product of equation (B43) and (B42a) giving:

$$\overset{V}{S}_1^t = \overset{V}{E}_1^t(z,t) x \overset{V}{H}^t(z,t)^* = \left(\frac{2\left|\overset{V}{E}_o^i\right|}{|\eta_0 + \eta_1|} \right)^2 \eta_1 e^{-2\gamma_1 z} e^{j2\omega t} \overset{V}{a}_z. \tag{B44}$$

For sine waves, the average power per unit area traveling in the plate is defined as one half the real part of the instantaneous power, which gives from equation (B44):

$$\left\langle \overset{V}{S}_1^t \right\rangle = \frac{1}{2} \left(\frac{2\left|\overset{V}{E}_o^i\right|}{|\eta_0 + \eta_1|} \right)^2 e^{-2\gamma_1 z} \overset{V}{a}_z real\{\eta_1\}. \tag{B45}$$

The average power per unit area absorbed in the plate is therefore the average power entering the plate at the boundary of media 0 and media 1. It is calculated using equation (B45) with z = +0:

$$\left\langle \overset{V}{S}_1^t \right\rangle = \frac{1}{2} \left(\frac{2\left|\overset{V}{E}_o^i\right|}{|\eta_0 + \eta_1|} \right)^2 \overset{V}{a}_z real\{\eta_1\} = \frac{2\left|\overset{V}{E}_o^i\right|^2}{|\eta_0 + \eta_1|^2} \overset{V}{a}_z real\{\eta_1\}. \tag{B46}$$

The total average power entering media 1 at the boundary is given by the product of the power per unit area and the surface area of the plate:

$$P^t = \left\langle \overset{V}{S}_1^t \right\rangle A_{surf} = \frac{2\left|\overset{V}{E}_o^i\right|^2 A_{surf}}{|\eta_0 + \eta_1|^2} real\{\eta_1\}. \tag{B47}$$

B.4 POWER FOR A PLATE OF MULTIPLE MATERIALS

Since the internal surface area of an enclosure (fairing/vehicle) is comprised of several different materials, it is necessary to consider the affects of replacing the single plate material with a plate made of several materials. This section addresses this condition.

Replace the media 1 plate at the boundary by a patchwork of several adjacent plates of different material as illustrated in Figure B-3. The incident power, the reflected power, and the absorbed power can be derived in terms of the incident E field and the impedances of the various materials using the equations in section 2.2.

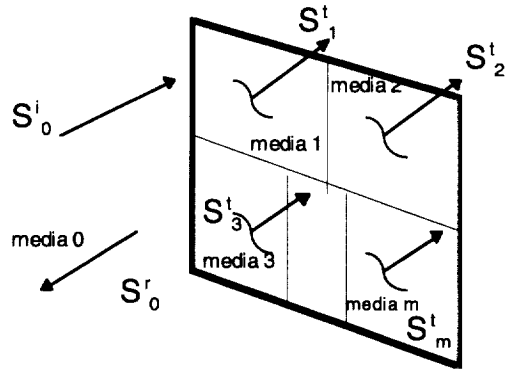

Figure B-3. RF waves at the boundary with several materials.

B.4.1 POWER OF THE INCIDENT WAVE ON MULTIPLE MATERIALS

The total incident power on several different plates is the sum of all the power incident on each plate, or using equation (B27a):

$$P_T^i = \left\langle \overset{\vee}{S}_1^i \right\rangle A_{1-surf} + \left\langle \overset{\vee}{S}_2^i \right\rangle A_{2-surf} + \cdots \left\langle \overset{\vee}{S}_k^i \right\rangle A_{k-surf} \quad \text{and}$$

$$P_T^i = \sum_{k=1}^{k=m} \left\langle \overset{\vee}{S}_k^i \right\rangle A_{k-surf} . \tag{B48}$$

The magnitude of the incident wave is the same for all plates although each plate would absorb different amounts of power. This means the incident electric field is constant for all plates, therefore substituting equation (B27) into equation (B48) and simplifying gives:

$$P_T^i = \frac{\left| \overset{\vee}{E}_o^i \right|^2}{2|\eta_0|^2} real(\eta_0) \left(\sum_{k=1}^{k=m} A_{k-surf} \right). \tag{B49}$$

Equation (B49) is the total of the average power which is incident on all plates.

B.4.2 POWER OF THE REFLECTED WAVES FROM MULTIPLE MATERIALS

The total power reflected from several different plates using equation (B37) is the sum of the reflected powers from each plate, or:

$$P_T^r = \left\langle \overset{\vee}{S}_1^r \right\rangle A_{1-surf} + \left\langle \overset{\vee}{S}_2^r \right\rangle A_{2-surf} + \cdots \left\langle \overset{\vee}{S}_k^r \right\rangle A_{k-surf} \quad \text{and} \tag{B50}$$

$$P_T^r = \frac{1}{2} \sum_{k=1}^{k=m} real \left\langle \overset{\vee}{S}_k^r \right\rangle A_{k-surf} . \tag{B51}$$

The incident wave magnitude is the same for all plates although each plate would absorb different amounts of power. This means the incident electric field is constant for all plates, therefore substituting equation

(B36) into equation (B51) and simplifying gives:

$$P_T^r = \frac{\left|\overset{\vee}{E}_o^i\right|^2 real\{\eta_0\}}{2|\eta_0|^2}\left(\sum_{k=1}^{k=m} A_{k-surf}\left(\frac{|\eta_0 - \eta_k|}{|\eta_0 + \eta_k|}\right)^2\right). \tag{B52}$$

Equation (B41) gives the average power reflected from all the materials.

B.4.3 POWER ENTERING THE SEVERAL MATERIALS

The total power absorbed by several plates of different materials using equation (B47) is the sum of all the power entering each individual plate, or:

$$P_T^t = \left\langle \overset{\vee}{S}_1^t \right\rangle A_{1-surf} + \left\langle \overset{\vee}{S}_2^t \right\rangle A_{2-surf} + \cdots \left\langle \overset{\vee}{S}_k^t \right\rangle A_{k-surf} \text{ and}$$

$$P_T^t = \sum_{k=1}^{k=m} \left\langle \overset{\vee}{S}_k^t \right\rangle A_{k-surf}. \tag{B53}$$

The incident wave magnitude is the same for all plates although each plate would absorb different amounts of power. This means the electric field is constant for all plates, therefore substituting equation (B46) into equation (B53) and simplifying gives:

$$P_T^t = 2\left|\overset{\vee}{E}_o^i\right|^2 \left(\sum_{k=1}^{k=m} \frac{A_{k-surf}\, real\{\eta_k\}}{|\eta_0 + \eta_k|^2}\right). \tag{B54}$$

Equation (B54) gives the total average power entering all the materials and is the key to solving for the field inside an enclosure.

B.5 DETERMINE THE ELECTRIC (E) FIELD IN AN ENCLOSURE

Consider an enclosure where the surface area is made up of several different materials. An antenna is radiating within the enclosure. RF energy will be reflected from the surface and will increase until the incident power on the surface reaches a level where the surface absorbs the amount of power being radiated by the antenna. The magnitude of the incident wave is first determined and then the equivalent E field standing wave inside the enclosure is determined.

B.5.1 VALUE OF THE INCIDENT WAVE IN THE ENCLOSURE

For M number of media making up the enclosure surface, the magnitude of the incident wave which would give the power loss is therefore determined by solving equation (B54) for the electric field giving:

$$\left|\overset{\vee}{E}_o^i\right| = \sqrt{\frac{\langle P \rangle}{\sum_{k=1}^{k=m} 2A_{k-surf}\, real\left\{\frac{\eta_k}{|\eta_o + \eta_k|^2}\right\}}}. \tag{B55}$$

This equation is exact, where P is the power in watts radiated by the antenna. However in evaluating the E field, care must be exercised to properly evaluate the real part of the impedance ratio term.

B.5.2 STANDING WAVE IN THE ENCLOSURE

In our problem the equivalent RF wave incident upon the surface is producing the loss of energy. A reflected wave is also present within the enclosure. The reflected wave and the incident wave combine to form a standing wave within the enclosure. A computation of the standing wave resulting from the reflection from the plate is desired.

a) In the air, the incident and reflected wave combine to form a standing wave defined by:

$$\vec{E}(z,t) = \left[\vec{E}_o^i e^{j(\omega t-\beta_1 z)} + \vec{E}_o^r e^{j(\omega t+\beta_1 z)}\right]\vec{a}_x \text{ and}$$
$$\vec{E}(z,t) = e^{j\omega t}\left[\vec{E}_o^i e^{j(-\beta_1 z)} + \vec{E}_o^r e^{j(\beta_1 z)}\right]\vec{a}_x . \tag{B56}$$

b) Solving in terms of the incident wave components:

Since: $$\vec{E}_o^r = -\left(\frac{\eta_0-\eta_1}{\eta_0+\eta_1}\right)\vec{E}_o^i. \tag{B57}$$

then equation (B56) becomes:

$$E(z,t) = \vec{E}_o^i e^{j\omega t}\left[e^{j(-\beta_1 z)} - \left(\frac{\eta_0-\eta_1}{\eta_0+\eta_1}\right)e^{j(\beta_1 z)}\right]\vec{a}_x. \tag{B58}$$

Using Euler's equation :

$$e^{ju} \equiv \cos u + j\sin u$$
and
$$e^{-ju} \equiv \cos u - j\sin u. \tag{B59}$$

for $e^{i(\beta z)}$ and $e^{i(-\beta z)}$ in equation (B58) results in:

$$\vec{E}(z,t) = \vec{E}_o^i e^{j\omega t}\left[\left(\frac{\eta_0+\eta_1}{\eta_0+\eta_1}\right)(\cos(\beta z) - j\sin(\beta z)) - \left(\frac{\eta_0-\eta_1}{\eta_0+\eta_1}\right)(\cos(\beta z) + j\sin(\beta z))\right]\vec{a}_x.$$

Collecting terms and simplifying gives:

$$\vec{E}(z,t) = \vec{E}_o^i e^{j\omega t}\left[\left(\frac{2\eta_1}{\eta_0+\eta_1}\right)\cos\beta z - \left(\frac{2\eta_0}{\eta_0+\eta_1}\right)j\sin\beta z\right]\vec{a}_x. \tag{B60}$$

Using Euler's equation for $e^{j\omega t}$ gives:

$$\overset{v}{E}(z,t) = \overset{v}{E}_o^i(\cos\omega t + j\sin\omega t)\left[\left(\frac{2\eta_1}{\eta_0+\eta_1}\right)\cos\beta z - \left(\frac{2\eta_0}{\eta_0+\eta_1}\right)j\sin\beta z\right]\overset{v}{a}_x. \tag{B61}$$

Equation (B61) gives the general computation defining the standing wave inside the enclosure. A highly reflective boundary occurs for values of $\eta_1 \cong 0$ and equation (B61) becomes:

$$\overset{v}{E}(z,t) \cong 2\overset{v}{E}_o^i \sin(\beta_1 z)[\sin(\omega t) - j\cos(\omega t)]\overset{v}{a}_x. \tag{B62}$$

Basically, the standing wave inside the enclosure is twice the incident wave magnitude.

B.6 CONCLUSION

Equation (B55) can be used to calculate the RF field strength inside an enclosure. The equation uses the surface areas of different materials and the complex impedance of the materials. Appendix C provides the equations for the complex impedance and intrinsic characteristics of materials. The standing wave in the enclosure has an upper boundary which is approximately twice the magnitude of the incident wave calculated by equation (B55). It should be noted that the value of the electric field given by equation (B55) is the magnitude of the wave. It should be multiplied by 0.707 to determine the RMS value.

APPENDIX C

Derivation of the Equations for a Media's Intrinsic Characteristics

by
Jerry Reddell

C.1 INTRODUCTION

An exact computation of the intrinsic characteristics of different materials or medias is needed when performing assessments of the reflections and transmission of electromagnetic waves in a system containing several materials. Many textbooks give approximate equations which are applicable to only one type of media and the form and units of the equation varies from textbook to textbook. In many cases considerable confusion exists on the meaning and applicability of the results to a particular problem. This appendix derives the generic equations for the characteristics. The equations defining the wave impedance and the wave propagation are developed. Metric units are used throughout. A media's intrinsic characteristics define the relationships between the electric and magnetic portions of the wave as well as the propagation losses and velocity within the media. A media's intrinsic characteristics depend on the media's physical properties:

$\mu \equiv$ permeability; (henry per meter),

$\varepsilon \equiv$ permittivity; (farad per meter), and

$\sigma \equiv$ conductivity; (mho per meter).

The characteristics also depend on the frequency of the wave:

$\omega \equiv$ frequency; (radians per second).

The propagation characteristic is related to three other important terms: (1) propagation velocity, (2) skin depth, and (3) wavelength; which are also derived from the propagation characteristic equations.

C.2 WAVE IMPEDANCE (η)

The wave impedance or intrinsic impedance defines the relationship between the magnetic portion of the wave and the electric portion. It is defined as:

$$\eta \equiv \frac{|\vec{E}|}{|\vec{H}|}. \tag{C1}$$

The wave impedance can be derived from these two Maxwell equations:

$$\nabla x\vec{H} = J_c + \frac{\partial \vec{D}}{\partial t} \quad \text{and} \tag{C2}$$

$$\nabla x\vec{E} = -\frac{\partial \vec{B}}{\partial t}. \tag{C3}$$

But

$$J_c = \sigma\vec{E}, \tag{C4}$$

$$\vec{D} = \varepsilon\vec{E}, \tag{C5}$$

$$\vec{B} = \mu\vec{H}, \tag{C6}$$

where $\vec{E} = Ee^{j\omega t}$ and $\vec{H} = He^{j\omega t}$.

Differentiating equations (C5) and (C6) with respect to time (t) gives:

$$\frac{\partial \vec{D}}{\partial t} = \frac{\partial(\varepsilon \vec{E})}{\partial t} = \varepsilon \frac{\partial(\vec{E})}{\partial t} = \varepsilon \frac{\partial(Ee^{j\omega t})}{\partial t} = j\omega\varepsilon Ee^{j\omega t} = j\omega\varepsilon\vec{E} \text{ and} \tag{C7}$$

$$\frac{\partial \vec{D}}{\partial t} = \frac{\partial(\varepsilon \vec{E})}{\partial t} = \varepsilon \frac{\partial(\vec{E})}{\partial t} = \varepsilon \frac{\partial(Ee^{j\omega t})}{\partial t} = j\omega\varepsilon Ee^{j\omega t} = j\omega\varepsilon\vec{E}. \tag{C8}$$

Substituting equations (C4) and (C7) into equation (C2), and substituting equation (C8) into equation (C3) gives:

$$\begin{aligned} &\vec{\nabla} x \vec{H} = (\sigma + j\omega\varepsilon)\vec{E} \text{ and} \\ &\vec{\nabla} x \vec{E} = -j\omega\mu\vec{H}\cdot \end{aligned} \tag{C9}$$

Solving equation (C1) for $\vec{E}$ gives $|\vec{E}| = \eta|\vec{H}|$ and substituting into equations (C9) gives:

$$\left|\vec{\nabla} x \vec{H}\right| = \left|(\sigma + j\omega\varepsilon)\eta\vec{H}\right| \text{ and} \tag{C10}$$

$$\left|\vec{\nabla} x \eta\vec{H}\right| = \eta\left|\vec{\nabla} x \vec{H}\right| = \left|-j\omega\mu\vec{H}\right|. \tag{C11}$$

Solving equation (C11) for the cross product gives:

$$\left|\vec{\nabla} x \vec{H}\right| = \left|\frac{-j\omega\mu}{\eta}\vec{H}\right|. \tag{C12}$$

Therefore equation (C12) and equation (C10) are equal and :

$$\left|\vec{\nabla} x \vec{H}\right| = \left|-\frac{j\omega\mu}{\eta}\right| * \left|\vec{H}\right| = \left|(\sigma + j\omega\varepsilon)\eta\right| * \left|\vec{H}\right|. \tag{C13}$$

From which is obtained:

$$\left|\frac{j\omega\mu}{\eta}\right| = \left|(\sigma + j\omega\varepsilon)\eta\right|. \tag{C14}$$

From which comes:

$$\eta^2 = \frac{j\omega\mu}{(\sigma + j\omega\varepsilon)} \tag{C15}$$

Therefore the wave or intrinsic impedance becomes:

$$\eta = \eta_R + j\eta_i = \sqrt{j\omega\mu/(\sigma + j\omega\varepsilon)}. \tag{C16}$$

This is the form of the equation which is normally presented in text books. A more desirable form can be derived. Dividing numerator and denominator by ωε gives:

$$\eta = \sqrt{\frac{\left(j\omega\mu/\omega\varepsilon\right)}{\left(j+\sigma/\omega\varepsilon\right)}} = \sqrt{\frac{j\left(\mu/\varepsilon\right)}{\left[\left(\sigma/\omega\varepsilon\right)+j\right]} * \frac{\left[\left(\sigma/\omega\varepsilon\right)-j\right]}{\left[\left(\sigma/\omega\varepsilon\right)-j\right]}}. \tag{C17}$$

Finally:

$$\eta = \sqrt{\frac{\left(\frac{\mu}{\varepsilon}\right) * \left[1+j\left(\sigma/\omega\varepsilon\right)\right]}{\left[1+\left(\sigma/\omega\varepsilon\right)^2\right]}}. \tag{C18}$$

The complex form under the radical requires additional operations to find a value for the impedance. This can be accomplished by determining the absolute value of the impedance. Let:

$$A = \sqrt{\frac{\left(\frac{\mu}{\varepsilon}\right)}{\left[1+\left(\sigma/\omega\varepsilon\right)^2\right]}}. \tag{C19}$$

Putting A in equation (C18) becomes:

$$\eta = A\sqrt{\left[1+j\left(\sigma/\omega\varepsilon\right)\right]}. \tag{C20}$$

Multiplying the term in the radical by the conjugate of the term gives:

$$\eta = A\sqrt{\sqrt{\left[1+j\left(\sigma/\omega\varepsilon\right)\right]*\left[1-j\left(\sigma/\omega\varepsilon\right)\right]}\angle \tan^{-1}\left(\sigma/\omega\varepsilon\right)} \text{ and} \tag{C21}$$

$$\eta = A\sqrt{\sqrt{\left[1^2+\left(\sigma/\omega\varepsilon\right)^2\right]}\angle \tan^{-1}\left(\sigma/\omega\varepsilon\right)} = A\sqrt{\sqrt{1^2+\left(\sigma/\omega\varepsilon\right)^2}}\angle\frac{1}{2}\tan^{-1}\left(\sigma/\omega\varepsilon\right). \tag{C22}$$

Therefore the absolute value of the wave impedance is:

$$|\eta| = A\sqrt{\sqrt{\left[1^2+\left(\sigma/\omega\varepsilon\right)^2\right]}}. \tag{C23}$$

Now inserting equation (C19) for A gives :

$$|\eta| = \sqrt{\frac{\left(\frac{\mu}{\varepsilon}\right) * \sqrt{\left[1+\left(\sigma/\omega\varepsilon\right)^2\right]}}{\left[1+\left(\sigma/\omega\varepsilon\right)^2\right]}} = \sqrt{\frac{\left(\frac{\mu}{\varepsilon}\right)}{\sqrt{\left[1+\left(\sigma/\omega\varepsilon\right)^2\right]}}} = \frac{\sqrt{\left(\frac{\mu}{\varepsilon}\right)}}{\sqrt[4]{\left[1+\left(\sigma_{\omega\varepsilon}\right)^2\right]}}. \tag{C24}$$

The magnitude of the associated angle is:

$$\theta = \sqrt{\angle \tan^{-1}\left(\sigma/\omega\varepsilon\right)} = (\frac{1}{2}) \tan^{-1}(\frac{\sigma}{\omega\varepsilon}). \tag{C25}$$

If $A = \tan^{-1}(\frac{\sigma}{\omega\varepsilon})$ then $\theta = \frac{A}{2}$ and

$$\cos(\theta) = \cos\left(\frac{A}{2}\right) = \sqrt{\frac{\cos(A)+1}{2}} = \sqrt{\frac{\cos\left(\tan^{-1}\left(\frac{\sigma}{\omega\varepsilon}\right)\right)+1}{2}}. \tag{C26}$$

But

$$\cos A = \cos\left(\tan^{-1}\left(\frac{\sigma}{\omega\varepsilon}\right)\right) = \frac{\omega\varepsilon}{\sqrt{\sigma^2+\omega^2\varepsilon^2}} = 1/\sqrt{1+\left(\frac{\sigma}{\omega\varepsilon}\right)^2}. \tag{C27}$$

Therefore equation (C26) becomes:

$$\cos\theta = \sqrt{\frac{1+\sqrt{\left(\frac{\sigma}{\omega\varepsilon}\right)^2+1}}{2\sqrt{1+\left(\frac{\sigma}{\omega\varepsilon}\right)^2}}}. \tag{C28}$$

The real part of wave impedance is therefore:

$$\eta_R = |\eta|\cos\theta = |\eta|\sqrt{\frac{\left(1/\sqrt{1+\left(\frac{\sigma}{\omega\varepsilon}\right)^2}\right)+1}{2}} = |\eta|\sqrt{\frac{1+\sqrt{1+\left(\frac{\sigma}{\omega\varepsilon}\right)^2}}{2\sqrt{1+\left(\frac{\sigma}{\omega\varepsilon}\right)^2}}}. \tag{C29}$$

Inserting equation (C24) for the absolute value of the impedance gives:

$$\eta_R = \frac{\sqrt{\left(\frac{\mu}{\varepsilon}\right)}}{\sqrt[4]{\left[1+\left(\sigma_{\omega\varepsilon}\right)^2\right]}} \sqrt{\frac{1+\sqrt{1+\left(\frac{\sigma}{\omega\varepsilon}\right)^2}}{2\sqrt{1+\left(\frac{\sigma}{\omega\varepsilon}\right)^2}}}. \tag{C30}$$

Finally the real portion of the impedance is simplified to:

$$\eta_R = \sqrt{\frac{\left(\frac{\mu}{\varepsilon}\right)\left(\sqrt{1+\left(\frac{\sigma}{\omega\varepsilon}\right)^2}+1\right)}{2\left(1+\left(\frac{\sigma}{\omega\varepsilon}\right)^2\right)}}. \tag{C31}$$

The imaginary part of wave impedance is similarly derived:

If $A = \tan^{-1}(\frac{\sigma}{\omega\varepsilon})$ then $\theta = \frac{A}{2}$ and using equation (C27) in the following gives:

$$\sin\theta = \sin\left(\frac{A}{2}\right) = \sqrt{\frac{\cos(A)-1}{2}} = \sqrt{\frac{\sqrt{1+\left(\frac{\sigma}{\omega\varepsilon}\right)^2}-1}{2\sqrt{1+\left(\frac{\sigma}{\omega\varepsilon}\right)^2}}}. \tag{C32}$$

and the imaginary part of equation (C16) becomes:

$$\eta_i = |\eta| * \sin\theta = \sqrt{\frac{\left(\frac{\mu}{\varepsilon}\right)\left(\sqrt{1+\left(\frac{\sigma}{\omega\varepsilon}\right)^2}-1\right)}{2\left(1+\left(\frac{\sigma}{\omega\varepsilon}\right)^2\right)}}. \tag{C33}$$

Equations (C31) and (C33) provide exact computations of the real and imaginary portions of the intrinsic or wave impedance while equation (C24) provides the exact computation for the absolute magnitude of the impedance for any material.

C.2.2 WAVE PROPAGATION CONSTANTS

The propagation of a wave through a media can also be determined using the equations (C9) which are repeated here:

$$\vec{\nabla} x \vec{H} = (\sigma + j\omega\varepsilon)\vec{E} \text{ and}$$
$$\vec{\nabla} x \vec{E} = -j\omega\mu\vec{H} \cdot \tag{C34}$$

Solving for the electric field and magnetic field gives:

$$\vec{H} = \vec{\nabla} x \vec{E}/(-j\omega\mu) \text{ and}$$
$$\vec{E} = \vec{\nabla} x \vec{H}/(\sigma + j\omega\varepsilon). \tag{C35}$$

Substituting equations (C35) into equations (C34) results in:

$$\vec{\nabla} x\left(\vec{\nabla} x \vec{E}\right) = -j\omega\mu(\sigma + j\omega\varepsilon)\vec{E} \text{ and} \tag{C36}$$

$$\vec{\nabla} x\left(\vec{\nabla} x \vec{H}\right) = -j\omega\mu(\sigma + j\omega\varepsilon)\vec{H}. \tag{C37}$$

The left portion of equations (C36) and (C37) are defined by the identity:

$$\vec{\nabla} x\left(\vec{\nabla} x \vec{A}\right) \equiv \vec{\nabla}\left(\vec{\nabla} \bullet \vec{A}\right) - \nabla^2 \vec{A}.$$

so equations (C36) and (C37) become:

$$\vec{\nabla}\left(\vec{\nabla} \bullet \vec{E}\right) - \nabla^2 \vec{E} = -j\omega\mu(\sigma + j\omega\varepsilon)\vec{E} \text{ and}$$
$$\vec{\nabla}\left(\vec{\nabla} \bullet \vec{H}\right) - \nabla^2 \vec{H} = -j\omega\mu(\sigma + j\omega\varepsilon)\vec{H}. \tag{C38}$$

Also from Maxwell's equations:

$$\nabla \bullet \vec{D} = \rho \tag{C39}$$

But

$$\vec{D} = \varepsilon\vec{E} \text{ and}$$
$$\nabla \bullet \vec{D} = \nabla \bullet \varepsilon\vec{E} = \varepsilon\left(\nabla \bullet \vec{E}\right) = \rho. \tag{C40}$$

Therefore:

$$\nabla \bullet \vec{E} = \frac{\rho}{\varepsilon}. \tag{C41}$$

Since there is no space charge in the region, then equation (C41) gives:

$$\nabla \bullet \vec{E} = \frac{\rho}{\varepsilon} = \frac{0}{\varepsilon} = 0. \tag{C42}$$

Another Maxwell equation is:

$$\nabla \bullet \vec{B} = 0 \tag{C43}$$

but

$$\vec{B} = \mu \vec{H} \tag{C44}$$

and therefore

$$\nabla \bullet \vec{B} = \nabla \bullet \left(\mu \vec{H}\right) = \mu\left(\nabla \bullet \vec{H}\right) = 0. \tag{C45}$$

So

$$\vec{\nabla} \bullet \vec{H} = 0. \tag{C46}$$

Therefore using equations (C42) and (C46) in equations (C38) reduce to:

$$\begin{aligned} &\nabla^2 \vec{E} = j\omega\mu(\sigma + j\omega\varepsilon)\vec{E} \equiv \gamma^2 \vec{E} \quad \text{and} \\ &\nabla^2 \vec{H} = j\omega\mu(\sigma + j\omega\varepsilon)\vec{H} \equiv \gamma^2 \vec{H}. \end{aligned} \tag{C47}$$

From equation (C47) the propagation constant γ is defined as:

$$\gamma^2 \equiv j\omega\mu(\sigma + j\omega\varepsilon) \tag{C48}$$

and therefore:

$$\gamma = \alpha + j\beta = \sqrt{j\omega\mu(\sigma + j\omega\varepsilon)} = \sqrt{\omega\mu(j\sigma - \omega\varepsilon)}. \tag{C49}$$

This is the equation normally given in text books for the propagation constant. A more desirable and useful form will now be developed.

$$\gamma = \sqrt{\omega\mu(j\sigma - \omega\varepsilon)} = \sqrt{\omega^2\mu\varepsilon(1 - j\frac{\sigma}{\omega\varepsilon})} \tag{C50}$$

Let

$$A = \omega\sqrt{\mu\varepsilon}. \tag{C51}$$

Substituting A into equation (C50) results in:

$$\gamma = A\sqrt{\left[1 - j\left(\sigma/\omega\varepsilon\right)\right]}. \tag{C52}$$

Multiplying the term in the radical by the conjugate of the term determines the absolute value giving:

$$\gamma = A\sqrt{\sqrt{\left[1 - j\left(\sigma/\omega\varepsilon\right)\right] * \left[1 + j\left(\sigma/\omega\varepsilon\right)\right]}\angle \tan^{-1}\left(-\sigma/\omega\varepsilon\right)}. \tag{C53}$$

Performing the multiplication:

$$\gamma = A\sqrt{\sqrt{\left[1^2 + \left(\sigma/\omega\varepsilon\right)^2\right]}\angle \tan^{-1}\left(-\sigma/\omega\varepsilon\right)} \text{ and} \tag{C54}$$

$$\gamma = A\sqrt{\sqrt{\left[1 + \left(\sigma/\omega\varepsilon\right)^2\right]}\angle \frac{1}{2}\tan^{-1}\left(-\sigma/\omega\varepsilon\right)}. \tag{C55}$$

Therefore the absolute value of the wave impedance is:

$$|\gamma| = A\sqrt{\sqrt{\left[1^2 + \left(\sigma/\omega\varepsilon\right)^2\right]}}. \tag{C56}$$

Substituting equation (C51) into equation (C56) gives:

$$|\gamma| = \omega\sqrt{\mu\varepsilon}\sqrt{1+\left(\frac{\sigma}{\omega\varepsilon}\right)^2}. \tag{C57}$$

The angle between the real and imaginary parts is determined from equation (C55):

$$\theta = \sqrt{\angle \tan^{-1}\left(-\sigma/\omega\varepsilon\right)} = \left(\frac{1}{2}\right)\left[\pi - \tan^{-1}\left(\frac{\sigma}{\omega\varepsilon}\right)\right]. \tag{C58}$$

If $A = \tan^{-1}\left(\frac{\sigma}{\omega\varepsilon}\right)$ then $\theta = \frac{\pi}{2} - \frac{1}{2}\tan^{-1}\left(\frac{\sigma}{\omega\varepsilon}\right)$

and the phase shift constant which is defined as the imaginary part of the propagation constant is:

$$\beta = |\gamma|\sin\theta = |\gamma|\sin\left(\frac{\pi}{2} - \frac{1}{2}\tan^{-1}\frac{\sigma}{\omega\varepsilon}\right) = |\gamma|\cos\left(\frac{1}{2}\tan^{-1}\frac{\sigma}{\omega\varepsilon}\right). \tag{C59}$$

Since $$\cos(\theta) = \cos\left(\frac{A}{2}\right) = \sqrt{\frac{\cos(A)+1}{2}}, \tag{C60}$$

then $$\cos A = \cos\left(\tan^{-1}\left(\frac{\sigma}{\omega\varepsilon}\right)\right) = \frac{\omega\varepsilon}{\sqrt{\sigma^2 + \omega^2\varepsilon^2}} = 1/\sqrt{1+\left(\frac{\sigma}{\omega\varepsilon}\right)^2}. \tag{C61}$$

Therefore substituting equation (C61) into equation (C60) gives:

$$\cos\theta = \sqrt{\frac{1+\sqrt{\left(\frac{\sigma}{\omega\varepsilon}\right)^2+1}}{2\sqrt{1+\left(\frac{\sigma}{\omega\varepsilon}\right)^2}}}. \tag{C62}$$

Then from equations (C62) and (C59) comes:

$$\beta = |\gamma| \sqrt{\frac{1}{2}\left(\frac{1}{\sqrt{1+\left(\frac{\sigma}{\omega\varepsilon}\right)^2}}+1\right)} = |\gamma| \sqrt{\frac{\sqrt{1+\left(\frac{\sigma}{\omega\varepsilon}\right)^2}+1}{2\sqrt{1+\left(\frac{\sigma}{\omega\varepsilon}\right)^2}}}. \tag{C63}$$

Using equation (C57) for the absolute value of propagation constant gives:

$$\beta = \omega\sqrt{\mu\varepsilon\sqrt{1+\left(\frac{\sigma}{\omega\varepsilon}\right)^2}} \sqrt{\frac{\sqrt{1+\left(\frac{\sigma}{\omega\varepsilon}\right)^2}+1}{2\sqrt{1+\left(\frac{\sigma}{\omega\varepsilon}\right)^2}}}. \tag{C64}$$

This reduces to give the phase shift constant as:

$$\beta = \omega\sqrt{\frac{\mu\varepsilon}{2}\left(\sqrt{1+\left(\frac{\sigma}{\omega\varepsilon}\right)^2}+1\right)}. \tag{C65}$$

Similarly the attenuation constant is defined as the real part of the propagation constant:

$$\alpha = |\gamma|\cos(\theta) = |\gamma|\cos\left(\frac{\pi}{2}-\frac{A}{2}\right) = |\gamma|\sin\left(\frac{A}{2}\right).$$

if $A = \tan^{-1}\left(\frac{\sigma}{\omega\varepsilon}\right)$ then:

$$\sin\left(\frac{A}{2}\right) = \sqrt{\frac{\cos(A)-1}{2}} = \sqrt{\frac{\sqrt{1+\left(\frac{\sigma}{\omega\varepsilon}\right)^2}-1}{2\sqrt{1+\left(\frac{\sigma}{\omega\varepsilon}\right)^2}}}. \tag{C66}$$

The attenuation constant can be calculated from:

$$\alpha = |\gamma| * \sin\theta = \omega\sqrt{\frac{\mu\varepsilon}{2}\left(\sqrt{1+\left(\frac{\sigma}{\omega\varepsilon}\right)^2}-1\right)}. \tag{C67}$$

Equation (C65) gives the exact computation of the phase shift constant in any material while equation (C67) provides the exact computation for the attenuation constant for any material.

C.3 OTHER CHARACTERISTICS

Three other terms can be determined from the propagation constants. They are wave velocity in the media, wavelength in the media, and skin depth.

C.3.1 WAVE VELOCITY IN THE MEDIA

The velocity of a RF wave in a media is dependent on the media properties. It is not, in general, the same as in a vacuum. The propagation velocity in any media (including vacuum) is given by:

$$U \equiv \frac{\omega}{\beta} = \omega / \omega \sqrt{\frac{\mu\varepsilon}{2}\left(\sqrt{1+\left(\frac{\sigma}{\omega\varepsilon}\right)^2}+1\right)} = 1/\sqrt{\frac{\mu\varepsilon}{2}\left(\sqrt{1+\left(\frac{\sigma}{\omega\varepsilon}\right)^2}+1\right)}. \tag{C68}$$

C.3.2 WAVELENGTH IN A MEDIA

The wavelength inside a material is not the same as in vacuum. The wavelength inside any media (including vacuum) is given by:

$$\lambda_m = 2\pi/\beta = 2\pi \Big/ \omega\sqrt{\frac{\mu\varepsilon}{2}\left(\sqrt{1+\left(\frac{\sigma}{\omega\varepsilon}\right)^2}+1\right)}. \tag{C69}$$

C.3.3 SKIN DEPTH

The skin depth is defined as the distance (z) inside the media at which the magnitude of the wave is attenuated to the factor 1/e, which means:

$$\begin{aligned}
&\vec{E}(z,t) = \vec{E}_0 e^{-1} e^{\beta z} e^{j\omega t} = \vec{E}_0 e^{-\alpha z} e^{\beta z} e^{j\omega t} \\
&or \\
&e^{-1} = e^{-\alpha z}, \\
&\therefore \alpha z = 1, \text{ and} \\
&z = \frac{1}{\alpha}.
\end{aligned} \tag{C70}$$

The skin depth is therefore defined by:

$$\delta \equiv \frac{1}{\alpha} = \frac{1}{\omega\sqrt{\frac{\mu\varepsilon}{2}\left(\sqrt{1+\left(\frac{\sigma}{\omega\varepsilon}\right)^2}-1\right)}}. \tag{C71}$$

This is the general or exact computation for the skin depth in any material (including vacuum). Two quick checks of the validity of equation (C71) are now made. A look at the equation (C71) for vacuum, which has a conductivity of zero, gives:

$$\delta_{vacuum} = \frac{1}{\omega\sqrt{\frac{\mu\varepsilon}{2}\left(\sqrt{1+\left(\frac{0}{\omega\varepsilon}\right)^2}-1\right)}} = \frac{1}{\omega\sqrt{\frac{\mu\varepsilon}{2}\left(\sqrt{1}-1\right)}} = \frac{1}{\omega\sqrt{\frac{\mu\varepsilon}{2}(0)}} = \frac{1}{0} = \infty.$$

A skin depth of infinity is what is intuitively expected for vacuum.

The skin depth equation which is normally presented in text books applies only to highly conductive materials and is an approximation determined from equation (C71). When the conductivity is large (> 100 mho per meter) then equation (C71) gives:

$$\delta \approx \frac{1}{\omega\sqrt{\frac{\mu\varepsilon}{2}\left(\sqrt{\left(\frac{\sigma}{\omega\varepsilon}\right)^2}\right)}} = \frac{1}{\sqrt{\frac{\omega^2\mu\varepsilon}{2}\left(\frac{\sigma}{\omega\varepsilon}\right)}} = \frac{1}{\sqrt{\frac{\omega\mu\sigma}{2}}} = \frac{1}{\sqrt{\pi f\mu\sigma}}.$$

This is the skin depth equation typically presented in textbooks.

C.4 SUMMARY

Equations (C24), (C30), and (C33) define the computations for the components of the complex wave impedance of a material. Equations (C57), (C65), and (C67) define the computations for the components of the complex wave propagation constant of a material. Equations (C68), (C69), and (C71) give the velocity, wavelength, and skin depth calculations for a material. These equations are exact and are valid for any material including vacuum.

APPENDIX D

Method for Determining the Effective Impedance of the Acoustic Blankets on a Surface

by
Jerry Reddell

D.1 INTRODUCTION

The evaluation of the RF field strength inside the Delta Launch Vehicle Fairing is complicated by the presence of acoustic blankets which line the inner surface of the fairing. These blankets are made of a layer of fiberglass batting covered on each side with a thin sheet of fiberglass cloth which has been coated with carbon loaded teflon. A method of evaluating the blankets affect on the RF fields is needed. Figure 1 illustrates the blanket construction and installation.

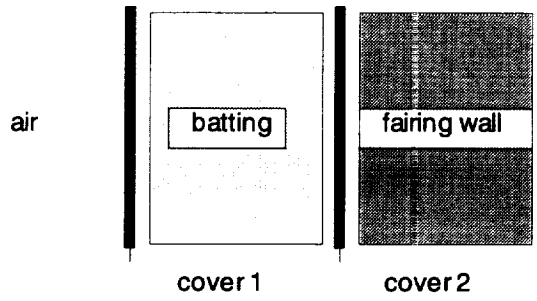

Figure D-1. Layers of material for the acoustic blanket installation on the fairing wall.

Equation (B55) of Appendix B indicates the blanketed area and its impedance are required to evaluate the affect on the RF field strength. The area is determined rather easily. However, the effective impedance of the blanket is not easily determined. The effective impedance is a function of three layers of material, each material's thickness, each layer's RF characteristics, and the RF characteristics of the wall. Previous attempts to assess the blanket's impact involved series summing of successive reflections and transmittances. The approach was computationally intense and results were not convincing. An accurate model for computing the effective impedance of the blanket covered area is needed. This note derives the mathematical equation used to accurately determine the effective impedance of the area covered by the blankets. The effective impedance can then be used to calculate the RF fields inside the fairing.

The acoustic blanket also covers the RF window in the fairing wall. A method of calculating the RF transmittance (insertion loss) of the acoustic blanket is also needed. This note also develops the equations which define the effective transmittance through the blanket covered window.

D.2 APPROACH

The analytical approach for solving the problem is:

a) Determine the equivalent impedance of the areas covered by layers of material (blankets). This requires knowing the RF characteristics and dimensions of the materials. The equivalent impedance can be determined by Equation D17 which is derived in section D.3 of this Appendix. The determination must start at the wall and proceed one layer at a time to the innermost layer to the center of the enclosure of fairing.
b) Having determined the impedances of the various areas, use equation B55 of Appendix B to calculate the RF field inside the fairing or enclosure.

c) Use equations D21, D22 and D23 and the impedances at each boundary (as determined in step a) to compute the RF field which is transmitted through each layer of material in the blanket, starting at the innermost material surface and proceeding toward the wall or open RF window. These equations are derived in section D.4 of this Appendix.

Section D.5 of this Appendix applies the equations to the blanket covered fairing wall to illustrate the methodology for arriving at the equivalent surface impedance and transmittance through the blanket.

D.3 EQUIVALENT IMPEDANCE OF A MATERIAL BOUNDED BY TWO MEDIA

Consider a boundary between two media as shown in Figure D-2.

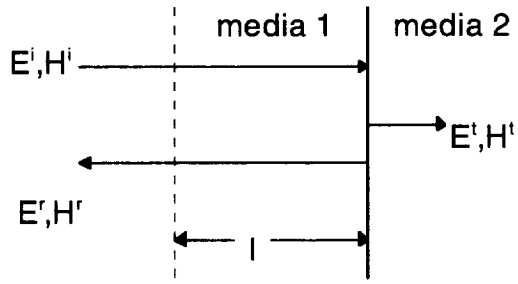

Figure D-2. RF waves at the boundary of two media.

An incident wave is traveling in media 1 toward the boundary. The reflected wave is traveling in media 1 away from the boundary. The incident and reflected waves, as a function of the distance (l) from the boundary, are described mathematically by equations (B23), (B24), and (B28) of Appendix B. The incident wave is defined by:

$$E^i = E^I e^{j\omega t} e^{-(\alpha_1 + j\beta_1)(-l)} \text{ and}$$
$$H^i = H^I e^{j\omega t} e^{-(\alpha_1 + j\beta_1)(-l)}. \tag{D1}$$

The reflected wave is:

$$E^r = E^R e^{j\omega t} e^{-(\alpha_1 + j\beta_1)(l)} \text{ and}$$
$$H^r = H^R e^{j\omega t} e^{-(\alpha_1 + j\beta_1)(l)}. \tag{D2}$$

Where the propagation constant (γ) has been replaced by its complex parts, the attenuation constant (α) and the phase shift constant (β_1).

The total field at distance (l_1) from the boundary is given by the sum of the incident and reflected fields, or:

$$E^{tot} = E^i + E^r,$$
$$E^{tot} = E^I e^{j\omega t} e^{(\alpha_1 + j\beta_1)l} + E^R e^{j\omega t} e^{-(\alpha_1 + j\beta_1)l}, \tag{D3}$$

$$H^{tot} = H^{i} + H^{r}, \text{ and}$$
$$H^{tot} = H^{I} e^{j\omega t} e^{(\alpha_1 + j\beta_1)l} + H^{R} e^{j\omega t} e^{-(\alpha_1 + j\beta_1)l}. \tag{D4}$$

The magnitudes of the reflected and incident waves are related by the complex impedances of the two media as defined in equations (C11) and (C18) of Appendix C such that:

$$E^{R} = \left(\frac{\eta_2 - \eta_1}{\eta_2 + \eta_1}\right) E^{I} \tag{D5}$$

and

$$H^{R} = \left(\frac{\eta_1 - \eta_2}{\eta_2 + \eta_1}\right) H^{I}. \tag{D6}$$

Using equation (D5) in equation (D3) gives:

$$E^{tot} = E^{I} e^{j\omega t} \left\{ e^{(\alpha_1 + j\beta_1)l} + \left[\frac{\eta_2 - \eta_1}{\eta_2 + \eta_1}\right] e^{-(\alpha_1 + j\beta_1)l} \right\}. \tag{D7}$$

Using equation (D6) in equation (D4) gives:

$$H^{tot} = H^{I} e^{j\omega t} \left\{ e^{(\alpha_1 + j\beta_1)l} + \left[\frac{\eta_1 - \eta_2}{\eta_2 + \eta_1}\right] e^{-(\alpha_1 + j\beta_1)l} \right\}. \tag{D8}$$

Using Euler's formula to define:

$$e^{j\beta_1 l} \equiv \cos(\beta_1 l) + j\sin(\beta_1 l) \text{ and}$$
$$e^{-j\beta_1 l} \equiv \cos(\beta_1 l) - j\sin(\beta_1 l).$$

Which are now used in equations (D7) and (D8) resulting in:

$$E^{Tot} = E^{I} e^{j\omega t} \left\{ e^{\alpha_1 l}(\cos\beta_1 l + j\sin\beta_1 l) + \left[\frac{\eta_2 - \eta_1}{\eta_2 + \eta_1}\right] e^{-\alpha_1 l}(\cos\beta_1 l - j\sin\beta_1 l) \right\} \tag{D9}$$

and

$$H^{Tot} = H^{I} e^{j\omega t} \left\{ e^{\alpha_1 l}(\cos\beta_1 l + j\sin\beta_1 l) - \left[\frac{\eta_2 - \eta_1}{\eta_2 + \eta_1}\right] e^{-\alpha_1 l}(\cos\beta_1 l - j\sin\beta_1 l) \right\}. \tag{D10}$$

Collecting the real and imaginary portions of (D9) and (D10) gives:

$$E^{Tot} = E^{I} e^{j\omega t} \left\{ \left(e^{\alpha_1 l} + \left[\frac{\eta_2 - \eta_1}{\eta_2 + \eta_1}\right] e^{-\alpha_1 l} \right) \cos\beta_1 l + j\sin\beta_1 l \left(e^{\alpha_1 l} - \left[\frac{\eta_2 - \eta_1}{\eta_2 + \eta_1}\right] e^{-\alpha_1 l} \right) \right\} \text{ and} \tag{D11}$$

$$H^{Tot} = H^I e^{j\omega t}\left\{\left(e^{\alpha_1 l} - \left[\frac{\eta_2 - \eta_1}{\eta_2 + \eta_1}\right]e^{-\alpha_1 l}\right)\cos\beta_1 l + j\sin\beta_1 l\left(e^{\alpha_1 l} + \left[\frac{\eta_2 - \eta_1}{\eta_2 + \eta_1}\right]e^{-\alpha_1 l}\right)\right\}. \quad \text{(D12)}$$

Multiplying equations (D11) and (D12) by $\frac{\eta_2 + \eta_1}{\eta_2 + \eta_1}$ gives:

$$E^{Tot} = \frac{E^I e^{j\omega t}}{\eta_2 + \eta_1}\left\{\left([\eta_2 + \eta_1]e^{\alpha_1 l} + [\eta_2 - \eta_1]e^{-\alpha_1 l}\right)\cos\beta_1 l + j\sin\beta_1 l\left([\eta_2 + \eta_1]e^{\alpha_1 l} - [\eta_2 - \eta_1]e^{-\alpha_1 l}\right)\right\} \quad \text{(D13)}$$

and

$$H^{Tot} = \frac{H^I e^{j\omega t}}{\eta_2 + \eta_1}\left\{\left([\eta_2 + \eta_1]e^{\alpha_1 l} - [\eta_2 - \eta_1]e^{-\alpha_1 l}\right)\cos\beta_1 l + j\sin\beta_1 l\left([\eta_2 + \eta_1]e^{\alpha_1 l} + [\eta_2 - \eta_1]e^{-\alpha_1 l}\right)\right\}. \quad \text{(D14)}$$

The impedance is defined as the ratio of the total E-field to the total H-field (the ratio of equation (D13) to equation (D14)):

$$\eta_L(l) = \frac{E^I}{H^I}\left\{\frac{\left[(\eta_2 + \eta_1)e^{\alpha_1 l} + (\eta_2 - \eta_1)e^{-\alpha_1 l}\right]\cos\beta_1 l + j\left[(\eta_2 + \eta_1)e^{\alpha_1 l} - (\eta_2 - \eta_1)e^{-\alpha_1 l}\right]\sin\beta_1 l}{\left[(\eta_2 + \eta_1)e^{\alpha_1 l} - (\eta_2 - \eta_1)e^{-\alpha_1 l}\right]\cos\beta_1 l + j\left[(\eta_2 + \eta_1)e^{\alpha_1 l} + (\eta_2 - \eta_1)e^{-\alpha_1 l}\right]\sin\beta_1 l}\right\}. \quad \text{(D15)}$$

Since $\frac{E^I}{H^I} \equiv \eta_1$ then equation (D15) becomes:

$$\eta_L(l) = \eta_1\left\{\frac{\left[(\eta_2 + \eta_1)e^{\alpha_1 l} + (\eta_2 - \eta_1)e^{-\alpha_1 l}\right]\cos\beta_1 l + j\left[(\eta_2 + \eta_1)e^{\alpha_1 l} - (\eta_2 - \eta_1)e^{-\alpha_1 l}\right]\sin\beta_1 l}{\left[(\eta_2 + \eta_1)e^{\alpha_1 l} - (\eta_2 - \eta_1)e^{-\alpha_1 l}\right]\cos\beta_1 l + j\left[(\eta_2 + \eta_1)e^{\alpha_1 l} + (\eta_2 - \eta_1)e^{-\alpha_1 l}\right]\sin\beta_1 l}\right\}. \quad \text{(D16)}$$

A simplified version of this equation often appears in text books when the media l is considered lossless (α_1=0). (See reference 4, page 288, section 7-09, equation 10, for an example).

$$\eta_L(l) = \eta_1\left\{\frac{\eta_2\cos\beta_1 l + j\eta_1\sin\beta_1 l}{\eta_1\cos\beta_1 l + j\eta_2\sin\beta_1 l}\right\}.$$

Equation (D16) shows that the impedance at a distance from the boundary is not the constant value of media 1 impedance. It is altered by the presence of the media 2 intrinsic impedance and varies with the distance from the boundary. An interesting result of equation (D16) occurs when the distance, 1, from media 1 is a multiple of a half wavelength, where the impedance is equal to the impedance of media 2.

Now consider the addition of a third media and a second boundary as shown in Figure D-3.

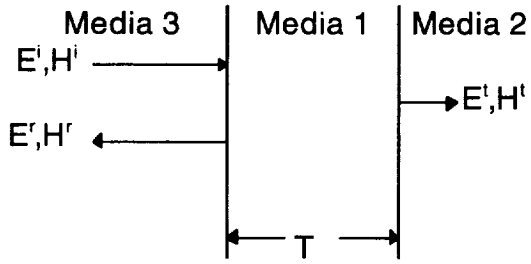

Figure D-3. RF waves at surface boundary with two layers of material.

The impedance at the boundary of media 3 and 1 is given by equation (D16) with "l" replaced by the thickness (T) of media 1 giving:

$$\eta_L(T) = \eta_1 \left\{ \frac{\left[(\eta_2+\eta_1)e^{\alpha_1 T} + (\eta_2-\eta_1)e^{-\alpha_1 T}\right]\cos\beta_1 T + j\left[(\eta_2+\eta_1)e^{\alpha_1 T} - (\eta_2-\eta_1)e^{-\alpha_1 T}\right]\sin\beta_1 T}{\left[(\eta_2+\eta_1)e^{\alpha_1 T} - (\eta_2-\eta_1)e^{-\alpha_1 T}\right]\cos\beta_1 T + j\left[(\eta_2+\eta_1)e^{\alpha_1 T} + (\eta_2-\eta_1)e^{-\alpha_1 T}\right]\sin\beta_1 T} \right\}. \quad \text{(D17)}$$

Media 1 is of thickness (T.) Media 2 impedance, η_2 can be thought of as a 'load' impedance which alters the intrinsic media 1 impedance at its boundary with media 3. Media 1 and media 2 can be replaced, as illustrated in Figure D-4, with an equivalent media impedance given by equation (D17) using the thickness (T) of media 1 for the value of "l."

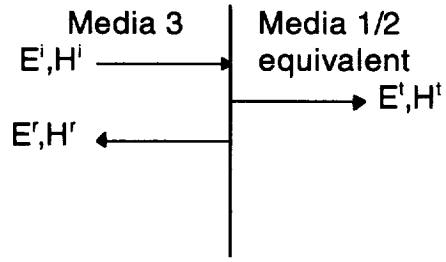

Figure D-4. RF waves at the boundary of an equivalent surface material.

Successive application of equation (D17) can reduce several layers of different media with varying thicknesses to a single boundary problem.

D.4 TRANSMITTANCE THROUGH A MEDIA OF THICKNESS, T

Considering Figure D-3, the transmittance into media 2 at its boundary is given by:

$$\begin{aligned} E^T &= E^I(0) + E^R(0) = E^{Tot}\big|_{l=0} \text{ and} \\ H^T &= H^I(0) + H^R(0) = H^{Tot}\big|_{l=0}. \end{aligned} \quad \text{(D18)}$$

The total field at the boundary of media 1 and 2 is determined from equations (D13) and (D14) by setting l =0. The field at boundary of media 3 and 1 is given by the equations when l = T. The ratio of the media

1 and 2 boundary total field to the field at the boundary of 2 and 3 (distance T) is given by:

$$\frac{E^{Tot}(0)}{E^{Tot}(T)} = \frac{2\eta_2}{\left([\eta_2+\eta_1]e^{\alpha_1 T}+[\eta_2-\eta_1]e^{-\alpha_1 T}\right)\cos\beta_1 T + j\sin\beta_1 T\left([\eta_2+\eta_1]e^{\alpha_1 T}-[\eta_2-\eta_1]e^{-\alpha_1 T}\right)}. \quad \text{(D19)}$$

and

$$\frac{H^{Tot}(0)}{H^{Tot}(T)} = \frac{2\eta_1}{\left([\eta_2+\eta_1]e^{\alpha_1 T}-[\eta_2-\eta_1]e^{-\alpha_1 T}\right)\cos\beta_1 T + j\sin\beta_1 T\left([\eta_2+\eta_1]e^{\alpha_1 T}+[\eta_2-\eta_1]e^{-\alpha_1 T}\right)}. \quad \text{(D20)}$$

Solve for the total field, $E^{Tot}(0)$ and $H^{Tot}(0)$, at media 2 boundary and substitute into equations (D18) gives

$$E^T = \frac{2\eta_2 E^{Tot}(T)}{\left([\eta_2+\eta_1]e^{\alpha_1 T}+[\eta_2-\eta_1]e^{-\alpha_1 T}\right)\cos\beta_1 T + j\sin\beta_1 T\left([\eta_2+\eta_1]e^{\alpha_1 T}-[\eta_2-\eta_1]e^{-\alpha_1 T}\right)} \quad \text{(D21)}$$

and

$$H^T = \frac{2\eta_1 H^{Tot}(T)}{\left([\eta_2+\eta_1]e^{\alpha_1 T}-[\eta_2-\eta_1]e^{-\alpha_1 T}\right)\cos\beta_1 T + j\sin\beta_1 T\left([\eta_2+\eta_1]e^{\alpha_1 T}+[\eta_2-\eta_1]e^{-\alpha_1 T}\right)}. \quad \text{(D22)}$$

Define four terms:

$$A_R = real\left([\eta_2+\eta_1]e^{\alpha_1 T}-[\eta_2-\eta_1]e^{-\alpha_1 T}\right),$$
$$A_i = imag\left([\eta_2+\eta_1]e^{\alpha_1 T}-[\eta_2-\eta_1]e^{-\alpha_1 T}\right),$$
$$B_R = real\left([\eta_2+\eta_1]e^{\alpha_1 T}+[\eta_2-\eta_1]e^{-\alpha_1 T}\right), \text{ and}$$
$$B_i = imag\left([\eta_2+\eta_1]e^{\alpha_1 T}+[\eta_2-\eta_1]e^{-\alpha_1 T}\right).$$

Substituting these four terms into equation D21 and D22 give:

$$E^T = \frac{2\eta_2 E^{Tot}(T)}{(B_R+jB_i)\cos\beta_1 T + j\sin\beta_1 T(A_R+jA_i)} \text{ and} \quad \text{(D22a)}$$

$$H^T = \frac{2\eta_1 H^{Tot}(T)}{(A_R+jA_i)\cos\beta_1 T + j\sin\beta_1 T(B_R+jB_i)}. \quad \text{(D22b)}$$

Collecting the real and imaginary terms in the denominator.

$$E^T = \frac{2\eta_2 E^{Tot}(T)}{\left(B_R \cos\beta_1 T - A_i \sin\beta_1 T\right) + j\left(A_R \sin\beta_1 T + B_i \cos\beta_1 T\right)} \text{ and} \tag{D22c}$$

$$H^T = \frac{2\eta_1 H^{Tot}(T)}{\left(A_R \cos\beta_1 T - B_i \sin\beta_1 T\right) + j\left(B_R \sin\beta_1 T + A_i \cos\beta_1 T\right)}. \tag{D22d}$$

Clearing the denominators of imaginary terms:

$$E^T = \frac{2\eta_2 E^{Tot}(T)\left[\left(B_R \cos\beta_1 T - A_i \sin\beta_1 T\right) - j\left(A_R \sin\beta_1 T + B_i \cos\beta_1 T\right)\right]}{\left(B_R \cos\beta_1 T - A_i \sin\beta_1 T\right)^2 + \left(A_R \sin\beta_1 T + B_i \cos\beta_1 T\right)^2} \text{ and} \tag{D22e}$$

$$H^T = \frac{2\eta_1 H^{Tot}(T)\left[\left(A_R \cos\beta_1 T - B_i \sin\beta_1 T\right) - j\left(B_R \sin\beta_1 T + A_i \cos\beta_1 T\right)\right]}{\left(A_R \cos\beta_1 T - B_i \sin\beta_1 T\right)^2 + \left(B_R \sin\beta_1 T + A_i \cos\beta_1 T\right)^2}. \tag{D22f}$$

These two equations (D22e and D22f) define the electric and magnetic field terms for the RF wave transmitted into media 2 in terms of the wave entering media 1 at the boundary between media 1 and media 3.

The conjugate of the magnetic field portion of the wave is taken from equation (D22f):

$$\left[H^T\right]^* = \frac{2\left[\eta_1\right]^* \left[H^{Tot}(T)\right]^* \left[\left(A_R \cos\beta_1 T - B_i \sin\beta_1 T\right) + j\left(B_R \sin\beta_1 T + A_i \cos\beta_1 T\right)\right]}{\left(A_R \cos\beta_1 T - B_i \sin\beta_1 T\right)^2 + \left(B_R \sin\beta_1 T + A_i \cos\beta_1 T\right)^2}. \tag{D22g}$$

Since the instantaneous power of a wave composed of complex phasors is determined by the product of the electric field and the conjugate of the magnetic field portions of the wave, then the instantaneous power per unit area entering media 2 is given by the product of equations (D22e) and (D22g) giving:

$$S^T = \left\{ \frac{4\eta_2\left[\eta_1\right]^* E^{Tot}(T)\left[H^{Tot}(T)\right]^* \left[\left(B_R \cos\beta_1 T - A_i \sin\beta_1 T\right) - j\left(A_R \sin\beta_1 T + B_i \cos\beta_1 T\right)\right]\left[\left(A_R \cos\beta_1 T - B_i \sin\beta_1 T\right) + j\left(B_R \sin\beta_1 T + A_i \cos\beta_1 T\right)\right]}{\left\{\left(B_R \cos\beta_1 T - A_i \sin\beta_1 T\right)^2 + \left(A_R \sin\beta_1 T + B_i \cos\beta_1 T\right)^2\right\}\left\{\left(A_R \cos\beta_1 T - B_i \sin\beta_1 T\right)^2 + \left(B_R \sin\beta_1 T + A_i \cos\beta_1 T\right)^2\right\}} \right\}.$$

Which simplifies to:

$$S^T = \left\{ \frac{4\eta_2\left[\eta_1\right]^* \left[\left(A_R B_R + A_i B_i\right) + j\left\{\left(A_R B_i - A_i B_R\right)\left(1 - 2\cos^2\beta_1 T\right) - \left(A_R^2 + A_i^2 - B_R^2 - B_i^2\right)\left(\cos\beta_1 T \sin\beta_1 T\right)\right\}\right]}{\left\{\left(B_R \cos\beta_1 T - A_i \sin\beta_1 T\right)^2 + \left(A_R \sin\beta_1 T + B_i \cos\beta_1 T\right)^2\right\}\left\{\left(A_R \cos\beta_1 T - B_i \sin\beta_1 T\right)^2 + \left(B_R \sin\beta_1 T + A_i \cos\beta_1 T\right)^2\right\}} \right\} S_1^T. \tag{D23}$$

where the term $S_1^T = E^{Tot}(T)\left[H^{Tot}(T)\right]^*$ is the instantaneous complex power entering media 1 at its boundary with media 3. Remember the average power would be one half the real part of equation (D23). The equation (D23) provides a means of determining the transmittance through a series of media layers and boundaries. Equation (D23) can be successively applied to each media (starting at the first incident boundary) to find the transmittance into the final media. This will be shown in Section D.5.2 for the acoustic blanket.

D.5 APPLICATION TO THE ACOUSTIC BLANKET INSTALLATION

The application of equations (D17,) (D21,) (D22,) and (D23) to the acoustic blanket installation in the Delta fairing will be described here. The process necessary to arrive at a solution for the effective impedance and the transmittance will also be described. The blanket analyzed here is one of several possible configurations. The blanket is similiar to a large pillow, having a conductive cover filled with none conductive batting. Figure D-1 illustrates the configuration analyze.

D.5.1 IMPEDANCE OF THE BLANKET-COVERED WALL

This section will describe the application of the equation (D17) to the acoustic blanket installation illustrated in Figure D-1. The inner fairing wall surface is the starting point and each layer of material is considered in turn.

D.5.1.1 Impedance of the Fairing Wall

The wall material is aluminum. Its RF characteristics (impedance, attenuation constant, and phase constant) can be computed from equations defined in Appendix C.

D.5.1.2 Impedance of Blanket Cover 2 and the Fairing Wall

Figure D-5 illustrates the cover and wall to be analyzed. Equation (D17) shows the RF characteristics of the cover and the wall are required for the computation. Section D.5.1.1 described the computation of the wall characteristics. Determination of the blanket cover intrinsic RF characteristics is complicated by its construction. It is made of several thin layers of materials. Some of the layers have carbon particles which make those layers conductive while other layers are non-conductive. Test data is available, however, which can be used to compute its RF characteristics. Appendix E provides the equations for the impedance, attenuation constant, and phase constant using the test data values for the complex dielectric constant.

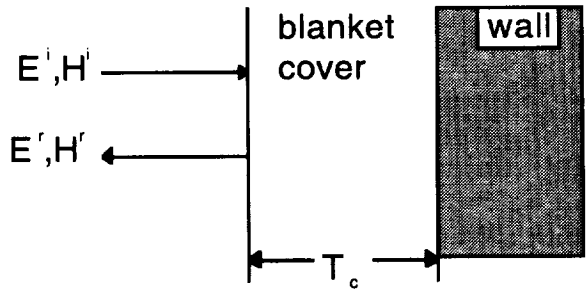

Figure D-5. RF wave at boundary for cover 2 and fairing wall.

Using the cover RF characteristics and aluminum wall RF characteristics (from Section D.5.1.1), the impedance at the surface of the blanket cover is given by equation (D17):

$$\eta_{L1}(Tc) = \eta_C \left\{ \frac{\left[(\eta_{alum}+\eta_C)e^{\alpha_c Tc} + (\eta_{alum}-\eta_C)e^{-\alpha_c Tc}\right]\cos\beta_c Tc + j\left[(\eta_{alum}+\eta_C)e^{\alpha_c Tc} - (\eta_{alum2}-\eta_C)e^{-\alpha_c Tc}\right]\sin\beta_c Tc}{\left[(\eta_{alum}+\eta_C)e^{\alpha_c Tc} - (\eta_{alum}-\eta_{1C})e^{-\alpha_c Tc}\right]\cos\beta_c Tc + j\left[(\eta_{alum}+\eta_C)e^{\alpha_c Tc} + (\eta_{alum}-\eta_C)e^{-\alpha_c Tc}\right]\sin\beta_c Tc} \right\}. \quad \text{(D24)}$$

D.5.1.3 Impedance at Surface of the Batting

Figure D-6 illustrates the next step in the process. The next surface for consideration is the inner surface of the batting. The batting is fiberglass. Its relative dielectric constant is estimated to be 1.02 and it is considered lossless. The value of the dielectric constant was determined using:

$$dielectric_{batting} = \frac{Density_{batting}}{Density_{glass}}\left(dielectric_{glass}\right).$$

The batting's RF impedance, attenuation, and phase constant are calculated using the equations in Appendix C.

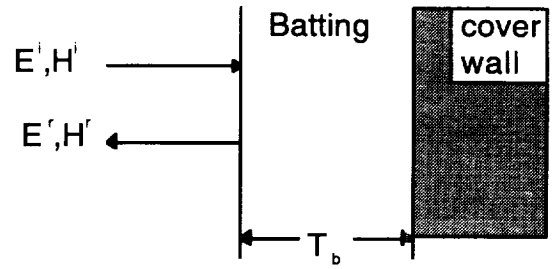

Figure D-6. Blanket batting and boundary with equivalent cover/wall material.

The impedance at the surface of the batting is calculated, using equation (D17), with the combined wall/cover impedance, η_{L1}, (from Section D.5.1.2 equation (D24)) and the batting RF characteristics giving:

$$\eta_{L2}(Tb) = \eta_{L1} \left\{ \frac{\left[(\eta_{L1}+\eta_{L2})e^{0} + (\eta_{L1}-\eta_{L2})e^{-0}\right]\cos\beta_b Tb + j\left[(\eta_{L1}+\eta_{L2})e^{0} - (\eta_{L1}-\eta_{L2})e^{-0}\right]\sin\beta_b Tb}{\left[(\eta_{L1}+\eta_{L2})e^{0} - (\eta_{L1}-\eta_{L2})e^{-0}\right]\cos\beta_b Tb + j\left[(\eta_{L1}+\eta_{L2})e^{0} + (\eta_{L1}-\eta_{L2})e^{-0}\right]\sin\beta_b Tb} \right\}. \quad \text{(D25)}$$

D.5.1.4 Impedance at Inner Surface of Blanket Cover

The final step is the impedance at the exposed surface of the blanket. This is illustrated in Figure D-7. The impedance of the cover was determined is Section D.5.2. The impedance of the batting-cover-wall is from equation (D24.)

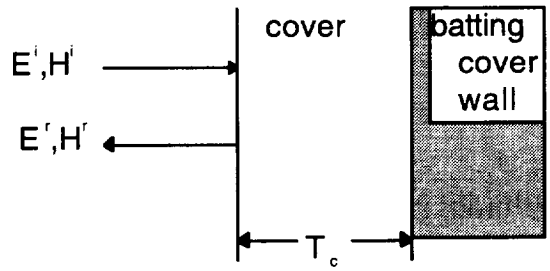

Figure D-7. RF waves at boundary with equivalent material for batting, cover sheet and wall.

Therefore the impedance at the exposed surface of the blanket cover is determined, using equation (D17), by the combined batting/cover/wall impedance (from Section D.5.1.4) and the cover characteristics (from Section D.5.1.2,) giving:

$$\eta_{L3}(Tc)=\eta_C\left\{\frac{\left[(\eta_{L2}+\eta_C)e^{\alpha_c Tc}+(\eta_{L2}-\eta_C)e^{-\alpha_c Tc}\right]\cos\beta_c Tc+j\left[(\eta_{L2}+\eta_C)e^{\alpha_c Tc}-(\eta_{L2}-\eta_C)e^{-\alpha_c Tc}\right]\sin\beta_c Tc}{\left[(\eta_{L2}+\eta_C)e^{\alpha_c Tc}-(\eta_{L3}-\eta_{1C})e^{-\alpha_c Tc}\right]\cos\beta_c Tc+j\left[(\eta_{L2}+\eta_C)e^{\alpha_c Tc}+(\eta_{L2}-\eta_C)e^{-\alpha_c Tc}\right]\sin\beta_c Tc}\right\}. \tag{D26}$$

This impedance can now be used to compute the reflection, transmittance, and loss of the blanket-covered wall.

D.5.2 TRANSMITTANCE THROUGH THE ACOUSTIC BLANKET

Transmittance through the acoustic blanket is of concern because the blanket covers the RF window in the fairing wall. Adequate signal is needed outside the fairing. Figure D-1 illustrates the problem if the wall is replaced by air. The calculation of the transmittance through the acoustic blanket starts at the inner cover 1 surface and proceeds one layer at a time through the blanket until reaching the RF window.

D.5.2.1 Power Entering the Blanket

The blanket-wall system impedance ($\eta_{L3}(T_c)$) resulting from section D.5.1.5 equation (D26) is used in Appendix B equations (B40) and (B41) to calculate the field entering the blanket's inner cover surface of Figure D-7. Using η_A for the impedance of air and $\eta_{L3}(T_c)$ as the equevalent impedance of the blanket and wall system, equations (B40) and (B41) give:

$$E_{c1}^T(T_c)=\left(\frac{2\eta_{L3}}{\eta_A+\eta_{L3}}\right)E^I \text{ and}$$
$$H_{c1}^T(T_c)=\left(\frac{2}{\eta_A+\eta_{L3}}\right)E^I. \tag{D27}$$

The conjugate of the magnetic field is:

$$\left[H_{c1}^T(T_c)\right]^*=\left(\frac{2[\eta_A+\eta_{L3}]}{|\eta_A+\eta_{L3}|^2}\right)\left[E^I\right]^*. \tag{D27a}$$

The instantaneous complex power entering the blanket's inner cover is the product of the electric field and the conjugate of the magnetic field giving:

$$S_{c1}^{T} = \left(\frac{2\eta_{L3}}{\eta_A + \eta_{L3}}\right)\left(\frac{2[\eta_A + \eta_{L3}]}{|\eta_A + \eta_{L3}|^2}\right)[E^I]^* E^I = \frac{4\eta_{L3}|E^I|^2}{|\eta_A + \eta_{L3}|^2}. \quad \text{(D27b)}$$

D.5.2.2 Transmittance Through the Blanket's Inner Cover into the Blanket's Batting Layer

The results of section D.5.2.1 become the field terms for use in equations (D22e), (D22f), and(D23) to determine the field entering the batting. The electric field entering the batting is:

$$E_b^T(T_b) = \frac{2\eta_{L2}E_{c1}^T(T_{c1})\left[\left(B_{Rc1}\cos\beta_{c1}T_{c1} - A_{ic1}\sin\beta_{c1}T_{c1}\right) - j\left(A_{Rc1}\sin\beta_{c1}T_{c1} + B_{ic1}\cos\beta_{c1}T_{c1}\right)\right]}{\left(B_{Rc1}\cos\beta_{c1}T_{c1} - A_{ic1}\sin\beta_{c1}T_{c1}\right)^2 + \left(A_{Rc1}\sin\beta_{c1}T_{c1} + B_{ic1}\cos\beta_{c1}T_{c1}\right)^2}. \quad \text{(D28)}$$

The magnetic field entering the batting is:

$$H_b^T(T_b) = \frac{2\eta_{c1}H_{c1}^T(T_c)\left[\left(A_{Rc1}\cos\beta_{c1}T_{c1} - B_{ic1}\sin\beta_{c1}T_{c1}\right) - j\left(B_{Rc1}\sin\beta_{c1}T_{c1} + A_{ic1}\cos\beta_{c1}T_{c1}\right)\right]}{\left(A_{Rc1}\cos\beta_{c1}T_{c1} - B_{ic1}\sin\beta_{c1}T_{c1}\right)^2 + \left(B_{Rc1}\sin\beta_{c1}T_{c1} + A_{ic1}\cos\beta_{c1}T_{c1}\right)^2}. \quad \text{(D29)}$$

The instantaneous complex power entering the batting is:

$$S_b^T(T_b) = \left\{\frac{4\eta_{L2}[\eta_{c1}]^*\left[\left(A_{Rc1}B_{Rc1} + A_{ic1}B_{ic1}\right) + j\left(\left(A_{Rc1}B_{ic1} - A_{ic1}B_{Rc1}\right)\left(1 - 2\cos^2\beta_{c1}T_{c1}\right) - \left(A_{Rc1}^2 + A_{ic1}^2 - B_{Rc1}^2 - B_{ic1}^2\right)\left(\cos\beta_{c1}T_{c1}\sin\beta_{c1}T_{c1}\right)\right)\right]}{\left\{\left(B_{Rc1}\cos\beta_{c1}T_{c1} - A_{ic1}\sin\beta_{c1}T_{c1}\right)^2 + \left(A_{Rc1}\sin\beta_{c1}T_{c1} + B_{ic1}\cos\beta_{c1}T_{c1}\right)^2\right\}\left\{\left(A_{Rc1}\cos\beta_{c1}T_{c1} - B_{ic1}\sin\beta_{c1}T_{c1}\right)^2 + \left(B_{Rc1}\sin\beta_{c1}T_{c1} + A_{ic1}\cos\beta_{c1}T_{c1}\right)^2\right\}}\right\} S_{c1}^T. \quad \text{(D30)}$$

Where the subscript 'c1' designates the blankets inner cover properties, $[\eta_{c1}]^*$ is the conjugate of the cover impedance, S_{c1}^T is the instantaneous complex power entering the inner cover sheet, and:

$$B_{Rc1} = real\left(\left[\eta_{L2} + \eta_{c1}\right]e^{\alpha_{c1}T_{c1}} + \left[\eta_{L2} - \eta_{c1}\right]e^{-\alpha_{c1}T_{c1}}\right),$$
$$B_{ic1} = imag\left(\left[\eta_{L2} + \eta_{c1}\right]e^{\alpha_{c1}T_{c1}} + \left[\eta_{L2} - \eta_{c1}\right]e^{-\alpha_{c1}T_{c1}}\right),$$
$$A_{Rc1} = real\left(\left[\eta_{L2} + \eta_{c1}\right]e^{\alpha_{c1}T_{c1}} - \left[\eta_{L2} - \eta_{c1}\right]e^{-\alpha_{c1}T_{c1}}\right), \text{ and}$$
$$A_{ic1} = imag\left(\left[\eta_{L2} + \eta_{c1}\right]e^{\alpha_{c1}T_{c1}} - \left[\eta_{L2} - \eta_{c1}\right]e^{-\alpha_{c1}T_{c1}}\right).$$

D.5.2.3 Transmittance Through the Blanket's Inner Cover and Batting into the Blanket's 2nd Cover Sheet

The results of section D.5.2.2 become the field terms for use in equations (D22e,) (D22f,) and (D23) to determine the field entering the second cover sheet. The electric field entering the second cover sheet is:

$$E_{c2}^T(T_{c2}) = \frac{2\eta_{L1}E_b^T(T_b)\left[\left(B_{Rb}\cos\beta_b T_b - A_{ib}\sin\beta_b T_b\right) - j\left(A_{Rb}\sin\beta_b T_b + B_{ib}\cos\beta_b T_b\right)\right]}{\left(B_{Rb}\cos\beta_b T_b - A_{ib}\sin\beta_b T_b\right)^2 + \left(A_{Rb}\sin\beta_b T_b + B_{ib}\cos\beta_b T_b\right)^2}. \quad \text{(D31)}$$

The magnetic field entering the second cover sheet is:

$$H_{c2}^{T}(T_{c2}) = \frac{2\eta_{L1} H_b^T(T_b)\left[\left(A_{Rb}\cos\beta_b T_b - B_{ib}\sin\beta_b T_b\right) - j\left(B_{Rb}\sin\beta_b T_b + A_{ib}\cos\beta_b T_b\right)\right]}{\left(A_{Rb}\cos\beta_b T_b - B_{ib}\sin\beta_b T_b\right)^2 + \left(B_{Rb}\sin\beta_b T_b + A_{ib}\cos\beta_b T_b\right)^2}. \tag{D32}$$

The instantaneous complex power entering the second cover sheet is:

$$S_{c2}^{T}(T_{c2}) = \left\{\frac{4\eta_{L1}\left[\eta_b\right]^*\left[\left(A_{Rb}B_{Rb} + A_{ib}B_{ib}\right) + j\left(\left(A_{Rb}B_{ib} - A_{ib}B_{Rb}\right)\left(1 - 2\cos^2\beta_b T_b\right) - \left(A_{Rb}^2 + A_{ib}^2 - B_{Rb}^2 - B_{ib}^2\right)\left(\cos\beta_b T_b \sin\beta_b T_b\right)\right)\right]}{\left\{\left(B_{Rb}\cos\beta_b T_b - A_{ib}\sin\beta_b T_b\right)^2 + \left(A_{Rb}\sin\beta_b T_b + B_{ib}\cos\beta_b T_b\right)^2\right\}\left\{\left(A_{Rb}\cos\beta_b T_b - B_{ib}\sin\beta_b T_b\right)^2 + \left(B_{Rc1}\sin\beta_b T_b + A_{ib}\cos\beta_b T_b\right)^2\right\}}\right\} S_b^T. \tag{D33}$$

Where the subscript 'b' designates the blanket's batting properties, $[\eta_b]^*$ is the conjugate of the cover impedance, S_b^T is the instantaneous complex power entering the inner cover sheet, and:

$$B_{Rc1} = real\left(\left[\eta_{L1} + \eta_b\right]e^{\alpha_b T_b} + \left[\eta_{L1} - \eta_b\right]e^{-\alpha_b T}\right),$$
$$B_{ib} = imag\left(\left[\eta_{L1} + \eta_b\right]e^{\alpha_b T_b} + \left[\eta_{L1} - \eta_b\right]e^{-\alpha_b T_b}\right),$$
$$A_{Rc1} = real\left(\left[\eta_{L2} + \eta_{c1}\right]e^{\alpha_{c1} T_{c1}} - \left[\eta_{L2} - \eta_{c1}\right]e^{-\alpha_{c1} T_{c1}}\right), \text{ and}$$
$$A_{ib} = imag\left(\left[\eta_{L1} + \eta_b\right]e^{\alpha_b T_b} - \left[\eta_{L1} - \eta_b\right]e^{-\alpha_b T_{b1}}\right).$$

D.5.2.4 Transmittance Through the Blanket and into the Air (Wall)

The results of section D.5.2.3 become the field terms for use in equations (D22e), (D22f), and (D23) to determine the field entering the air (wall.) The electric field entering the air (wall) is:

$$E_w^T = \frac{2\eta_w E_{c2}^T(T_{c2})\left[\left(B_{Rc2}\cos\beta_{c2} T_{c2} - A_{ic2}\sin\beta_{c2} T_{c2}\right) - j\left(A_{Rc2}\sin\beta_{c2} T_{c2} + B_{ic2}\cos\beta_{c2} T_{c2}\right)\right]}{\left(B_{Rc2}\cos\beta_{c2} T_{c2} - A_{ic2}\sin\beta_{c2} T_{c2}\right)^2 + \left(A_{Rc2}\sin\beta_{c2} T_{c2} + B_{ic2}\cos\beta_{c2} T_{c2}\right)^2}. \tag{D34}$$

The magnetic field entering the air (wall) is:

$$H_w^T = \frac{2\eta_{c2} H_{c2}^T(T_{c2})\left[\left(A_{Rc2}\cos\beta_{c2} T_{c2} - B_{ic2}\sin\beta_{c2} T_{c2}\right) - j\left(B_{Rc2}\sin\beta_{c2} T_{c2} + A_{ic2}\cos\beta_{c2} T_{c2}\right)\right]}{\left(A_{Rc2}\cos\beta_{c2} T_{c2} - B_{ic2}\sin\beta_{c2} T_{c2}\right)^2 + \left(B_{Rc2}\sin\beta_{c2} T_{c2} + A_{ic2}\cos\beta_{c2} T_{c2}\right)^2}. \tag{D35}$$

The instantaneous complex power entering the air (wall) is:

$$S_a^T = \left\{\frac{4\eta_a\left[\eta_{c2}\right]^*\left[\left(A_{Rc2}B_{Rc2} + A_{ic2}B_{ic2}\right) + j\left(\left(A_{Rc2}B_{ic2} - A_{ic2}B_{Rc2}\right)\left(1 - 2\cos^2\beta_{c2} T_{c2}\right) - \left(A_{Rc2}^2 + A_{ic2}^2 - B_{Rc2}^2 - B_{ic2}^2\right)\left(\cos\beta_{c2} T_{c2}\sin\beta_{c2} T_{c2}\right)\right)\right]}{\left\{\left(B_{Rc2}\cos\beta_{c2} T_{c2} - A_{ic2}\sin\beta_{c2} T_{c2}\right)^2 + \left(A_{Rc2}\sin\beta_{c2} T_{c2} + B_{ic2}\cos\beta_{c2} T_{c2}\right)^2\right\}\left\{\left(A_{Rc2}\cos\beta_{c2} T_{c2} - B_{ic2}\sin\beta_{c2} T_{c2}\right)^2 + \left(B_{Rc2}\sin\beta_{c2} T_{c2} + A_{ic2}\cos\beta_{c2} T_{c2}\right)^2\right\}}\right\} S_{c2}^T. \tag{D36}$$

Where the subscript, 'c2', designates the blanket's second cover properties,$[\eta_{c2}]^*$ is the conjugate of the cover impedance, S_{c2}^T is the instantaneous complex power entering the second cover sheet, and:

$$B_{Rc2} = real\left([\eta_w + \eta_{c2}]e^{\alpha_{c2}T_{c2}} + [\eta_w - \eta_{c2}]e^{-\alpha_{c2}T_{c2}}\right),$$
$$B_{ic2} = imag\left([\eta_w + \eta_{c2}]e^{\alpha_{c2}T_{c2}} + [\eta_w - \eta_{c2}]e^{-\alpha_{c2}T_{c2}}\right),$$
$$A_{Rc2} = real\left([\eta_w + \eta_{c2}]e^{\alpha_{c2}T_{c2}} - [\eta_w - \eta_{c2}]e^{-\alpha_{c2}T_{c2}}\right), \text{ and}$$
$$A_{ic2} = imag\left([\eta_w + \eta_{c2}]e^{\alpha_{c2}T_{c2}} - [\eta_w - \eta_{c2}]e^{-\alpha_{c2}T_{c2}}\right).$$

D.6 CONCLUSION

Equation (D17) can be used to develop the RF impedance model for the blanket covered walls of the fairing. Equations (D21) and (D22) can be used to define the field leaving the RF window. The application of the equations can be implemented easily using numerical values of the various material impedances in a computer program or spreadsheet. Hopefully this note provides the insight necessary to apply the equations to any combination of layered materials that might be encountered.

APPENDIX E

Calculating RF Characteristics of the Acoustic Blanket Cover Sheets

by
Jerry Reddell

The acoustic blankets used in the Delta metal fairing are built of two cover sheets and fiberglass batting material. The cover sheets in turn are built from a thin sheet of fiberglass cloth which has been dipped in Teflon and carbon loaded Teflon. Test measurements of the RF characteristics of the cover sheets were performed. The test data on the cover sheets defines the loss tangent and therefore the complex relative dielectric constant of the sheet. Equations are needed to compute the other sheet parameters from the complex dielectric constant; this Appendix develops the necessary equations. The equations are applicable to any material for which the complex dielectric constant is known.

The intrinsic impedance (a complex number) is given by Appendix C equation (C15) as:

$$\eta^2 = \frac{j\omega\mu}{\sigma + j\omega\varepsilon}. \tag{E1}$$

where: η is the intrinsic impedance,
ω is the frequency in radians per second,
σ is the conductivity in mhos per meter,
μ is the permeability in henrys per meter, and
ε is the permittivity in farads per meter.

Using the denominator and rearranging factors gives:

$$\sigma + j\omega\varepsilon = j\omega\varepsilon\left(1 + \frac{\sigma}{j\omega\varepsilon}\right) \tag{E2}$$

or

$$\sigma + j\omega\varepsilon = j\omega\varepsilon\left(1 - j\frac{\sigma}{\omega\varepsilon}\right). \tag{E3}$$

The permittivity of the material is a complex number defined by:

$$\varepsilon = \varepsilon_O\left(\varepsilon' + j\varepsilon''\right)$$

and the loss tangent is defined as

$$\tan\delta = \frac{\varepsilon''}{\varepsilon'}.$$

Equation (E3) now becomes:

$$\sigma + j\omega\varepsilon_m = j\omega\varepsilon_0\varepsilon'\left(1 - j\frac{\varepsilon''}{\varepsilon'}\right). \tag{E4}$$

Then comparison of equations (E3) and (E4) shows equivalent terms:

$$\frac{\sigma}{\omega\varepsilon_0\varepsilon'} = \frac{\varepsilon''}{\varepsilon'}. \tag{E5}$$

Solving equation (E5) for conductivity gives:

$$\sigma = \omega\varepsilon_0\varepsilon''. \tag{E6}$$

Inserting equation (5) into equation (1) gives:

$$\eta^2 = \frac{j\omega\mu}{j\omega\varepsilon_0\varepsilon'\left(1 - j\frac{\varepsilon''}{\varepsilon'}\right)}. \tag{E7}$$

Multiplying equation (7) by $\frac{\left(1 + j\frac{\varepsilon''}{\varepsilon'}\right)}{\left(1 + j\frac{\varepsilon''}{\varepsilon'}\right)}$ gives:

$$\eta^2 = \frac{\mu}{\varepsilon_0\varepsilon'\left(1 - j\frac{\varepsilon''}{\varepsilon'}\right)}\frac{\left(1 + j\frac{\varepsilon''}{\varepsilon'}\right)}{\left(1 + j\frac{\varepsilon''}{\varepsilon'}\right)} = \frac{\left(\frac{\mu}{\varepsilon_0\varepsilon'}\right)}{1 + \left(\frac{\varepsilon''}{\varepsilon'}\right)^2}\left(1 + j\frac{\varepsilon''}{\varepsilon'}\right). \tag{E8}$$

Which reduces to:

$$\eta^2 = \frac{\left(\frac{\mu}{\varepsilon_0\varepsilon'}\right)}{1 + \left(\frac{\varepsilon''}{\varepsilon'}\right)^2}\sqrt{1 + \left(\frac{\varepsilon''}{\varepsilon'}\right)^2}\angle\theta = \frac{\left(\frac{\mu}{\varepsilon_0\varepsilon'}\right)}{\sqrt{1 + \left(\frac{\varepsilon''}{\varepsilon'}\right)^2}}\angle\theta. \tag{E9}$$

Where: $\theta = \tan^{-1}\left(\frac{\varepsilon''}{\varepsilon'}\right)$.

Therefore the real part of the impedance is given by:

$$\eta_R = |\eta|\cos\left(\frac{\theta}{2}\right) = \sqrt{\frac{Cos\theta + 1}{2}} = \sqrt{\frac{\frac{\mu}{\varepsilon_0\varepsilon'}\left(\sqrt{1 + \left(\frac{\varepsilon''}{\varepsilon'}\right)^2} + 1\right)}{2\left[1 + \left(\frac{\varepsilon''}{\varepsilon'}\right)^2\right]}}. \tag{E10}$$

and the imaginary part is given by:

$$\eta_I = |\eta|\sin\left(\frac{\theta}{2}\right) = \sqrt{\frac{Cos\theta - 1}{2}} = \sqrt{\frac{\frac{\mu}{\varepsilon_0\varepsilon'}\left(\sqrt{1 + \left(\frac{\varepsilon''}{\varepsilon'}\right)^2} - 1\right)}{2\left[1 + \left(\frac{\varepsilon''}{\varepsilon'}\right)^2\right]}}. \tag{E11}$$

To derive the attenuation and phase constant, we use the propagation constant relationship defined by equation (C16) of Appendix C:

$$\gamma = \alpha + j\beta = \sqrt{j\omega\mu\left(\sigma + j\omega\varepsilon\right)}. \tag{E12}$$

Where: γ is the propagation constant of the material,
α is the attenuation constant of the material, and
β is the phase shift constant of the material.

But using equation (E4) in equation (E12) gives:

$$\gamma = \sqrt{j\omega\mu\left\{j\omega\varepsilon_0\varepsilon'\left(1 - j\frac{\varepsilon''}{\varepsilon'}\right)\right\}} = \omega\sqrt{-\mu\varepsilon_0\varepsilon'\left(1 - j\frac{\varepsilon''}{\varepsilon'}\right)} \text{ and}$$
$$\gamma = \omega\sqrt{-\mu\varepsilon_0(\varepsilon' - j\varepsilon'')} = \omega\sqrt{\mu\varepsilon_0\left[\sqrt{(\varepsilon')^2 + (\varepsilon'')^2}\right]}\angle\theta. \tag{E13}$$

Where:

$$\theta = \frac{\pi}{2} - \frac{1}{2}\tan^{-1}\left(\frac{\varepsilon''}{\varepsilon'}\right) \tag{E14}$$

and therefore:

$$\cos\theta = \sin\left(\frac{1}{2}\tan^{-1}\left(\frac{\varepsilon''}{\varepsilon'}\right)\right),$$

$$\sin\theta = \cos\left(\frac{1}{2}\tan^{-1}\left(\frac{\varepsilon''}{\varepsilon'}\right)\right),$$

$$\cos\left(\frac{A}{2}\right) = \sqrt{\frac{\cos A + 1}{2}}, \text{ and}$$

$$\sin\left(\frac{A}{2}\right) = \sqrt{\frac{\cos A - 1}{2}}.$$

Then:

$$\cos\theta = \sin\left(\frac{1}{2}\tan^{-1}\left(\frac{\varepsilon''}{\varepsilon'}\right)\right) = \sqrt{\frac{\cos\left(\tan^{-1}\left(\frac{\varepsilon''}{\varepsilon'}\right)\right) + 1}{2}} = \sqrt{\frac{\sqrt{1 + \left(\frac{\varepsilon''}{\varepsilon'}\right)^2} - 1}{2 * \sqrt{1 + \left(\frac{\varepsilon''}{\varepsilon'}\right)^2}}} \text{ and} \tag{E15}$$

$$\sin\theta = \cos\left(\frac{1}{2}\tan^{-1}\left(\frac{\varepsilon''}{\varepsilon'}\right)\right) = \sqrt{\frac{\cos\left(\tan^{-1}\left(\frac{\varepsilon''}{\varepsilon'}\right)\right)-1}{2}} = \sqrt{\frac{\sqrt{1+\left(\frac{\varepsilon''}{\varepsilon'}\right)^2}+1}{2*\sqrt{1+\left(\frac{\varepsilon''}{\varepsilon'}\right)^2}}}. \tag{E16}$$

The attenuation constant is the real part of the wave impedance, thus:

$$\alpha = |\gamma|\cos\theta = \omega\sqrt{\mu\varepsilon_0\sqrt{(\varepsilon')^2+(\varepsilon'')^2}}\left[\sin\left(\frac{1}{2}\tan^{-1}\frac{\varepsilon''}{\varepsilon'}\right)\right]$$

giving

$$\alpha = \omega\sqrt{\mu\varepsilon_0\varepsilon'\sqrt{1+\left(\frac{\varepsilon''}{\varepsilon'}\right)^2}}\sqrt{\frac{\sqrt{1+\left(\frac{\varepsilon''}{\varepsilon'}\right)^2}-1}{2*\sqrt{1+\left(\frac{\varepsilon''}{\varepsilon'}\right)^2}}} = \omega\sqrt{\frac{\mu\varepsilon_0\varepsilon'}{2}\left[\sqrt{1+\left(\frac{\varepsilon''}{\varepsilon'}\right)^2}-1\right]}. \tag{E17}$$

The phase constant is the imaginary part of the wave impedance, thus:

$$\beta = |\gamma|\sin\theta = \omega\sqrt{\mu\varepsilon_0\sqrt{(\varepsilon')^2+(\varepsilon'')^2}}\left[\cos\left(\frac{1}{2}\tan^{-1}\frac{\varepsilon''}{\varepsilon'}\right)\right]$$

resulting in

$$\beta = \omega\sqrt{\mu\varepsilon_0\varepsilon'\sqrt{1+\left(\frac{\varepsilon''}{\varepsilon'}\right)^2}}\sqrt{\frac{\sqrt{1+\left(\frac{\varepsilon''}{\varepsilon'}\right)^2}+1}{2*\sqrt{1+\left(\frac{\varepsilon''}{\varepsilon'}\right)^2}}} = \omega\sqrt{\frac{\mu\varepsilon_0\varepsilon'}{2}\left[\sqrt{1+\left(\frac{\varepsilon''}{\varepsilon'}\right)^2}+1\right]}. \tag{E18}$$

Equations (E6), (E10), (E11), (E17), and (E18) provide the necessary RF characteristics for the cover sheet from the measured complex dielectric constant.

REPORT DOCUMENTATION PAGE

Form Approved
OMB No. 0704-0188

1. AGENCY USE ONLY *(Leave blank)*	2. REPORT DATE	3. REPORT TYPE AND DATES COVERED
	August, 1998	Technical Publication

4. TITLE AND SUBTITLE
Technique for Predicting the RF Field Strength Inside an Enclosure

5. FUNDING NUMBERS

6. AUTHOR(S)
M. Hallett, J. Reddell

7. PERFORMING ORGANIZATION NAME(S) AND ADDRESS (ES)
Orbital Launch Services (OLS) Project
Goddard Space Flight Center
Greenbelt, Maryland 20771

8. PEFORMING ORGANIZATION REPORT NUMBER
98B00064

9. SPONSORING / MONITORING AGENCY NAME(S) AND ADDRESS (ES)
National Aeronautics and Space Administration
Washington, DC 20546-0001

10. SPONSORING / MONITORING AGENCY REPORT NUMBER
TP—1998–206864

11. SUPPLEMENTARY NOTES
J. Reddell, Boeing Corp, Seabrook, Maryland

12a. DISTRIBUTION / AVAILABILITY STATEMENT
Unclassified - Unlimited
Subject Category: 33
Report available from the NASA Center for AeroSpace Information,
7121 Standard Drive, Hanover MD 21076-1320 (301) 621-0390.

12b. DISTRIBUTION CODE

13. ABSTRACT *(Maximum 200 words)*

This Memorandum presents a simple analytical technique for predicting the RF electric field strength inside an enclosed volume in which radio frequency radiation occurs. The technique was developed to predict the radio frequency (RF) field strength within a launch vehicle's fairing from payloads launched with their telemetry transmitters radiating and to the impact of the radiation on the vehicle and payload. The RF field strength is shown to be a function of the surface materials and surface areas. The method accounts for RF energy losses within exposed surfaces, through RF windows, and within multiple layers of dielectric materials which may cover the surfaces. This Memorandum includes the rigorous derivation of all quations and presents examples and data to support the validity of the technique.

14. SUBJECT TERMS
RF electric, field strength, radio frequency, radiation, telemetry transmitters, RF windows, dielectric materials

15. NUMBER OF PAGES
90

16. PRICE CODE

17. SECURITY CLASSIFICATION OF REPORT	18. SECURITY CLASSIFICATION OF THIS PAGE	19. SECURITY CLASSIFICATION OF ABSTRACT	20. LIMITATION OF ABSTRACT
Unclassified	Unclassified	Unclassified	UL